Effects of time-dependent faradaic currents on electric double-layer capacitance

Effects of time-dependent faradaic currents on electric double-layer capacitance

時間依存ファラデー電流が電気二重層キャパシタンスに与える影響

by

Yuanyuan Liu

劉 圓圓

A Thesis

for the degree of *Doctor of Engineering*

Submitted to Advanced Interdisciplinary Science and Technology

Graduate School of Engineering

University of Fukui

in September 2024

Abstract

The electric double layer (EDL) structure, is a physical framework for understanding electrochemical reactions, and revealing and controlling its structure in advancing electrochemical fields such as batteries, capacitors, and sensors. It has been believed that mass transport, which is related to the faradaic current, has no relation with the EDL structure so far. Recently, the diffusion-controlled faradaic currents in a short time can be suppressed by the EDL. The suppression of the diffusion-controlled faradaic currents is caused by one kind of capacitive current on the EDL, which is charging the dipole moment of the solvent molecules to compensate for the newly generated dipole moment of a pair of oxidant or (reductant) and the counter ion. The orientation of the new dipole moment is opposite to that of the solvent dipoles through the faradaic reactions. When the current by the newly dipole moment exceeds that of the solvent dipoles, the observed capacitance has a negative value, which is called the negative capacitance (NC). This concept has been confirmed by using the AC impedance and stripping voltammetry. Also, fast-scan cyclic voltammetry is a suitable electrochemical technique for detecting the NC because it shows voltage-variations at a short time response. It provides not only the properties of the NC but also the determination of reaction mechanisms.

The NC for the one-electron transfer reaction of a ferrocenyl derivative was evaluated to be –64 $\mu F\ cm^{-2}$ for 1 mM redox concentration. The values were found to be proportional to their concentrations. It was shown that the NC leads to a larger peak separation in the voltammograms. It should be not

related to the heterogenous kinetics of the electrode transfer reactions.

The concept of the NC was extended to the two-electron reduction of hydrogen ions. The voltammograms showed two peaks, the first of which was attributed to the reduction of adsorbed hydrogen ions. The second one showed the NC behavior, similar to the ferrocenyl derivative. The NC causes the potential shift at high scan rates owing to the relaxation of the electric field for the faradaic reaction. The values of NC were twice more than that of the ferrocenyl derivative at the same concentration.

The NC was extended further to the four-electron transfer such as the oxidation of hydroxide ion. The voltammograms showed the diffusion-controlled one-electron rather than four-electron transfer reaction. The product could be assigned to hydrogen peroxide in the adsorbed state. The anodic peak current being lower than the diffusion-controlled one was ascribed to the NC rather than the heterogeneous kinetics. The values of NC were invariant to the concentrations of hydroxide ions because of the destruction of dipoles by agitation of hydroxyl radicals.

The EDL capacitance (EDLC) is known to have the properties of power law. The similarity of the NC to the EDLC was obtained with the comparison of the two in power-law by chronoamperometry. The chronoamperometric curves for the oxidation of the ferrocenyl derivative showed diffusion-controlled currents less than the theoretical ones. This deviation was ascribed to NC not the heterogeneous kinetics. The NC was proportional to the time of the power of -0.9, which is close to that of EDL capacitive currents. As a result, the NC can be ascribed to the orientation of solvent dipoles triggered

by the faradaic reactions. Ultimately, the effects of NC lead to a decrease in reaction rates, which can be considered as one of the factors contributing to the slow generation rates in water electrolysis in practical applications.

Acknowledgment

Time has swiftly passed, and as I approach the end of the thesis at the Advanced Interdisciplinary Science and Technology, Graduate School of Engineering, University of Fukui under the supervision of **Associate Professor Ryoichi ISHIMATSU**. I have reflected on the nearly six years since I arrived in Japan in October. 2018. With Dr.Ishimatsu for half of my doctoral career, I have learned from Dr. Ishimatsu the fresh perspectives in our research group, exposing us to new areas within electrochemistry such as electrochemiluminescence and homogeneous reaction kinetics. I would like to thank for his guidance in academic research and conference participation. Also, thanks to him for helping me out with troubleshooting.

Special thanks to **Emeritus Professor Koichi Jeremiah AOKI** (University of Fukui) for his invaluable support throughout my master's and doctoral studies. His enthusiasm for the electrochemical concept has inspired my scientific endeavors and instilled a profound commitment to my research work. Thanks for not only his mentorship in basic theoretic electrochemistry and logical thinking but also the encouragement that directed my foundation in scientific research. I still remember his statement when I started my Ph.D career three years ago: “Even if I were lying in the hospital, you could come to discuss the data with me”.

I'm also grateful to **Associate Professor Toyohiko NISHIUMI** for his insightful discussions during the seminar, as well as assistance with

presentations, which have been fundamental to my research growth.

The other appreciation goes to **Emeritus Professor Jingyuan CHEN** (University of Fukui) for highlighting a balance between life and research. She has reminded me that there's more important in the value of life than just academic pursuits.

I'm grateful for the camaraderie in the joyous moments during BBQs and year-end parties with my Lab members. Also, I encountered friends who worked part-time jobs with long conversations all night. I thank **Mrs. KASAJIMA**, who shared in seeing the cherry blossoms and tasting the delicious food in Fukui. The invaluable friendships with **Mr. Zhongkai ZHAO** formed through late-night experimental and research work sessions and heartwarming conversations. I also give special thanks to my encourager **Mr. Jinao FENG** who has enriched this journey with his encouragement and companionship.

Last but not the least, my heartfelt gratitude is dedicated to **my family** for their unwavering support and understanding, especially during the challenging times of the novel Coronavirus. Their messages of care and financial support were on my pillars of strength.

I also extend my thanks to **Mitani Company** for the scholarship, which has significantly eased my financial burden, allowing me to devote myself more passionately to my research.

Everyone’s life experience is very important and non-uniform. Be grateful for everyone I meet and everything I go through. Ultimately, it will

encourage my future to keep going.

Table of Contents

Chapter 1

Introduction

1.1.Electrode|Solution interface

Electrochemistry is the research field that focuses on the chemical changes when electric currents pass through the electrode|solution interface [1,2,3,4]. Even if currents are observed to be zero, electric potentials often provide thermodynamic information on chemical reactions at the interface. Since electrochemical processes occur at the interface between these different phases, they belong to heterogeneous reactions rather than homogenous ones [1,4].

Electrochemical processes are classified into a faradaic and a non-faradaic process [1,2,4,5,7]. The former is accompanied by charge transfer reactions at the interface, called oxidation or reduction. In contrast, the latter is caused by charging or discharging at the interfacial capacitor without oxidation or reduction. Electrochemical processes are always carried out with the assistance of electrodes for the input and output of electrical energy, where the interface is a site of the electrode reaction [6]. The electric current flowing through the faradaic reaction is a measure of the time-variation of the electric charge or rate of charge transfer, while the potential is a measure of the possibility of electrochemical charge transfer [7,8,9,10]. When an electrode is inserted into a solution, a chemical potential within the electrode phase is always different from that in the solution phase [11,12]. Unless any

faradaic reaction occurs, the equilibrium is maintained by the generation of electric potential in each phase so that a sum of the chemical potential and electric potential in the electrode, called an electrochemical potential, is common to the two phases in equilibrium [1,3,4,5,11,12, 13 , 14 , 15]. Obviously, the applied electric potential is inevitable. When an electric potential is applied to an external circuit so that the equilibrium may not be maintained, currents flow [1-12,16,17]. Currents vary the concentration of species relevant to the electrochemical reactions to make the non-uniform distribution of concentrations. Then mass transport occurs to make currents flow again so that the concentration may tend to be uniform gradually [1-8,18]. As a result, concentrations near the interface vary with time. The potential region with any currents or any faradaic reaction is called an unpolarized potential domain, whereas the region without currents is called a polarized potential domain [19,20,21,22].

I consider potential variations near the interface when the external voltage is applied to the interface. Then, a solution phase with the potential energy $\overline{U_S}$ comes in contact with an electrode with the potential energy $\overline{U_E}$, the energy varies drastically at the boundary, as shown in Fig.1.1. The electric field acting on one particle was distributed the difference of the potential energy $\bar{U}$ with respect to the distance x, $-\frac{\partial U}{\partial x}$. The maximum force should lie at the interface, where a particle would be transferred to the other phase associated with changing the molecular structure including the transfer of electric charge [23,24]. The transfer (faradaic reaction) makes the particle-stabilized in the transferred phase [24,25,26,27]. The change in the

molecular structure at the interface is nothing but an electrode reaction. Even if no molecular change or transfer occurs (non-faradaic reaction), the strong electric field of more than 10^9 V cm^{-1} at the interface may vary the distribution of ions and/or orientation of solvents [1-6,28,29]. The interface without any current can be regarded as in thermodynamic equilibrium [30].

Electrochemical work has been advanced from not only the thermodynamic equilibrium viewpoints, but also the kinetic ones [1,2,4,5,12,14,15,31]. The former has been directed experimentally to the polarized potential domains. Since the equilibrium potentials represent concentrations of redox species through the Nernst equation [32], they can work as potentiometric detectors. The concept of the equilibrium is helpful for the identification of redox species even for electrochemical dynamics if one pays attention only to potentials near zero currents. The polarized domains have been utilized for study on EDLC, which are responsible for functions of electrode reactions at the interface from a physicochemical viewpoint, as will be described in the next section.

In contrast, the kinetic behavior in unpolarized potential domains is a main concern in electrochemistry. Since heterogeneity of redox species near the interface is caused by currents, it is relaxed with mass transport and/or chemical reactions to yield temporal variations of the related components. Therefore, the electrochemical responses should vary not only with currents and voltages but also with time. One of the three variables is controlled externally in conventional electrochemical experiments. For example: 1) Chronoamperometry at which voltage or potential is controlled to measure

current vs. time curves; 2) Chronopotentiometry at which current is controlled to obtain voltage vs. time curves, and 3) Steady-state method at which mass transport is controlled sufficiently enough to maintain steady-state to measure current vs. voltage curves. There are also other techniques for combining the two variables into one, such as linear sweep voltammetry, pulse voltammetry, and alternating current voltammetry. They have been often utilized for conveniently electrochemical tools. These electrochemical techniques have been used in the field of fuel cells [8,33,34,35], medical tests [36,37,38], the characterization of biological neurotransmitters [39,40], and the detection of gases and toxic substances involving sea-water electrolysis called soda industry [41,42,43], the generation of hydrogen and oxygen from water electrolysis [44,45,46], the electrowinning of copper or the extraction of aluminum, and alkali metals [47,48], electrochemical processing through the dissolution of metals [49,50], the development of electrical energy storage devices known as batteries [51,52,53,54] or capacitors [53,55,56], and the preparation of electroanalytical sensors [57,58], to name a few.

In general, the simplest electrochemical system is in equilibrium without charge transfer steps. There is no charge transfer reaction at the electrode|solution interface under the control of specific electrochemical parameters, but rather the structure of its interface is altered during the electrochemical reaction. This is realized in the EDL, which exhibits abnormal behavior owing to the heterogeneity at the interface. An electrochemically accessible measure is capacitance. It will be described in the Section.1.2, along with its history. It will be extended to faradaic

processes caused mainly by diffusion relevant to the EDLC.

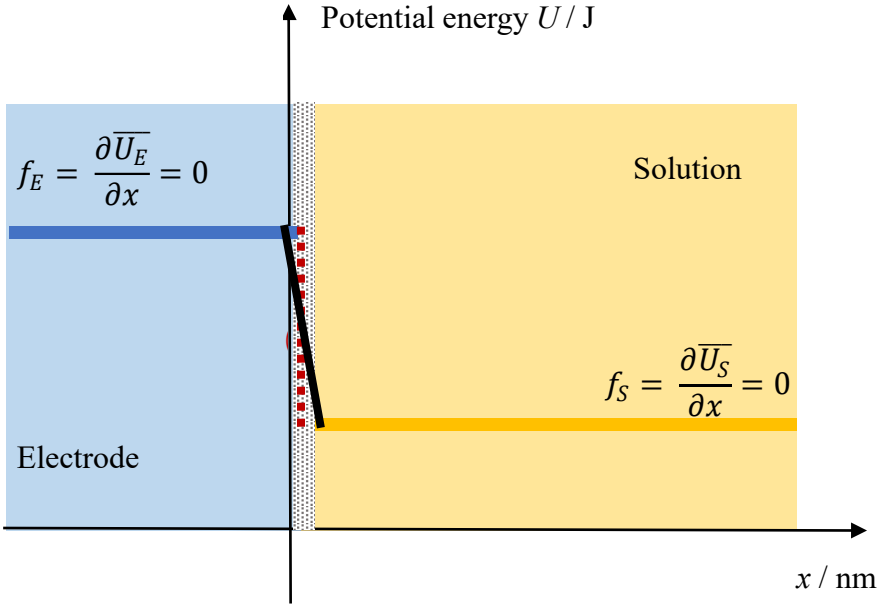

Fig.1.1 Illustration of the potential energy distribution between electrodes and solutions. The X-axis is the distance from the electrode surface, and the Y-axis is the potential energy.

1.2.Electric double layer (EDL)

1.2.1. Helmholtz model

The term of the "electric double layer" was first introduced in the early works from Helmholtz, dating back to 1853 [59] and 1879 [60]. This concept hypothesizes that the arrangement of charges at the electrode surface forms a tightly packed monolayer, as illustrated in Fig.1.2, while a parallel layer with opposite charges forms in the solution relative to the electrode surface. Helmholtz believed that the interface structure of the EDL adhered to the

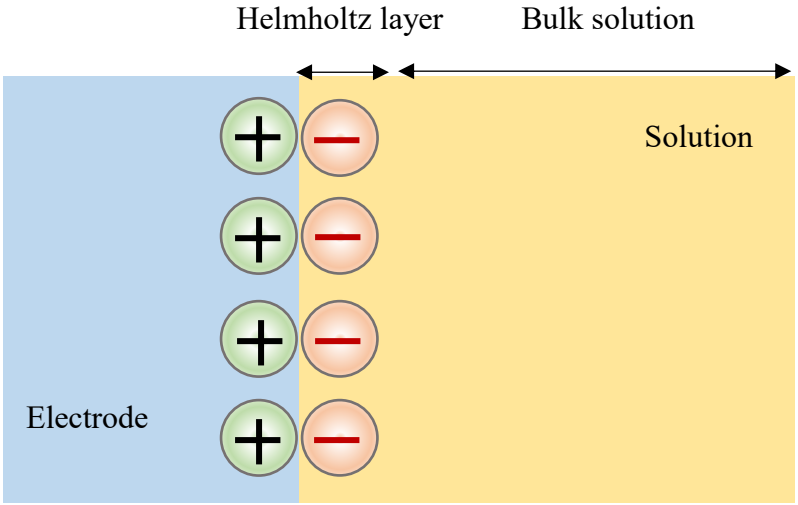

Fig.1.2 Schematic diagram of Helmholtz model of the electric double layer

theory of interfacial charge separation [60]. Then, the total amount of charges stored, Q, at the electrode|solution interface is governed by the equation $Q = CV$, where C represents the interfacial EDLC, and V is the voltage difference between the two phases. This assumption is akin to a parallel-plate capacitor.

The stored energy in the Helmholtz model, U, is related to the ideal capacitance as follows [61]:

$$U = \int_0^V Q\, dV = \int_0^V CV\, dV = \frac{1}{2} CV^2 \quad (1.2.1)$$

Herein C is a constant value. It applies to ideal capacitors. However, it is important to note that in real systems. The ionic composition of the solution could influence the values of the C, thereby making it a variable rather than a constant.

1.2.2. Gouy-Chapman (GC) model

Experimental data have shown that the value of the EDLC is not constant but varies with the potential and also increases with the rise in concentration of the ionic solution. Building upon the foundation laid by the Helmholtz model, a French electrochemist Maurice Gouy and a British electrochemist David Chapman significantly refined Helmholtz's model around 1910 [62,63], leading to what is now known as the Gouy-Chapman (GC) model. This model acknowledges that the charge at the electrode surface attracts ions near the electrode|solution interface due to electrostatic attraction. The EDL becomes very rigid. However, the GC model accounts for the thermal motion of ions, which increases the entropy of the system and results in the formation of a diffuse layer. This makes the GC model less compact compared to Helmholtz's one. Gouy and Chapman introduced the concept of a diffuse layer of charged solution, marking a significant advancement in our understanding of electrochemical interfaces. Fig.1.3 illustrates the schematic of the GC model for an ionic distribution caused by an electric field and thermal balance by electrostatics and statistical mechanics. The former is governed by the Poisson equation, which is related to the Galvani potential, while the latter follows the Boltzmann statistical

equation. By conceptualizing the solution as several thin layers parallel to the electrode, each with a thickness of dx, and assuming thermal equilibrium among all layers, the distribution of ions can be analyzed in detail. According to electrostatic mechanics, the charge density $\rho(x)$ and the electrostatic potential $\varphi(x)$ at any distance x from the electrode surface are expressed by the Poisson equation:

$$\frac{d^2\varphi(x)}{dx^2} = -\frac{\rho(x)}{\varepsilon\varepsilon_0} \tag{1.2.2}$$

Here, ε represents the dielectric constant of the solvent in the solution, and ε_0 is the vacuum permittivity with a value of approximately 8.9×10^{-12} C^2 N^{-1} m^{-2}.

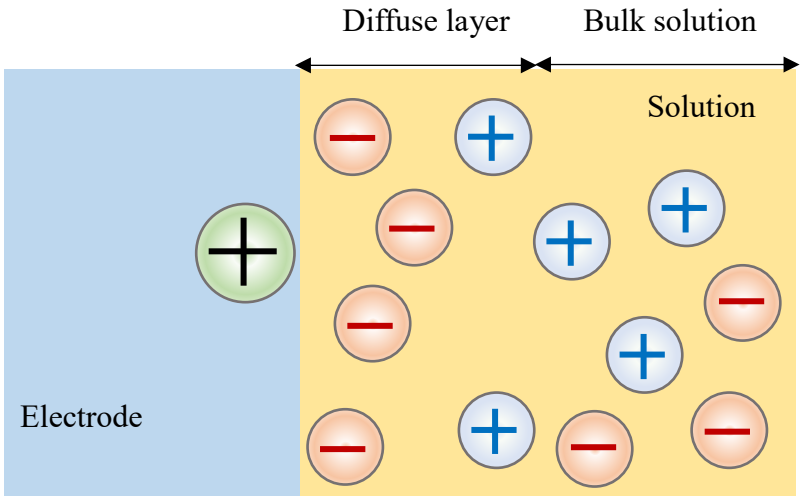

Fig.1.3 Schematic diagram of GC model of the electric double layer

On the assumption that the solution includes monovalent cation and anion with concentrations of c_+ and c_-, respectively. In the region of larger potential, particularly near the electrode|solution interface, the charge density of cations decreases while that of anions increases. The charge density of all ions is governed by the following equation:

$$\rho(x) = (c_+ - c_-)e \tag{1.2.3}$$

Where e is the elementary charge. The concentration of ions at any distance with the electrostatic potential $\varphi(x)$ follows Boltzmann statistical mechanics and is expressed as:

$$c_+(x) = c_0 \mathrm{e}^{-\frac{F\varphi(x)}{RT}} \tag{1.2.4}$$

$$c_-(x) = c_0 \mathrm{e}^{\frac{F\varphi(x)}{RT}} \tag{1.2.5}$$

Here, c_0 is the standard ionic concentration, F is the Faraday constant, R is the gas constant and T is the temperature. If the value of $F\varphi$ is close to zero, the total charge density can be approximated as:

$$\rho(x) = c_0 e \mathrm{e}^{-\frac{F\varphi(x)}{RT}} - c_0 e \mathrm{e}^{\frac{F\varphi(x)}{RT}} \cong 2c_0 e \frac{F\varphi(x)}{RT} \tag{1.2.6}$$

Integrating this into Equation 1.2.2, we derive:

$$\frac{d^2\varphi(x)}{dx^2} = 2c_0 e \frac{F\varphi(x)}{\varepsilon\varepsilon_0 RT} \tag{1.2.7}$$

$$-2c_0 e \frac{F\varphi(x)}{\varepsilon\varepsilon_0 RT} \equiv L^{-2}\,\varphi(x) \tag{1.2.8}$$

Where L, the Debye length, is defined as:

$$L = \sqrt{\frac{\varepsilon\varepsilon_0 RT}{2c_0 e^2 F^2}} = \sqrt{\frac{\varepsilon\varepsilon_0 RTN_\mathrm{A}}{2c_0 F^2}} \tag{1.2.9}$$

Under the boundary conditions where $\varphi = \varphi_0$ as x tends to 0 and x approaches infinity∞, $\varphi = 0$, the solution to the Equation becomes:

$$\varphi(x) = \varphi_0 e^{-\frac{x}{L}} \tag{1.2.10}$$

Fig.1.4 illustrates the distribution of the electrostatic potential across this interface. The relationship between the potential and the charge density of the diffuse layer is given by the following equation:

$$\sigma = \varepsilon\varepsilon_0 \left(\frac{d\varphi_{\Delta,0}}{dx}\right)_{x=0} = (8RT\varepsilon\varepsilon_0 c_0)^{1/2} \sinh\left(\frac{eF\varphi_{\Delta,0}}{2RT}\right)$$

$$\varphi_{\Delta,0} = \varphi_0 - \varphi_S = E \tag{1.2.11}$$

With the approximation in Eq.(1.2.6), the expression for σ is given by:

$$\sigma = \varepsilon\varepsilon_0 \left(\frac{d\varphi_{\Delta,0}}{dx}\right)_{x=0} = \sqrt{\frac{2\varepsilon\varepsilon_0 c_0}{RTN_A}}\, F\varphi_{\Delta,0} \tag{1.2.12}$$

Here, σ denotes the surface charge density of the diffuse layer. The potential $\varphi_{\Delta,0}$ defined as the difference between the electrode potential φ_0 and the potential in the bulk solution φ_S, is equivalent to the polarized potential *E*, as shown in Equation (1.2.11). The polarized potential usually is controlled by the applied electric potential. This relationship crucially links the electrostatic properties of the electrode|solution interface with the applied electrochemical potential. Ultimately, the variation of the total charge stored on the interface with the applied potential can be described by differential capacitance.

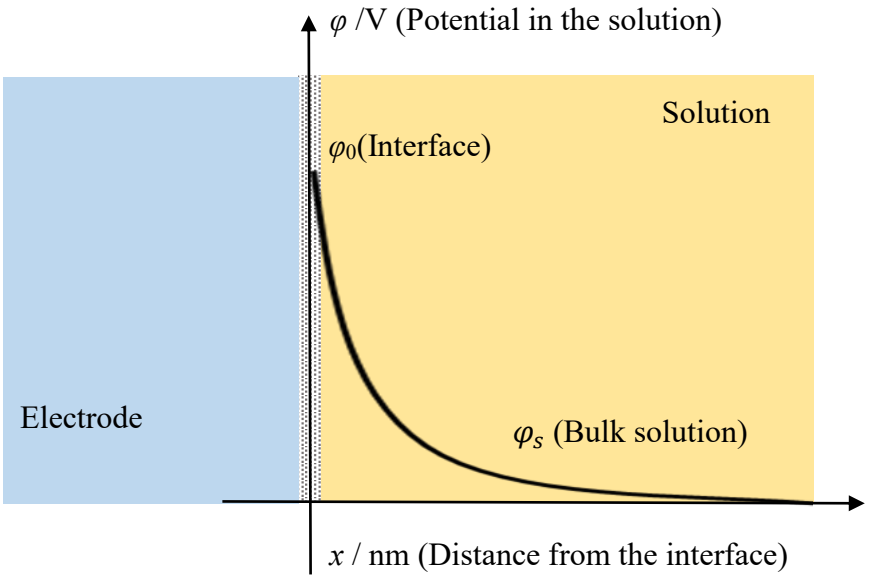

Fig.1.4 Potential contribution of GC model of the electric double layer

Differentiating the expression for the surface charge density yields the differential capacitance, denoted as C_{GC}. This can be expressed as the derivative of the surface charge density with respect to the potential:

$$C_{\mathrm{GC}} = \frac{\partial \sigma}{\partial \varphi_{\Delta,0}} = \sqrt{\frac{2\varepsilon\varepsilon_0 c_0 e^2 F^2}{RT}} \cosh\left(\frac{eF\varphi_{\Delta,0}}{2RT}\right) = \frac{\varepsilon\varepsilon_0}{L} \cosh\left(\frac{eF\varphi_{\Delta,0}}{2RT}\right) \tag{1.2.13}$$

Numerical values of C_{GC} at conventional values of the parameters are calculated from:

$$C_{\mathrm{GC}} = \frac{\varepsilon\varepsilon_0}{L} \cosh\left(\frac{eFE}{2RT}\right) = 228\sqrt{c_0}\cosh(19.5E) \tag{1.2.14}$$

This equation indicates that the capacitance of the GC model exhibits a "V-shaped" curve as a function of the polarized potential E as well as the ionic concentration c. This characteristic behavior is illustrated in Fig.1.5.

The differential capacitance by the GC model tends to increase

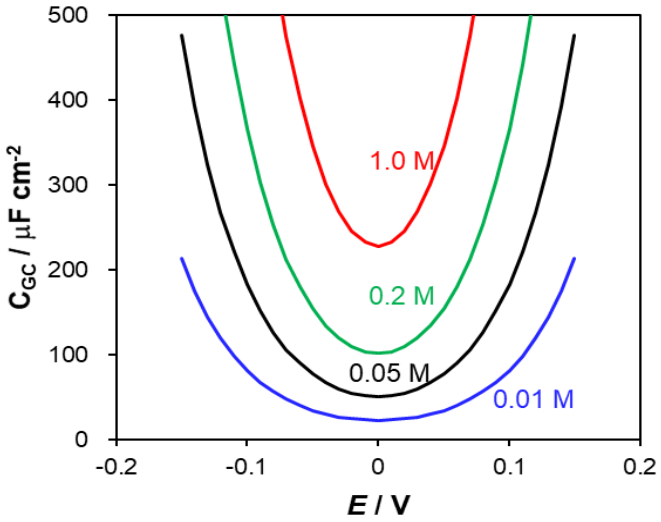

Fig.1.5 Differential capacitance C_{GC} against the polarized potential and ionic concentration.

infinitely with an increase in potential. This model assumes that the position of ions in solution is not spatially restricted and is treated as point charges that can approach the electrode surface arbitrarily closely. The assumption of a point charge causes ions to get unreliably high concentrations near the electrode. In reality system, ions have a finite size and cannot be so close to the surface as to be smaller than its radius. A significant limitation of the GC model is its failure to account for the physical dimensions of the ions, which plays a crucial role in determining the actual behavior of the electrode|solution interface. Thus, the capacitance by the GC model does not include the extra amount of charge by the nearest electric force at the electrode.

1.2.3. GC-Stern (GC-S) model

The experimental data on NaF NaCl, NaF, Na_2SO_4, and NaOH electrolyte solutions were measured and interpreted by David C. Granhame in detail, as shown in Fig.1.6. The capacitance observed at lower concertation

of electrolyte was close to the GC model assumed. However, no "trough" was observed at high one, suggesting the GC model seemed to have drawbacks [64].

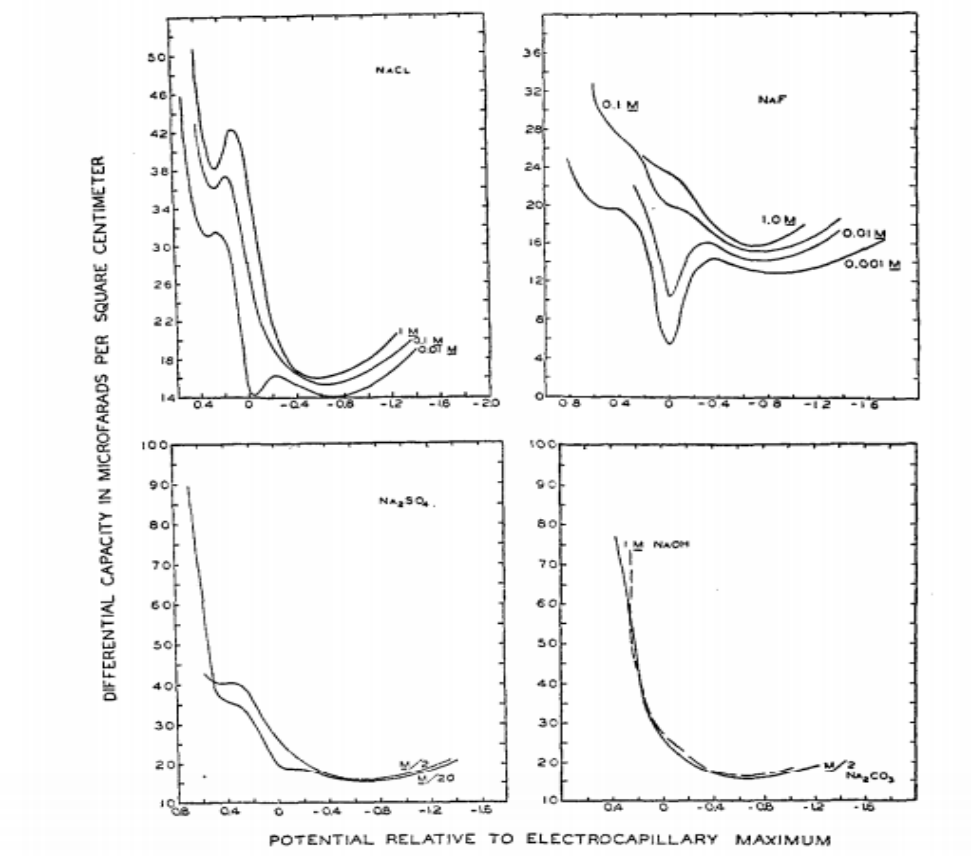

Fig.1.6 Differential capacity of the electric double layer between mercury and aqueous solutions of the salts named for NaCl, NaF, Na_2SO_4, and NaOH solution, $T = 25°C$ [64].

One critical aspect overlooked by the GC model is the solvation of ions near the electrode surface. It is essential to consider the thickness x of the solvent shell layer, which is added to the effective radius of the ion. In a low electrolyte concentration, the solvation of the ions has a negligible effect on the capacitance due to the significantly larger thickness of the diffuse layer compared to x. Conversely, the charges at very high concentrations of electrolyte accumulate to the interface at x_0, resembling the Helmholtz model

more closely. The plane of x_0 is known as the Helmholtz plane, x_H, becomes a critical factor.

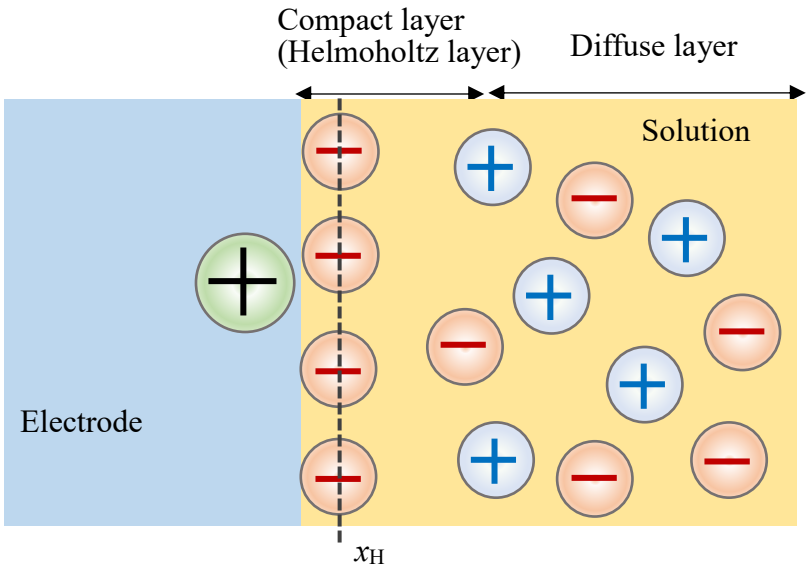

Fig.1.7 Schematic diagram of GC-Stern Model of the electric double layer.

In 1924, Stern [65] proposed a model of the interface that incorporated principles from both the Helmholtz and GC models. It describes a compact layer extending from the electrode surface to the Helmholtz plane and an additional diffusion layer, as shown in Fig.1.7.

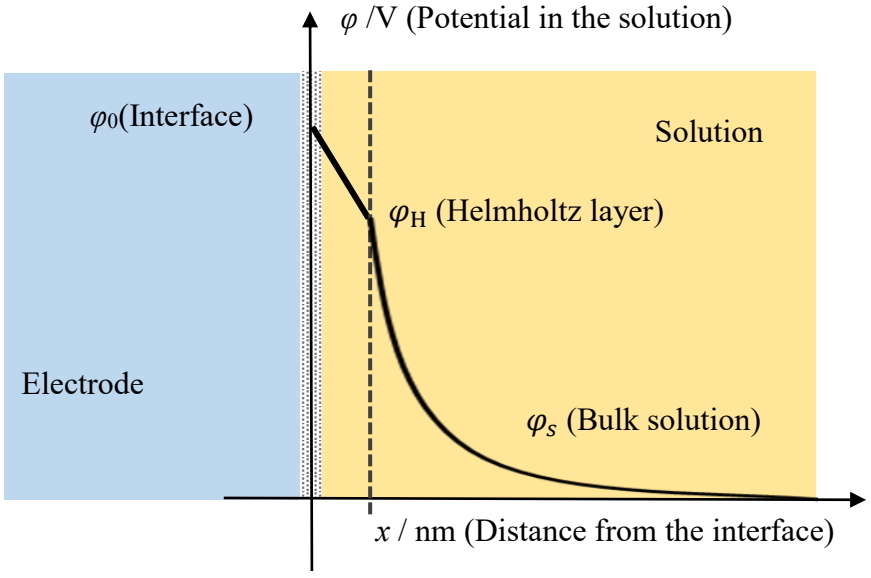

Fig.1.8 Potential contribution of GC-Stern model of the electric double layer

In the compact layer of the GC-Stern model, potentials are linearly distributed to the freedom of charge movement. Conversely, the potential contribution in the diffuse layer aligns with the predictions of the GC Model. Fig.1.8 illustrates the potential distribution across these two interfacial layers in the GC-Stern model.

Mathematical derivations suggested that the capacitances in the compact layer (C_{H}) and in the diffuse layer (C_{D}) are effectively connected in series. Hence, the reciprocal of the total capacitance in the GC-Stern model ($C_{\mathrm{GC-Stern}}$) is the sum of the reciprocals of C_{H} and C_{D}, expressed as:

$$\frac{1}{C_{\mathrm{GC-stern}}} = \frac{1}{C_{\mathrm{H}}} + \frac{1}{C_{\mathrm{D}}} = \frac{x_H}{\varepsilon\varepsilon_0} + \frac{L}{\varepsilon\varepsilon_0 \cosh\left(\frac{eF\varphi_{\Delta,0}}{2RT}\right)} \tag{1.2.15}$$

In this model, C_{H} is considered independent of the potential, whereas C_{D} exhibits a V-shaped with potential, as discussed previously. The total capacitance demonstrated complex behavior, varies with electrolyte concentration or the polarized potential, as illustrated below (Fig.1.9).

It is expected to exhibit a V-shaped characteristic near zero potential, primarily influenced by C_{D} at low electrolyte concentration. At higher electrolyte concentrations, it is attributed to the C_{D} becoming so pronounced that it virtually makes no contribution to the total capacitance. The GC-Stern model effectively reproduced key features of real systems and provided an explanation for the observed V-shaped differential capacitance versus potential behavior in the mercury electrode, as shown in Fig.1.6. However, there may be deviations due to C_{H} owing to the failure of the GC theory.

Importantly, this theory of the GC-Stern model does not account for the effects of ion-ion interactions within the EDL and the non-specific strong interactions between ions and electrode surface. Additionally, the chemical adsorption at the electrode surface may also influence the measurement of capacitance [66].

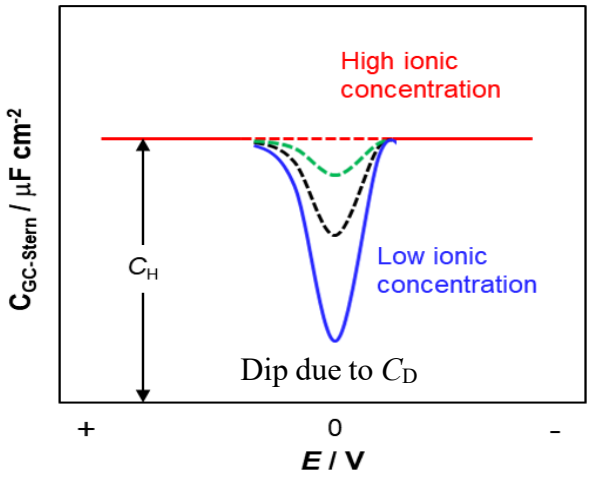

Fig.1.9 The variation of capacitance $C_{GC\text{-}Stern}$ with the polarized potential.

1.2.4. Grahame's model

In 1947, Grahame simultaneously considered ions that exhibited specifically adsorpted ions on the Helmholtz layer, and those solvated shell-lost ions (typically anions). The latter ions have smaller radii to approach closer to the electrode surface [64]. Consequently, the Helmholtz layer presented distinct demarcations. These two separate boundaries are referred to as the Inner Helmholtz Plane (IHP) and the Outer Helmholtz Plane (OHP). Overall, the EDL structure is primarily divided into three regions, encompassing the IHP, OHP, and the Diffuse layer, as depicted in Fig.1.10

below. Within the IHP, there were small-sized ions without a hydration shell and adsorbed anions. Despite the potential repulsion between the adsorbed anions and the opposite charge or anions in the solution, the adsorbed anions remained stably adhered due to the predominance of adsorptive forces over electrostatic repulsions. Furthermore, the OHP is typically characterized by solvated ions. Electrode redox reactions occur in this layer. The Diffuse layer mentioned here is consistent with the descriptions provided in the preceding sections. This section does not elaborate further on it. On the other hand, the

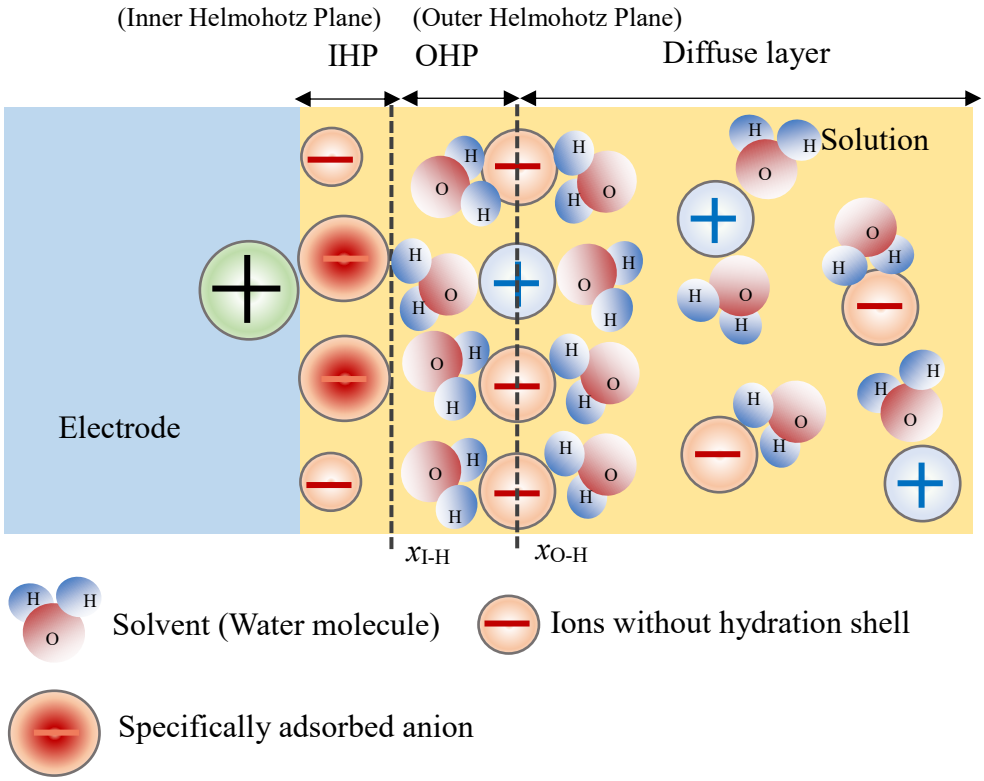

Fig.1.10 Schematic diagram of Grahame-Model of the electric double layer.

test species used in this thesis have no specially adsorption behavior. There will be not considered for adsorbed ion in the latter Chapter.

1.2.5. BDM model

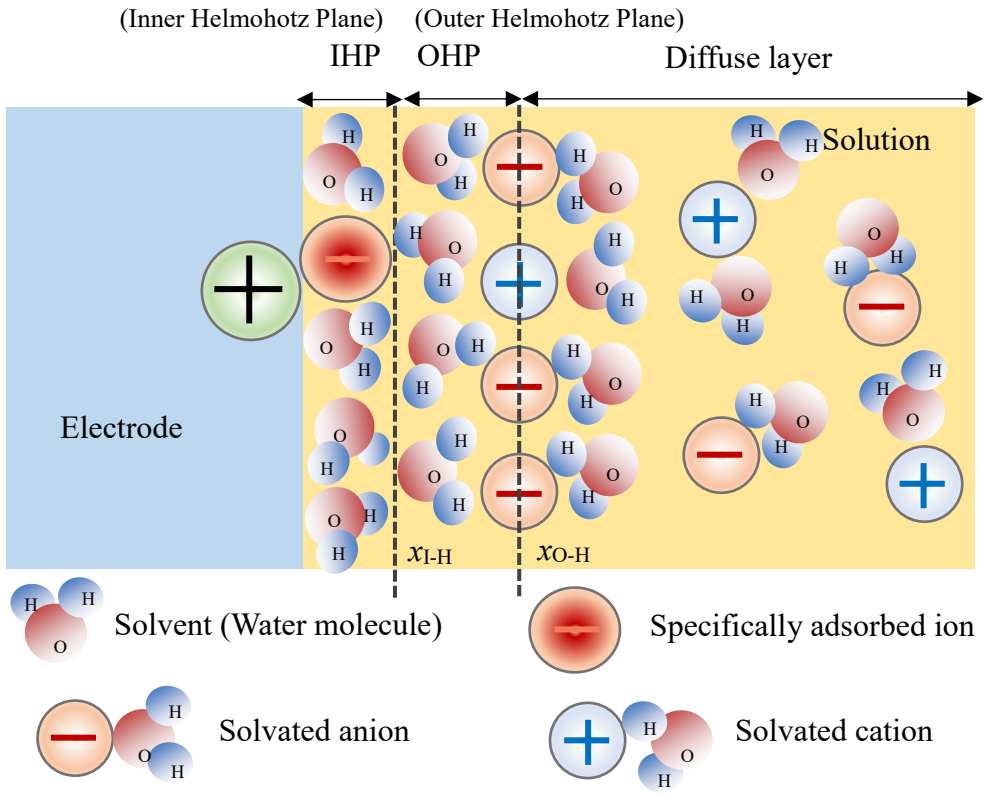

Fig.1.11 Schematic diagram of BDM model of the electric double layer.

Currently, our depiction of the model of the electric double layer is based on the BDM (Bockris, Devanathan, and Muller) model, as shown in Fig.1.11. BDM hypothesized that a layer of orientated adsorbed water molecules existed at the electrode surface due to high hydration-free energy or the strong association of most anions with water molecules [67]. According to their model, the inner layer is constituted by solvent dipoles and specifically adsorbed ions. The outer layer, meanwhile, aligns with the GC model. It is important to note that the observed capacitance is not solely dependent on the polarized potential but also influenced by the distribution of ions near the electrode|solution interface and the types of solvents in the

solution. This aspect of the model allows for an explanation of the variations in capacitance observed at different electrolyte concentrations and the polarized potential.

1.2.6. Further development

Prof. Cheng from Xiamen University in China and colleagues have simulated the Pt(111)|aqueous solution interfacial structures at various potentials [68]. They proposed a scientific viewpoint that the change in the coverage degree of chemisorbed water at the point of zero charge (PZC), contributes negatively to the interface capacitance. A simple model is used to describe this concept, as illustrated in Fig.1.12.

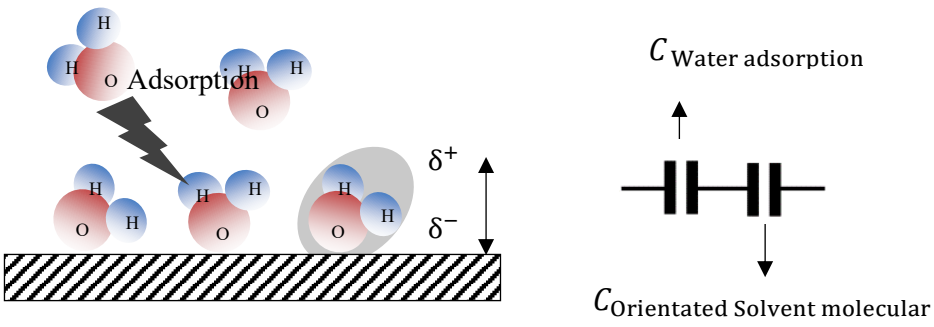

Fig.1.12 Schematic model used to describe the water adsorption-induced change in Helmholtz electric capacitance from Ref.[68].

The total differential capacitance in this model, C_H, of the Helmholtz layer is composed of the capacitance due to water chemisorption, C_{ads}, and the capacitance due to orientated water molecular as solvent dipoles, C_{sol}, connected in series [68]:

$$\frac{1}{C_{\text{H}}} = \frac{1}{C_{\text{Orientated Solvent molecular}}} + \frac{1}{C_{\text{Water adsorption}}} \tag{1.2.16}$$

Since the dipole orientation of chemisorbed water is opposite to the direction of the applied electric field, the value of C_{ads} is negative, reaching its maximum at the PZC. This accounts for the observed "bell-shaped" differential capacitance curve in electrochemical experiments, offering a coherent explanation [69,70].

Recently, a groundbreaking research by the team of Professor Marc T.M. Kopper, a member of the Royal Society of Chemistry working at Leiden University, discovered that the values of the measured capacitance in an

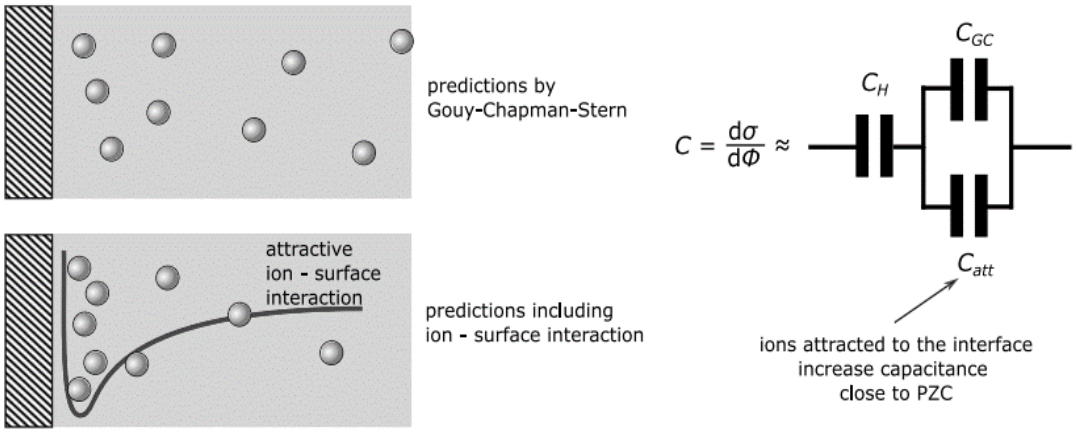

Fig.1.13 Schematic model of the mean-field model used to describe attractive ion-surface interaction from Ref.[71].

ideally polarized Pt(111)-aqueous electrolyte system were higher than those predicted by the GC-S model, especially at low electrolyte concentrations [71]. This deviation appeared to be independent of the nature of the ions. Following a fitting to the Parsons-Zobel curve, they proposed an updated version of the advanced EDL model. Their model primarily considered the presence of organized, adsorbed water molecules on the electrode surface,

aligning with the BDM model with the weak attractive interaction between ions and the electrode surface. Further, they considered the variation in the hydration energy of water molecules with ions, leading to a non-uniform ion concentration near the electrode surface. The revised model perfectly matched the calculated one by the theory with experimental values across different electrolytic solutions and concentrations and more. Fig.1.13 demonstrates this model and its corresponding electric circuit diagram. The formula for the EDLC adheres to the following [71]:

$$\frac{1}{C} = \frac{1}{C_{\mathrm{H}}} + \frac{1}{C_{\mathrm{GC}} + C_{\mathrm{att}}} \tag{1.2.17}$$

$$\frac{1}{C_{\mathrm{H}}} = \frac{1}{C_{\mathrm{Orientated\ Solvent}}} + \frac{1}{C_{\mathrm{Water\ adsorption}}}$$

These works provided a new perspective for understanding and simulating the EDL structure of electrochemical interfaces.

1.3.EDL capacitance (EDLC)

The determination of EDLC is of significant importance to the understanding of electrochemical interfacial structures from a microscopic viewpoint, greatly enhancing our knowledge of microstructures. The models discussed previously provided insights into the inherent potential dependence of EDLCs. They also served as basic theoretical support for the electrochemical behavior of charge transfer reactions and specific adsorption occurring at the electrode|solution interface. However, they still cannot maintain validity with experimental results of properties of the interface, such as frequency dependence [72].

1.3.1. Constant Phase Element or frequency dispersion of EDLCs

In the early 1970s, electrochemists have discovered the frequency dependence of EDLCs at solid-liquid interfaces [73, 74, 75, 76, 77]. It describes how its value differs from an ideal capacitor, changing with the frequency of the applied electric field. Those works, integrating equivalent circuits and specific electrochemical impedance measurement methods, allowed for the electrode impedance (Z) of an ideal polarizable electrode (*"ideal" means* C_d *is independent of AC voltage and AC frequency*) to be represented by a series connection of solution resistance (R_s) and ideal double-layer capacitance (C_d) [78]:

$$Z = R_s + \frac{1}{iwC_d} \qquad (1.3.1)$$

where i is the imaginary unit, and ω is the angular frequency, representing

the ideal double-layer capacitance. Variations of the imaginary impedance, $-Z_2$ (= $1/iwC_d$) with the real one, Z_1 (= R_s) yield a Nyquist plot. The Nyquist plot for an ideal capacitor element shows a line vertical to the x-axis at R_s point as shown in Fig.1.14(a). However, a real EDLC with frequency

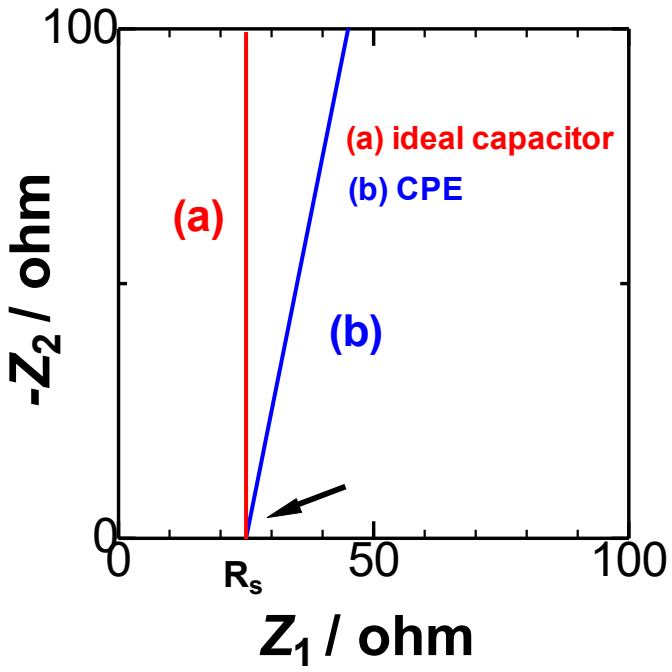

Fig.1.14 Nyquist Plot of Eq. (1.3.1) for an ideal capacitor and Eq. (1.3.2) for the CPE. The following parameters are R_s = 25 Ω, α = 1 or 0.9.

dependence showed a sloped line rather than a vertical one in Fig.1.14(b). This "constant phase angle" behavior, which was first named by Fricke [79], led to the real EDLC component being called a "Constant Phase Element" (CPE). The concept of CPE has been widely applied in various field date, playing a significant role in the study and interpretation of complex electrochemical behavior [72, 80 , 81 , 82]. The impedance Z_{CPE} can be expressed with the help of a parameter α, by [83,84]:

$$Z_{\mathrm{CPE}} = R_s + \frac{1}{(iw)^{-\alpha}Q} \qquad (1.3.2)$$

Here Q is a constant with a conventional unit of F $s^{\alpha-1}$ or F $cm^{\alpha-2}$ $s^{\alpha-1}$. The parameter of Q does not scale with the electrode surface area. Consequently, the use of CPE impedance which implies proportionality to surface area, is inappropriate for this context [85]. If the numerical values of α are close to unity, those of Q are similar to the values of the EDLC. The real and imaginary components in Eq. (1.3.2) are $R_s + Q^{-1}\omega^{-\alpha}\cos(\alpha\pi/2)$ and $-Q^{-1}\omega^{-\alpha}\sin(\alpha\pi/2)$, of which the ratio yields:

$$-Z_2 / (Z_1 - R_s) = \tan(\alpha\pi/2) \quad (1.3.3)$$

This accurately captures the variation depicted in Fig.1.14(b). The condition of α=1, corresponds to an ideal capacitor. Conversely, it corresponds only to the resistance circuit of $R_s + Q^{-1}$at α=0. This encapsulates the fundamental concept of the CPE. Currently, CPE behavior is also referred to as the frequency dispersion [86,87,88,89,90,91,92] of EDLCs or the power law of frequency [93,94]. The variation is due to differing perspectives on the issue. In detail, the CPE behavior has been attributed to surface heterogeneity, roughness, or other electrochemical phenomena. Compared to this, the concept of frequency dispersion is more encompassing, acting as a general term for experimental outcomes. The power law as described is merely an articulation of a mathematical relationship, offering a refined description of the variations in EDLCs. The Aoki's group has provided scientific insights into the interrelation among the frequency dispersion. They have pointed out a lack of description regarding the physical significance of Q in Eq. 1.3.2 within the CPE concept. The concept is based on the time derivative of charge, q (= It) = CV, which also serves as a theoretical basis for the general

phenomenon of frequency dispersion [95,96]. Extensively experimental results elucidated the origin of CPE or frequency dispersion of EDLCs. These experimental findings have been supported by different electrochemical techniques, such as ac-impedance [72,87,88,89,90,93,97,98] and chronoamperometry [99]and chronopotentiometry [100]. The next section will describe the results obtained by means of AC-impedance and chronoamperometry.

1.3.2. EDLCs by means of AC impedance

AC impedance, also known as Electrochemical Impedance Spectroscopy, is a technique for analyzing resistance (which impedes the flow of electric current) and capacitance (the ability to store electric charge) within a system by applying AC signals of varying frequencies to obtain dynamic responses. It typically spans frequencies from a few Hertz to several thousand Hertz or higher. The key to AC impedance is to find the correspondence between equivalent circuits and the interfacial and chemical properties. However, to date, the equivalent circuits have only been determined empirically or by trial and error to lead significant uncertainty when interpreting the experimental data obtained. The Aoki's group proposed a mathematical technique for demonstrating the frequency dispersion to address this issue [72,90]. The frequency dependence, which is defined by dC/dw or dC/dt, is obtainable from the time derivative of the charge q accumulated in the capacitor, where $q = CV$, and V is the applied AC voltage. The time derivative of q gives the AC current, i.e.

$$I = \frac{\mathrm{d}\,(CV)}{\mathrm{d}t} = C\,\frac{\mathrm{d}V}{\mathrm{d}t} + V\frac{\mathrm{d}C}{\mathrm{d}t} \tag{1.3.4}$$

When the AC voltage is represented as $V_0 e^{i\omega t}$ with an amplitude V_0, the first term on the right side of the Eq.1.3.4 is given by $i\omega CV$. For the final term, introducing a new time t' is necessary, which can help transform time into frequency. Obviously, it differs from the t in the Eq.1.3.4. Conceptually, the reciprocal of frequency or angular velocity should correspond to time such as $\omega = 1/t' = 2\pi f$ or ambiguous by a constant. The term of $\mathrm{d}C/\mathrm{d}t$ can be represented through variable transformation as:

$$\frac{\mathrm{d}C}{\mathrm{d}t} = \frac{\mathrm{d}C}{\mathrm{d}\omega}\,\frac{\mathrm{d}\omega}{\mathrm{d}f}\,\frac{\mathrm{d}f}{\mathrm{d}t} = -2\pi\omega^2\frac{\mathrm{d}C}{\mathrm{d}\omega} \tag{1.3.5}$$

Then, the Eq.1.3.4 can be written as:

$$I = i\omega CV - 2\pi\omega^2 V\frac{\mathrm{d}C}{\mathrm{d}\omega} = V\left[i\omega C - 2\pi\omega^2\frac{\mathrm{d}C}{\mathrm{d}\omega}\right] \tag{1.3.6}$$

The Eq.1.3.6 here shows that the equivalent circuit is a parallel combination of the capacitor, $C_\mathrm{p} = i\omega C$ and the resistance, $R_\mathrm{p}^{-1} = -[2\pi\omega^2(\mathrm{d}C/\mathrm{d}\omega)]^{-1}$, as illustrated in Fig.1.15, where the subscript p means the parallel combination.

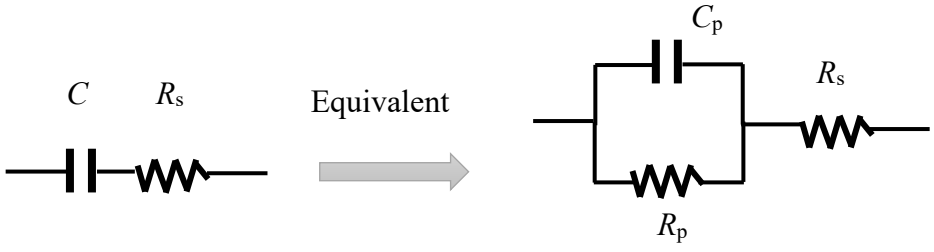

Fig.1.15 Equivalent circuit for the frequency-dependent capacitance. The EDL impedance as demonstrated by the CPE concept is shown on the left hand side.

The linearity in Fig.1.14(b) implies that the $-\omega^2(\mathrm{d}C/\mathrm{d}\omega)$ (come from $-Z_2$) should be proportional to ωC (come from R_s-subtracted, Z_1). The negative slope was defined as λ. That means the $[\omega^2(\mathrm{d}C_\mathrm{p}/\mathrm{d}\omega)]/\omega C_\mathrm{p} = \lambda$ as a

real constant in the real system. The differential equation by a mathematical solution for EDLCs, C_p with respect to ω can be written as:

$$C_p = k\omega^{-\lambda} = C_{p,1Hz}\, f^{-\lambda} \tag{1.3.7}$$

This expression is called the power-low of capacitance. The conclusion can be demonstrated in accurate experimental results. The plot of logC_p against log$f$ obtained by Hou, Wang et al was represented in the figure below [87,88,89,93].

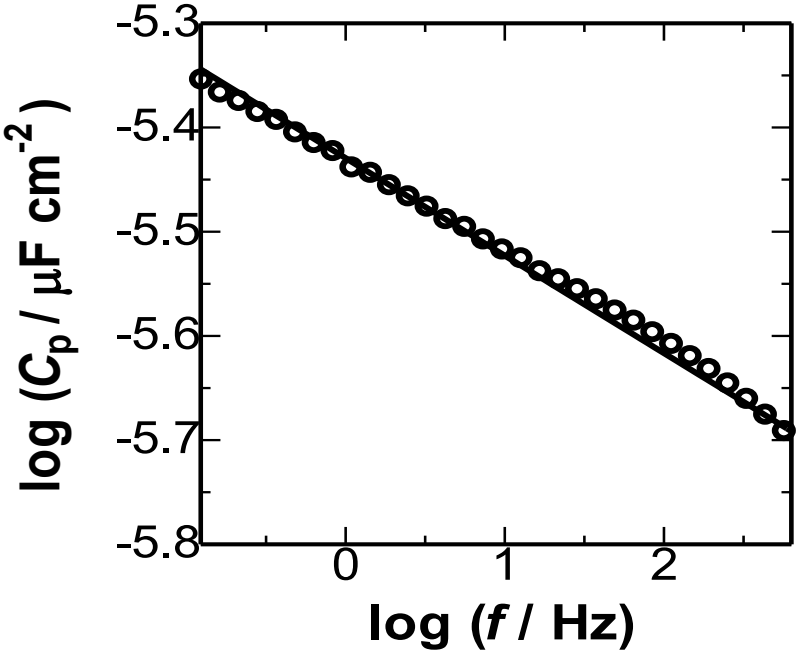

Fig.1.16 Plots of log (C_p) against the logarithm of the f in the 0.5 M KCl solution at the Pt electrode.

When the electrode materials are platinum and HOPG, the values of λ from the slopes are all close to 0.1, whereas are from 0.001 to 0.1 at PANI-coated electrode experimentally.

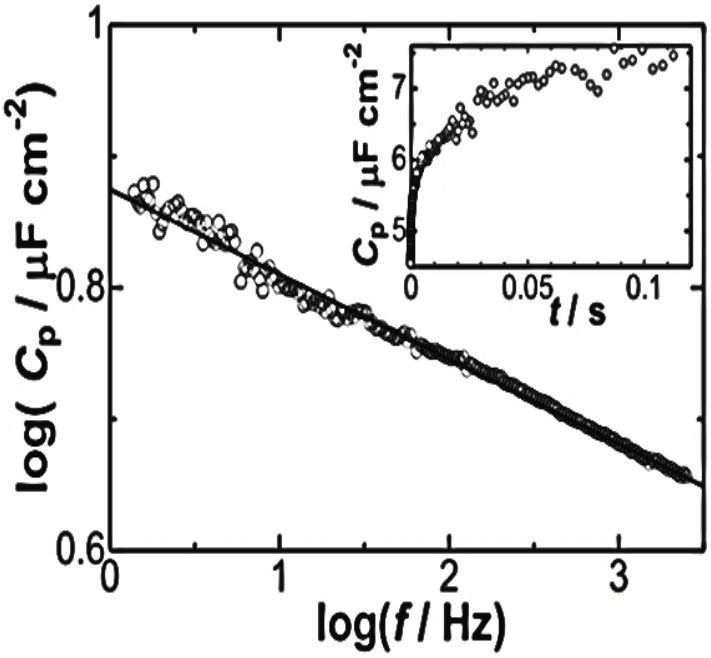

Fig.1.17 Plots of log (C_p) against the logarithm of the f in the 0.5 M KCl solution at the HOPG electrode. The inset is the variation of C_p with the t which is equal to $1/2\pi f$.

1.3.3. EDLCs by means of chronoamperometry

According to experiment result by the AC impedance as described in Section.1.3.2, the capacitance has been empirically expressed by $C_{\mathrm{p}} = C_{\mathrm{p,1Hz}}\, f^{-\lambda}$, where f is the AC-frequency, λ is a positive constant variously, and $C_{\mathrm{p,1Hz}}$ is the EDLC at f = 1Hz. An important concept is to replace frequency with the chronoamperometric time t, through $2\pi f = 1/t$, the time variation of the capacitance yields:

$$C_{\mathrm{p}} = C_{\mathrm{p,1Hz}}\, f^{-\lambda} = C_{\mathrm{p,1s}}\, t^{-\lambda} \qquad (1.3.8)$$

Where $C_{\mathrm{p,1s}}$ is the capacitive value at t = 1s, given by $C_{1\mathrm{s}} = (2\pi)^{\lambda}\, C_{\mathrm{p,1Hz}}$. The expression indicated that the EDLCs can be simply evaluated over a time scale of 1s. The assessment of the power law, λ, was experimentally

determined through the observation of the plots of logarithmic chronoamperometric currents against the time. He, *et al*. have found that the current initially decreases linearly for times shorter than 0.1 milliseconds, and subsequently follows a power-law plot in the millisecond domain. The results are shown in Fig.1.18. The theoretical expression can be derived through the differential equation with respect to *t*:

$$I = \frac{\mathrm{d}\,(CV)}{\mathrm{d}t} = \frac{\mathrm{d}\left(C_{\mathrm{p,1s}} t^{\lambda} V\right)}{\mathrm{d}t} = \lambda V C_{\mathrm{p,1s}} t^{\lambda-1} \tag{1.3.9}$$

$$\log I = \log\left(\lambda V C_{\mathrm{p,1s}} t^{\lambda-1}\right) = (\lambda - 1)\log t + \log\left(\lambda V C_{p,1s}\right) \tag{1.3.10}$$

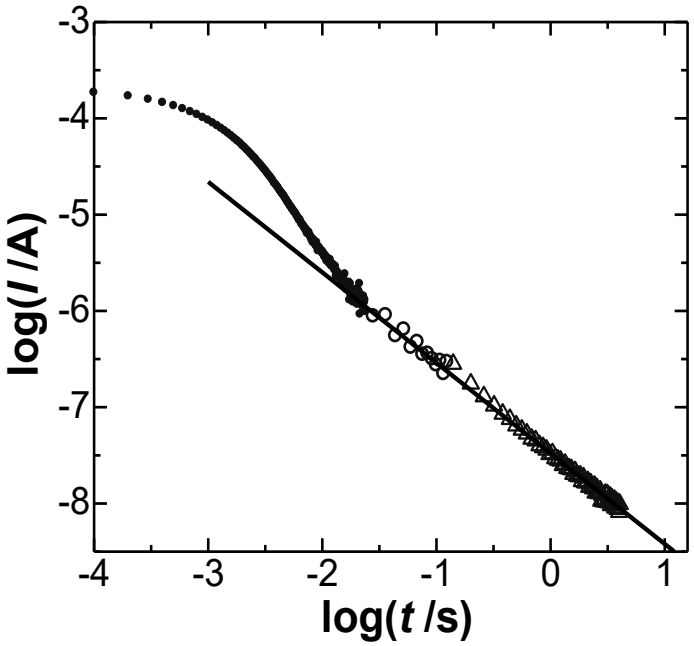

Fig.1.18 Plots of the logarithm of the chronoamperometric current against the logarithm of time observed at the 0.1 V step in the solution of the concentration of 0.01 M KCl.

The EDLCs followed a power number near 0.1 by the theory and chronoamperometric curves aligning with AC impedance. The assigned value of 0.1 may reflect the ratio of the equilibrium energy of the orientation to the activation energy of the kinetics. The following section will focus on

interpreting the frequency dispersion of EDLCs from a molecular level in the viewpoint of thermodynamics.

1.3.4. Origin of frequency dispersion of EDLCs

It is important to know what the variable controlling the EDLCs is before exploring the cause of frequency dispersion. In 2013, Hou, *et al*. had measured the impedance in 13 kinds of solvents, providing effective answers [88]. Fig.1.19 shows variation of $(C_p)_{f=1Hz}$ with the inverse of the length of the oriented molecules, d_{or} for these 13 solvents.

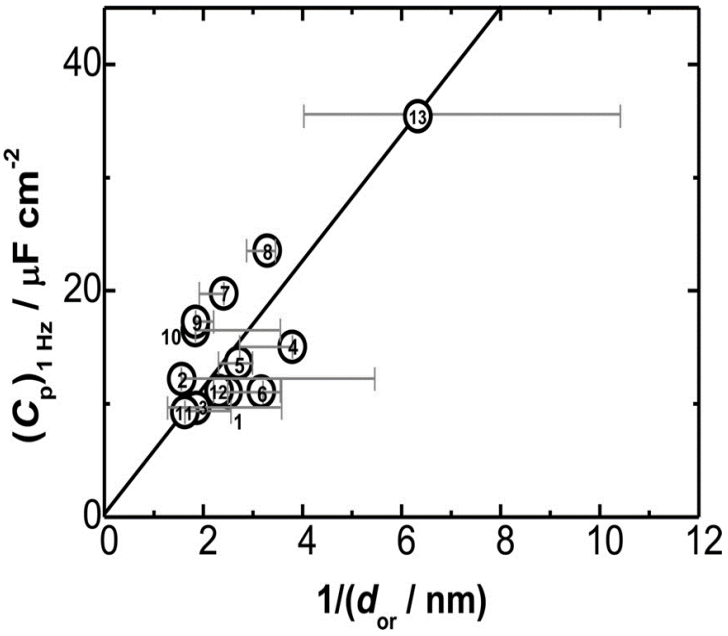

Fig.1.19 Variation of the EDLCs with the inverse of molecular diameter obtained from the solvent molecule.

The EDLCs are inversely proportional to the length of a solvent molecule along the dipole moment. From this, it can be understood that the EDLCs are primarily influenced by the localization of charge of solvent dipoles in response to the external electric field. Further, the Aoki's group has considered the origin of frequency dispersion or time dependence of

EDLCs based on several experimental results as follows:

An externally applied electric field seems to orient solvent dipoles in a uniform direction to decrease electrostatic energy, as illustrated in Fig.1.20.A. If the solvent dipoles were to be arranged only by electric field, it would take a period of the nano-second scale owing to the orientation of the dipoles. The actual relaxation time is as long as second-order, as experimental results have shown in Fig.1.16, Fig.1.17 and Fig.1.18. It should be composed of other interactions in pair energy as play. The interaction energy of hydrogen bonds (Solvent-solvent interaction) on electrodes is ten times larger than field-oriented (Solvent-electrode interaction) energy, and thus neighboring water dipoles are alternately oriented, as shown in Fig.1.20.B.

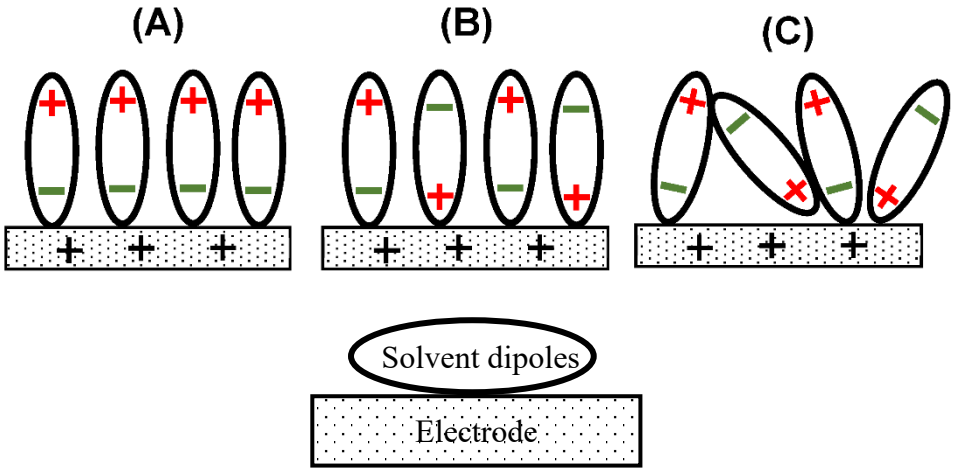

Fig.1.20 Illustrations of the orientation of solvent dipoles responding to positive voltage at an electrode when A) the interaction only by external field, B) the interaction among the dipoles is stronger, and C) it is balanced with the latter energy and thermally fluctuated.

As a result, the reason for the frequency dispersion is that the external field cannot orient uniform solvent dipoles on the electrode owing to the solvent-solvent dipole interaction which is ten times larger than the field-oriented dipole energy. It caused the relaxation time is not uniform. Then,

the thermal fluctuation agitates the turnover of the solvent dipoles to yield an average value of the two-directional orientation. This value provides the EDLC following the model which is as shown in Fig.1.20.C.

1.4.Faradaic reaction

A faradaic reaction is caused by charge transfer steps triggered with application of applied voltage. Then, under the influence of an applied voltage, the faradaic current dynamically flows until the equilibrium is established. The exploration of this step is called electrochemical kinetics. A comprehensive understanding of the electrochemical behavior occurring at the electrode|solution interface during faradaic reaction necessitates the viewpoint of both equilibrium and kinetics.

1.4.1 The view of equilibrium

Zero current is observed either in an equilibrium state of a single charge transfer reaction or in a balanced current state with a mixed potential of two or more reactions. The former potential is determined by the equality of the electrochemical potential of a reduced species with that of an oxidized one. For an n-electron transfer reaction, $R \leftrightarrow O + ne^-$, the equilibrium incorporated with the electrode potential, E_{eq}, is given by the Nernst equation:

$$E_{\mathrm{eq}} = E^0 + \frac{RT}{nF} \ln \frac{\gamma_{\mathrm{ox}}[\mathrm{Ox}]}{\gamma_{\mathrm{red}}[\mathrm{Red}]} \qquad (1.4.1)$$

where E^0 is the standard electrode potential of the redox couple, [Ox] and [Red] are the concentrations of oxidized and reduced species at the electrode surface. In particular, they are the same as the bulk concentration under the

equilibrium conditions. γ is the activity coefficient. In case of difficulty in evaluationg γ, which is usually assumed to be unity in dilute solutions, it is convenient to express the Nernst equation with a uniform one. Replacing E^0-$(RT/nF)\ln(\gamma_{ox}/\gamma_{red})$ by the formal potential, $E^{0'}$, yield:

$$E_{eq} = E^{0'} + \frac{RT}{nF}\ln\frac{[Ox]}{[Red]} \qquad (1.4.1A)$$

When the potential scan past the equilibrium potential by the voltage-step method, the oxidation or reduction of electroactive species is initiated and detected as peaks. The values of the peak potential can provide us with the means to determine the position of the reaction equilibrium. These concepts will be used in the latter chapters.

1.4.2 The view of kinetics

An electrochemically kinetics perspective informs us of the rate at which electrode reaction occurs to reach the equilibrium. Then, the Nernstian behavior does not hold and the electrode is kinetically limited [101]. We have used conventionally the Butler-Volmer (BV) equation to describe the potential dependence of electron transfer reactions at the electrode|solution interface. For a first-order heterogeneous oxidation and reduction reaction [66,102,103]:

$$Ox + ne^- \underset{k_{ox}}{\overset{k_{red}}{\rightleftharpoons}} Red^{n-} \qquad (1.4.2)$$

The rate constants for oxidation and reduction reactions are represented by k_{ox} and k_{red}, respectively. Their equations are given by:

$$k_{ox} = k_0 \exp\left[\frac{(1-\alpha)nF}{RT}(E - E^0)\right] \qquad (1.4.3)$$

$$k_{\mathrm{red}} = k_0 \exp\left[\frac{-\alpha nF}{RT}(E - E^0)\right] \quad (1.4.4)$$

Here, k_0 is the standard rate constant. It is due to the equilibrium conditions where $k_{\mathrm{ox}}c^*_{\mathrm{red}} = k_{\mathrm{red}}c^*_{\mathrm{ox}}$, leading to $k_{\mathrm{ox}} = k_{\mathrm{red}} = k_0$. The physical significance is that it reflects how quickly the reaction reaches a new equilibrium through mass transport when the applied external voltage is changed. α is the transfer coefficient, generally close to 0.5. The value of α changes with the voltage strictly speaking.

The dynamic current equals the difference in the reversible reaction, which can be expressed as [102,104]:

$$I = nFA[k_{\mathrm{red}}c_{\mathrm{ox}}(0,t) - k_{\mathrm{ox}}c_{\mathrm{red}}(0,t)]$$

$$= nFAk_0\left[c_{\mathrm{ox}}(0,t)\mathrm{e}^{\frac{-\alpha nF(E-E^0)}{RT}} - c_{\mathrm{red}}(0,t)\mathrm{e}^{\frac{(1-\alpha)nF(E-E^0)}{RT}}\right] \quad (1.4.5)$$

This is the renowned BV equation.

1.5.EDLCs involving the faradaic reaction

1.5.1 The basic concept

When discussing EDLC involving faradaic reaction, both EDL capacitive current and faradaic current flow through the real system. The mechanism of the faradaic current is a charge transfer step for a Lithium battery, while the EDL causes a time variation of accumulated charge. Faradaic current arises from a chemical process, typically generating direct current (DC), whereas the EDL involves a physical process. The basic difference between these mechanisms indicates that two currents are essentially independent of each other. As early as 1933, Frumkin predicted

possible “dependence” if electrolyte concentration was low. He thought that the observed faradaic currents may depend on concentrations of salt or structure of EDL which associated with EDL capacitive current. However, Frumkin’s concept has not been supported experimentally. This is due to the difficulty in measurements at experimental conditions.

In addition, when exploring the relation between faradaic current and EDL capacitive currents from the perspective of practical applications, the focus often shifts towards supercapacitors, hybrid capacitors, or pseudo-capacitors. Supercapacitors, as the name implies, refer to capacitors capable of storing a large amount of electrical energy. The first device resembling a supercapacitor was designed by H.I. Becker in 1954 [105]. His design allowed the capacitor to achieve very high capacitance even at low voltages. In that era, the designed supercapacitors were all based on the properties of EDLC. It was not until 1970 that researchers commercialized standard supercapacitors by using a high surface area of activated carbon as electrode material. It has been realized that the performance of supercapacitors, such as energy density (the ability to store energy), power density (the ability to charge and discharge quickly), and cycle life, greatly depend on the electrode materials. This discovery inspired Brian Evans Conway to give attention to electrode materials such as transition metal oxides (e.g., RuO_2, IrO_2, MnO_2) from 1962 to 1990 [106, 107]. The introduction of these materials significantly increased the energy density of capacitors. This type of capacitive behavior is caused by charge transfer through a faradaic reaction on the electrode interface, rather than being purely a physical phenomenon

like EDLC. Conway defined this capacitive behavior involving faradaic reactions as pseudo-capacitance. Later, conductive polymers (e.g., polyaniline or polythiophene derivatives) were also found to exhibit pseudo-capacitance behavior through doping into electrodes accompanied by intercalation or electrical adsorption reactions and were used in the development of pseudo-capacitors. The collective term for EDLC and pseudo-capacitors as supercapacitors was first proposed by Conway in 1999 and has been in use ever since. In recent years, due to market demand, researchers have developed hybrid capacitors that combine the characteristics of supercapacitors and batteries. For example, hybrid ion supercapacitors contain an activated carbon electrode (as a EDL capacitive type electrode) and a lithium-based intercalation compound electrode (as a battery electrode); another type consists of an asymmetric supercapacitor made of an activated carbon electrode (as a EDL capacitive type electrode) and a composite electrode based on pseudo-capacitive active material (as a pseudo-capacitive type electrode). Both of the above capacitors have been widely used in electric vehicles, renewable energy storage systems, mobile devices, and other chemical fields.

The development history is based on practical commercial applications of EDLC involving faradaic reactions, as described in the previous paragraphs. The performance parameters of faradaic capacitors such as energy density, power density, and capacitance values can be determined by some testing techniques, for example, cyclic voltammetry and constant current charge-discharge. The measured values of faradaic capacitance have

been reported which are hundreds to thousands of times higher than those of EDLCs alone. From a fundamental conceptual standpoint, the understanding of the mechanism for energy storage encompasses not only the accumulation of non-faradaic charges at the electrode|solution interface but also the storage of charges through faradaic reactions. In fact, the interpretation of the accurate mechanism varies among researchers.

Since the faradaic reaction often involves multiple steps of charge transfer, mass transport, or adsorption behaviors, understanding the mechanism of faradaic reactions in EDL structure is highly challenging. The approach to resolving this is through the use of an equivalent circuit, which can simplify the analysis of the entire electrochemical process and also allow for precise, independent analysis of each step. This enables the exploration of whether a faradaic reaction in the EDL structure offers a high energy density similar to that of pseudo-capacitance.

1.5.2 The equivalent circuit when a faradaic reaction occurs

The equivalent circuit for EDLC, C_p, is mentioned in Section 1.3. Here our initial focus is on establishing an equivalent circuit when a faradaic reaction occurs. In this thesis, we only involve redox species that are controlled by diffusion. Therefore, the faradaic reactions considered here are only subjected to control by the charge transfer steps and diffusion steps. The

Fig.1.21 Equivalent circuit for the faradaic impedance.

resulting faradaic impedance, Z_F, includes the resistive component, R_{ct}, representing the charge transfer resistance, and a general impedance, Z_W, caused by the diffusion step, known as the Warburg impedance on the EDL impedance [108].

It is necessary to consider the relationship between faradaic impedance and EDLC impedance. According to the description in the previous section, it is intuitively suggested that in supercapacitors undergoing faradaic reactions, the electrical energy is expected to surpass the sum of only the energy from the EDL capacitive behavior and that from the faradaic reactions alone. In other words, the observed current, I_{obs}, must be greater than the simple sum of the capacitive current, I_C, and the faradaic current, I_F. If one considers these components to be in series in an equivalent circuit, the total current, $I_{obs,S}$, mathematically equals to $I_C I_F/(I_C+I_F)$, which would necessarily result in $I_{obs,S}$ being less than their sum, a proposition that cannot stand. Thus, they would be in parallel, where the observed current, $I_{obs,p}$, should be the simple sum of I_C and I_F. The parallel relationship physically signifies that both are generated at the interface but functionally, the faradaic impedance and its EDL impedance are independent. This leads to the currents induced by each one to be independent as well [96].

In earlier years, Warburg and others have demonstrated through diffusion equations that the real and imaginary parts of the Warburg impedance are equal [109,110,111]. The Aoki's group has utilized this crucial finding as a foundation to elucidate the relationship between faradaic impedance and EDL impedance.

This exploration into the interplay between faradaic and EDL capacitive responses not only enriches our understanding of electrochemical interfaces but also guides the right mechanism of supercapacitors for enhanced performance. The extensive experimental data from the Aoki's group have yielded contrary results.

1.5.3 AC-impedance of determining the negative capacitance

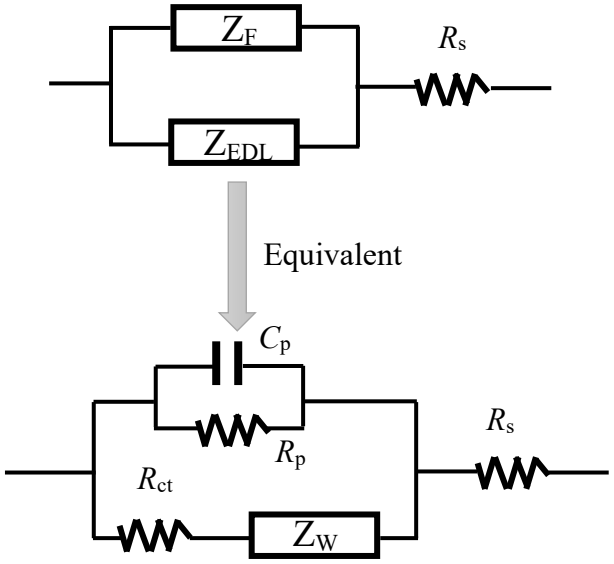

Fig.1.22 Equivalent circuit when the diffusion-controlled faradaic reaction occurs, which includes the EDL impedance and faradaic impedance.

The equivalent circuit, where the faradaic impedance is in parallel with the EDL impedance, is shown in Fig.1.22. The EDLC current density, j_{EDL}, and its faradaic AC current density, j_{F}, are given by the following Equation, respectively [22,95,112].

$$j_{\mathrm{EDL}} = \frac{\mathrm{d}C_{\mathrm{p}}V_{\mathrm{ac}}}{\mathrm{d}t} = \frac{C_{\mathrm{p}}\mathrm{d}V_{\mathrm{ac}}}{\mathrm{d}t} + \frac{V_{\mathrm{ac}}\mathrm{d}C_{\mathrm{p}}}{\mathrm{d}t} \tag{1.5.1}$$

$$j_{\mathrm{F}} = (1+i)c^{*}F^{2}\sqrt{D\omega}V_{\mathrm{ac}}\left[\sqrt{2}RT\cosh^{2}\left(\frac{\zeta_{\mathrm{dc}}}{2}\right)\right]^{-1} \tag{1.5.2}$$

$$\zeta_{\mathrm{dc}} = \frac{(E-E^{0})F}{RT} \tag{1.5.3}$$

Where the AC voltage $V_{ac} = V_0 e^{i\omega t}$ was applied to the electrode, c^* is the sum of the bulk concentration of the oxidized and reduced species and D is the diffusion coefficient. Since the concept of admittance is typically analogous to the current, the admittance of EDLC, when considering its property of frequency dependence, can be depicted as follows:

$$Y_{EDL} \equiv \frac{1}{Z} = (\lambda + i)\omega C_p \quad (1.5.4)$$

When the EDL impedance is considered to be independent of the Warburg impedance, the observed current is a simple sum of the currents through the EDL and the Warburg impedance. Then, the real admittance Y_1 and the imaginary admittance Y_2 are given by:

$$Y_1 = \lambda\omega C_p + Y_W = \lambda k_1 f^{-\lambda} + k_2 f^{-1/2} \quad (1.5.5)$$

$$Y_2 = \omega C_p + Y_W = k_3 f^{-\lambda} + k_4 f^{-1/2} \quad (1.5.6)$$

Here,

$$Y_W = c^* F^2 \sqrt{D\omega}\left[\sqrt{2}RT\cosh^2\left(\frac{\zeta_{dc}}{2}\right)\right]^{-1} \quad (1.5.7)$$

The Aoki's group conducted AC impedance measurements on the ferrocene derivatives, i.e. ferrocenylmethyl tetramethylammmounium involving simple one-electrode transfer faradaic reaction. They plotted the relationship between log Y_1 and log Y_2 against log f, as shown in Fig.1.23. A clear trend of deviation at high frequencies was observed. Tang. *et al*. in their measurements on different redox species (hexaammineruthenium and hexachlorirridium), observed a similar phenomenon [112]. This phenomenon is characterized by decreased EDLCs. Therefore, it is referred

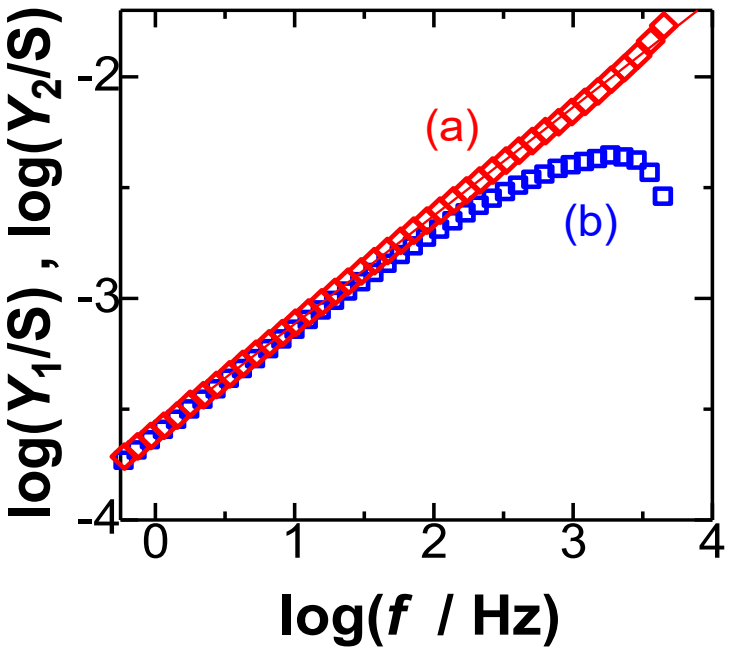

Fig.1.23 Variations of log Y_1(a) and log Y_2(b) with log f at the unpolarized potential in the solution of 1 mM $FcTMA^+$ + 0.5 M KCl.

to as the “Negative Capacitance” phenomenon.

1.5.4 The concept of negative capacitance

When a faradaic reaction occurs at the electrode|solution interface, a positive charge is generated electrochemically. It is easy to be neutralized with the negative one from the solution or partial charge of solvent molecules. It is called the redox charge dipole. This diploe is oriented in the direction opposite to that of the field-oriented solvent dipoles [22,95,112, 113]. Therefore, it works to suppress EDLC, as shown in Fig.1.24. When its contribution overcomes the EDLC current, the observed capacitance has a negative value. This is an explanation of the phenomenon of negative capacitance (NC).

The new evidence for the explanation of the physical meaning behind the phenomenon of NC had been provided in 2019 and 2023. The anodic and cathodic stripping voltammetry were used to investigate the deposition and stripping of silver ions [114,115]. An imbalance of charge was observed between the deposition and stripping. The formation of redox charge dipoles from silver ions (Ag^+) and counter ions (NO_3^-) was the fundamental cause of this imbalance. It was clearly demonstrated that as the concentration of NO_3^- increases, the values of NC also increase [116]. The effect of NC is closely related to the lifetime of the redox charge dipoles.

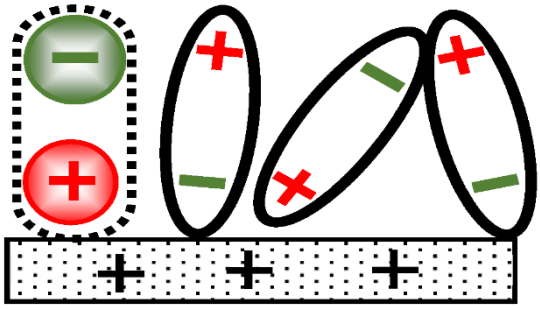

Fig.1.24 Illustrations of the orientation of solvent dipoles responding to the positive voltage at an electrode when the redox charge dipole generated through the faradaic reaction.

1.6.Objectives

Electrochemical processes including non-faradaic and faradaic reactions (Section 1.1) at the electrode|solution interface have been understood by analyzing electrochemical behaviors under various experimental conditions. For non-faradaic reactions, the EDLC can be observed at the thermodynamic equilibrium primarily due to the arrangement of solvent dipoles rather than the non-uniform of ions. It exhibits both the

voltage (Section 1.2) and time dependence (Section 1.3.1). The voltage dependency is typically governed by the electric field generated by the applied external voltage, while the time dependency arises from cooperative phenomena among solvent dipoles. These findings have been substantiated by extensive experimental evidence in our Lab (Section 1.3). Traditionally, faradaic reactions have been considered to be independent of the behavior of the EDLC. However, the arrangement of dipoles by the field is akin to the formation of redox species, as shown in Fig.1.24. Faradaic currents at a short time should include the capacitive currents, of which sign is opposite to the EDLC currents. It is caused by the generation of “a redox charge dipole”, which is by the redox species and a counterion. Its capacitance is called NC. Our research group has attempted to measure faradaic capacitance suppressed with a kind of EDLC using the AC impedance and stripping voltammetry (Section.1.5). The formation of NC has braked the conventional understanding of independence. Since the NC decreases observed faradaic currents, it looks like a delay or blocking of currents owing to heterogeneous kinetics. This thesis aims to disclose the significance of the NC for measurements of time-dependent curves and to offer a scientific explanation at a molecular level. The experimental techniques are fast-scan cyclic voltammetry or chronoamperometry to measure the faradaic reactions involving different electron transfers. It also aims to obtain the explanation by investigating the time-dependence of NC from the viewpoint of thermodynamics and kinetics. The step-by-step objective is enumerated in terms of hypothesis and advantages of techniques:

i. An extensively used technique with the time-voltage dependence is fast-scan voltammetry. It can also reveal the kinetic information. A simple one-electron transfer reaction ($FcTMA^{+} \rightarrow FcTMA^{2+}$) is used for demonstration of the NC in contrast with the heterogenous kinetics.

ii. Fast-scan cyclic voltammetry can manifest reaction mechanisms if the NC effect is subtracted. The classic half-reaction of water electrolysis, where the reduction of H^{+} ($H^{+} \rightarrow H_2$), involves two-electron transfer steps. Our research aims to extend the aforementioned studies on a simple one-electron transfer reaction to this complex one. A question arises whether the generation of intermediates might influence the values of NC.

iii. Dioxygen in basic solution has been recognized to arise from the reaction, $4OH^{-} \rightarrow O_2 + 2H_2O + 4e^{-}$. The four-electron transfer indicates some complications by various stepwise involving unknown intermediates in adsorbed states or dissolved ones with irreversible reactions. Intermediates can be detected by analyzing fast-scan cyclic voltammetry in light of the effects of the NC.

iv. The redox charge dipole causes a time-delay in faradaic reactions as long as the EDLC. It is interesting to examine a possibility of whether the time dependence of EDLCs is reflected in the NC or not. The electrochemical technique such as chronoamperometry is the simplest ones. The similarity will be examined for $FcTMA^{+}$ species.

1.7.Scope of the study in this thesis

Chapter 1 describes the significance of the electrode|solution interface. Several physical models related to the interfacial structure are discussed. The EDLC in the presence of faradaic reactions is addressed from both thermodynamic and kinetic scientific perspectives as the background of this thesis.

Chapter 2 introduces the electrochemical methods used in this research work, such as fast-scan cyclic voltammetry and chronoamperometry, related theoretical parts, and derive equations for these methods.

Chapter 3 focuses on determining the phenomenon of the NC using fast-scan cyclic voltammetry, with one single electrode transfer redox reaction as the oxidation of $FcTMA^+$.

Chapter 4 applies the theoretic concept of the NC to the reduction of hydrogen ions, H^+, which is one of the half-reactions in water electrolysis.

Chapter 5 deals with another half-reaction in water electrolysis, the oxidation of hydroxide ions, OH^- involving adsorptive ions. The fast-scan voltammetry method was used to confirm adsorptive substances and also to verify the NC.

Chapter 6 verifies the frequency dependence of the EDLC and the NC using chronoamperometry, where the capacitance exhibits a power law of 0.9. The faradaic reaction makes solvent molecules rearrange exhibiting a total power law of 0.4.

Chapter 7 is the conclusion part of the thesis.

References for Chapter 1 are given at the end of the first section. References

for the remaining chapters are given at the end of the thesis.

References

[1] A.J.Bard and L.R.Faulkner,Electrochemical Methods:Fundamentals and Applications, 2nd Edition. Wiley Global Education, 2000.

[2] Amulya K N Reddy, J. O'mara, and M. E. Gamboa-Aldeco, Modern electrochemistry. New York: Plenum Press, 1998.

[3] A. Bard, Standard Potentials in Aqueous Solution. Routledge, 2017.

[4] K. Oldham and J. Myland, Fundamentals of Electrochemical Science. Elsevier, 2012.

[5] P. W. Atkins and Julio De Paula, Physical chemistry. New York: W.H. Freeman, 2006.

[6] AROTE, Energy Storage Devices Basic Principle. Iop Renewable and Sustainable, 2021.

[7] N. Anna , "Investigation of electrochemical properties and performance of stimulation/sensing electrodes for pacemaker applications," 2005.

[8] R. J. Kee, H. Zhu, and D. G. Goodwin, "Modeling Electrochemistry and Solid-Oxide Fuel Cells: Part 1. Basic Principles," *ChemInform*, vol. 37, no. 34, Aug. 2006, DOI: https://doi.org/10.1002/chin.200634232.

[9] R. Vasquez, J. Waelder, Y. Liu, H. Bartels, and S. Maldonado, "A Gauss's law analysis of redox active adsorbates on semiconductor electrodes: The charging and faradaic currents are not independent," *Proceedings of the National Academy of Sciences of the United States of America*, vol. 119, no. 36, Aug. 2022, DOI: https://doi.org/10.1073/pnas.2202395119.

[10] G. Pataro, G. Donsì, and G. Ferrari, "Modeling of Electrochemical Reactions During Pulsed Electric Field Treatment," *In: Miklavcic, D.(eds) Handbook of Electroportion. Springer eBooks Cham*, pp. 1–30, Jan. 2016, DOI: https://doi.org/10.1007/978-3-319-26779-1_5-1.

[11] S. W. Boettcher *et al.*, "Potentially Confusing: Potentials in Electrochemistry," *ACS Energy Letters*, vol. 6, no. 1, pp. 261–266, Dec. 2020, DOI: https://doi.org/10.1021/acsenergylett.0c02443.

[12] Y. Demirel and V. Gerbaud, "Fundamentals of Equilibrium

Thermodynamics," *Nonequilibrium Thermodynamics*, pp. 1–85, 2019, DOI: https://doi.org/10.1016/b978-0-444-64112-0.00001-0.

[13] E. R. Cohen and I. Mills, *Quantities, units and symbols in physical chemistry*. Cambridge: RSC Publishing, 2007, p. 73.

[14] D. Mandler, "Allen J. Bard, György Inzelt, Fritz Scholz (Eds.): Electrochemical dictionary, 2nd ed.," *Analytical and Bioanalytical Chemistry*, vol. 405, no. 21, pp. 394–395, Jun. 2013, DOI: https://doi.org/10.1007/s00216-013-7079-7.

[15] A. J. Bard, György Inzelt, F. Scholz, and I. Ebrary, *Electrochemical dictionary*. New York: Springer, 2012.

[16] G. Inzelt, "Crossing the bridge between thermodynamics and electrochemistry. From the potential of the cell reaction to the electrode potential," *ChemTexts*, vol. 1, no. 1, Nov. 2014, DOI: https://doi.org/10.1007/s40828-014-0002-9.

[17] S. Grimnes and Ø. G. Martinsen, "Electrodes," *Bioimpedance and Bioelectricity Basics*, Chapter 7, pp. 179–254, 2015, DOI:

https://doi.org/10.1016/b978-0-12-411470-8.00007-6.

[18] Administrator, "Mass Transport," *www.ceb.cam.ac.uk*, Nov. 14, 2013. https://www.ceb.cam.ac.uk/research/groups/rg-eme/Edu/mass-transport.

[19] H. A. Haus and J. R. Melcher, *Electromagnetic Fields and energy.* Englewood Cliffs: Prentice-Hall, 1989, p. Chapter 6, Polarization.

https://mitocw.ups.edu.ec/resources/res-6-001-electromagnetic-fields-and-energy-spring-2008/chapter-6/06.pdf

[20] N. Perez, *Electrochemistry And Corrosion Science.* Springer, 2018, pp. 71–121, 121–154.

[21] Z. Wang, "Frequency-Dependence of Double Layer Capacitance by Electrode Reactions," Doctoral Thesis, *University of Fukui*, 2018.

[22] K.J Aoki, J. Chen, X. Zeng, and Z. Wang, "Decrease in the double layer capacitance by faradaic current," *RSC Advances*, vol. 7, no. 36, pp. 22501–22509, Jan. 2017, DOI: https://doi.org/10.1039/c7ra01770g.

[23] M. Schwartz, *Principles of Electrodynamics*. Courier Corporation,

2012.

[24] P. W. Atkins, J. De Paula, and J. Keeler, *Atkins' Physical Chemistry*, 11th ed. Oxford: Oxford University Press, 2019.

[25] H. Imai, "faradaic Rectification and Electrode Processes. IV," *The Journal of Physical Chemistry*, vol. 66, no. 9, pp. 1744–1746, Sep. 1962, DOI: https://doi.org/10.1021/j100815a508.

[26] P. M. Biesheuvel and J. Dykstra, "The difference between faradaic and NonFaradaic processes in Electrochemistry," *arXiv: Chemical Physics*, Sep. 2018, Accessed: Mar. 06, 2024. [Online]. Available: https://api.semanticscholar.org/CorpusID:105202354.

[27] Y. Liu, S. P. Jiang, and Z. Shao, "Intercalation pseudocapacitance in electrochemical energy storage: recent advances in fundamental understanding and materials development," *Materials Today Advances*, vol. 7, p. 100072, Sep. 2020, DOI: https://doi.org/10.1016/j.mtadv.2020.100072.

[28] A. Fruchtman, "Electric Field in a Double Layer and the Imparted Momentum," *Physical Review Letters*, vol. 96, no. 6, Feb. 2006, DOI: https://doi.org/10.1103/physrevlett.96.065002.

[29] J. K. Taylor, G. Raghu, and R. M. West, "Insights into the Kinetics of Electrostatic Denaturation of Surface-Bound DNA," *ECS Meeting Abstracts*, vol. MA2020-01, no. 27, pp. 1948–1948, May 2020, DOI: https://doi.org/10.1149/ma2020-01271948mtgabs.

[30] R. K. Franklin, S. M. Martin, T. D. Strong, and R. B. Brown, "2.12 - Chemical Sensors," *Comprehensive Microsystems*, pp. 433–461, 2008, DOI: https://doi.org/10.1016/b978-044452190-3.00044-6.

[31] J. Phojaroen, M. Raita, V. Champreda, N. Laosiripojana, S. Assabumrungrat, and S. Chuetor, "Thermodynamic and Kinetic Equilibrium for Adsorption of Cellulosic Xylose of Commercial Cation-Exchange Resins," *ACS Omega*, vol. 9, no. 2, pp. 3006–3016, Jan. 2024, DOI: https://doi.org/10.1021/acsomega.3c09246.

[32] R. Compton, "Equilibrium Electrochemistry and the Nernst Equation," *Understanding Voltammetry*, pp. 1–35, Jun. 2018, DOI: https://doi.org/10.1142/9781786345271_0001.

[33] H. Zhu, R. J. Kee, V. M. Janardhanan, O. Deutschmann, and D. G. Goodwin, “Modeling Elementary Heterogeneous Chemistry and Electrochemistry in Solid-Oxide Fuel Cells,” *Journal of The Electrochemical Society*, vol. 152, no. 12, p. A2427, 2005, DOI: https://doi.org/10.1149/1.2116607.

[34] J. Neri, A. Cammarata, and Alessandro Donazzi, “Experimental and Model Investigation of a Solid Oxide Fuel Cell Operated Under Low Fuel Flow Rate,” *Journal of The Electrochemical Society*, vol. 170, no. 12, pp. 124506–124506, Dec. 2023, DOI: https://doi.org/10.1149/1945-7111/ad1166.

[35] P. Ramakrishnan and A. Sahoo, “A Study on Mass Transfer Modelling in SOFC anode: Comparison of Diffusion Mass Transfer Models for Estimation of Diffusion Overpotential,” *Inzynieria Chemiczna I Procesowa*, pp. 4–4, Jan. 2024, DOI: https://doi.org/10.24425/cpe.2022.142293.

[36] Y. Wang, H. Xu, J. Zhang, and G. Li, “Electrochemical Sensors for Clinic Analysis,” *Sensors*, vol. 8, no. 4, pp. 2043–2081, Mar. 2008, DOI: https://doi.org/10.3390/s8042043.

[37] M. E. Gertner and M. Schlesinger, “Electrochemistry and Medical Devices: Friend or Foe?,” *The Electrochemical Society Interface*, vol. 12, no. 3, pp. 20–24, Sep. 2003, DOI: https://doi.org/10.1149/2.f05033if.

[38] C. Lu, J. Han, X. Sun, and G. Yang, “Electrochemical Detection and Point-of-Care Testing for Circulating Tumor Cells: Current Techniques and Future Potentials,” *Sensors*, vol. 20, no. 21, p. 6073, Oct. 2020, DOI: https://doi.org/10.3390/s20216073.

[39] F. Bettazzi and I. Palchetti, “Photoelectrochemical genosensors for the determination of nucleic acid cancer biomarkers,” *Current Opinion in Electrochemistry*, vol. 12, pp. 51–59, Dec. 2018, DOI: https://doi.org/10.1016/j.coelec.2018.07.001.

[40] M.do P. Ferreira, S. F. Yamada-Ogatta, and C. R. Teixeira Tarley, “Electrochemical and Bioelectrochemical Sensing Platforms for Diagnostics of COVID-19,” *Biosensors*, vol. 13, no. 3, p. 336, Mar. 2023, DOI: https://doi.org/10.3390/bios13030336.

[41] M. M. P. M., “On the Present Condition Of the Soda Industry,” *Nature*,

vol. 27, no. 695, pp. 401–402, Feb. 1883, DOI: https://doi.org/10.1038/027401a0.

[42] J.B.C.K, "The Applications of Electrolysis in Chemical Industry," *Nature*, vol. 103, no. 2585, pp. 203–203, May 1919, DOI: https://doi.org/10.1038/103203a0.

[43] P. Farràs, P. Strasser, and A. J. Cowan, "Water electrolysis: Direct from the sea or not to be?," *Joule*, vol. 5, no. 8, pp. 1921–1923, Aug. 2021, DOI: https://doi.org/10.1016/j.joule.2021.07.014.

[44] X. Wei *et al.*, "Improvement of the critical current density of alkaline water electrolysis based on the hydrodynamic similarity between boiling and water electrolysis," *International Journal of Heat and Mass Transfer*, vol. 214, no. 0017-9310, pp. 124420–124420, Nov. 2023, DOI: https://doi.org/10.1016/j.ijheatmasstransfer.2023.124420.

[45] N.-T. Suen, S.-F. Hung, Q. Quan, N. Zhang, Y.-J. Xu, and H. M. Chen, "Electrocatalysis for the oxygen evolution reaction: recent development and future perspectives," *Chemical Society Reviews*, vol. 46, no. 2, pp. 337–365, 2017, DOI: https://doi.org/10.1039/c6cs00328a.

[46] Z. Yu, J. Xu, T. Yang, and L. Liu, "Efficient hydrogen production by saline water electrolysis at high current densities without the interfering chlorine evolution," *Journal of Materials Chemistry A*, vol. 9, no. 39, pp. 22248–22253, Jan. 2021, DOI: https://doi.org/10.1039/d1ta05703k.

[47] J. T. Vardner *et al.*, "Vanadium (II) Sulfate for the Reductive Leaching of Chalcopyrite: Replacing Smelting with Electrolysis for Copper Production," *ChemElectroChem*, vol. 9, no. 24, Dec. 2022, DOI: https://doi.org/10.1002/celc.202200920.

[48] Sherif, "Electrochemical behavior of aluminum and some of its alloys in chloroaluminate ionic liquids: electrolytic extraction and electrorefining," *Journal of Solid State Electrochemistry*, vol. 16, no. 2, pp. 775–783, May 2011, DOI: https://doi.org/10.1007/s10008-011-1425-5.

[49] N. D. Hung, M. V. Phuoc, N. M. Thuy, and N. N. Tru, "Preparation of Nanosilver Colloidal Solution by Anodic Dissolution under High DC Voltage," *Electrochemistry*, vol. 81, no. 6, pp. 454–459, 2013, DOI: https://doi.org/10.5796/electrochemistry.81.454.

[50] L. Ding, X. Wang, S. Yang, W. Xu, Y. Yan, Y. Xue, F. Ma,

"Electrochemical extraction mechanism of Nd on Ga-Al alloy electrode," *Separation and Purification Technology*, vol. 306, no. 1383–5866, pp. 122543–122543, Feb. 2023, DOI: https://doi.org/10.1016/j.seppur.2022.122543.

[51] K. Detka and K. Górecki, "Selected Technologies of Electrochemical Energy Storage—A Review," *Energies*, vol. 16, no. 13, p. 5034, Jan. 2023, DOI: https://doi.org/10.3390/en16135034.

[52] S. Rudra, H. W. Seo, S. Sarker, and D. M. Kim, "Supercapatteries as Hybrid Electrochemical Energy Storage Devices: Current Status and Future Prospects," *Molecules*, vol. 29, no. 1, pp. 243–243, Jan. 2024, DOI: https://doi.org/10.3390/molecules29010243.

[53] Dr. Suman Gandi, Dr. Saidi Reddy Prame, and Dr. Damodar Reddy Edla, "Electrochemical energy storage systems and devices", *Multi Spectrum Publications*, 2021.

[54] J. Xiao *et al.*, "Perspective—Electrochemistry in Understanding and Designing Electrochemical Energy Storage Systems," *Journal of The Electrochemical Society*, vol. 169, no. 1, pp. 010524–010524, Jan. 2022, DOI: https://doi.org/10.1149/1945-7111/ac4a55.

[55] S. Sharma and P. Chand, "Supercapacitor and electrochemical techniques: A brief review," *Results in Chemistry*, vol. 5, p. 100885, Jan. 2023, DOI: https://doi.org/10.1016/j.rechem.2023.100885.

[56] Abhishek Panghal, D. Sahoo, Deepak Deepak, S. Deshmukh, Bhaskar Kaviraj, and Susanta Sinha Roy, "Single-Step Synthesis of Ni-Doped MoS_2 Nanostructures for Symmetrical Supercapacitor Devices," *ACS Applied Nano Materials*, Feb. 2024, DOI: https://doi.org/10.1021/acsanm.3c06139.

[57] S. Campuzano, M. Pedrero, P. Yáñez-Sedeño, and J. M. Pingarrón, "New challenges in point of care electrochemical detection of clinical biomarkers," *Sensors and Actuators B: Chemical*, vol. 345, p. 130349, Oct. 2021, DOI: https://doi.org/10.1016/j.snb.2021.130349.

[58] W. Wang, "Preparation of Electrochemical Sensor Based on Magnetic Graphene Nanocomposite for Determination of Dopamine," *International Journal of Electrochemical Science*, p. ArticleID:220232, Feb. 2022, DOI: https://doi.org/10.20964/2022.02.33.

[59] H. Helmholtz, "Ueber einige Gesetze der Vertheilung elektrischer

Ströme in körperlichen Leitern mit Anwendung auf die thierisch-elektrischen Versuche," *Annalen der Physik und Chemie*, vol. 165, no. 6, pp. 211–233, 1853, DOI: https://doi.org/10.1002/andp.18531650603.

[60] H. Helmholtz, "Studien über electrische Grenzschichten," *Annalen der Physik und Chemie*, vol. 243, no. 7, pp. 337–382, 1879, DOI: https://doi.org/10.1002/andp.18792430702.

[61] S. J. Ling, J. Sanny, and W. Moebs, "8.3 Energy Stored in a Capacitor -University Physics Volume 2 | OpenStax," *openstax.org*, Oct. 06, 2016. https://openstax.org/books/university-physics-volume-2/pages/8-3-energy-stored-in-a-capacitor (accessed Aug. 04, 2021).

[62] G. Gouy, "Sur la constitution de la charge électrique à la surface d'un électrolyte," *Journal de Physique Théorique et Appliquée*, vol. 9, no. 1, pp. 457–468, 1910, DOI: https://doi.org/10.1051/jphystap:019100090045700.

[63] G. Gouy, "In the constitution of the electric charge on the surface of an electrolyte [Sur la constitution de la charge électrique ala surface d'un électrolyte]," *Compt. Rend*, vol. 149, pp. 654–657, 1909.

[64] D. C. Grahame, "The Electrical Double Layer and the Theory of Electrocapillarity.," Chemical Reviews, vol. 41, no. 3, pp. 441–501, Dec. 1947, DOI: https://doi.org/10.1021/cr60130a002.

[65] O. Stern, "ZUR THEORIE DER ELEKTROLYTISCHEN DOPPELSCHICHT," *Zeitschrift für Elektrochemie und angewandte physikalische Chemie*, vol. 30, no. 21–22, pp. 508–516, Nov. 1924, DOI: https://doi.org/10.1002/bbpc.192400182.

[66] A. D. Clegg, N. V. Rees, O. V. Klymenko, B. A. Coles, and R. G. Compton, "Marcus theory of outer-sphere heterogeneous electron transfer reactions: High precision steady-state measurements of the standard electrochemical rate constant for ferrocene derivatives in alkyl cyanide solvents," *Journal of Electroanalytical Chemistry*, vol. 580, no. 1, pp. 78–86, Jun. 2005, DOI: https://doi.org/10.1016/j.jelechem.2005.03.013.

[67] J. O'm. Bockris, M. A. V. Devanathan, and K. Müller, "On the structure of charged interfaces," *Proceedings of the Royal Society of London*, vol. 274, no. 1356, pp. 55–79, Jun. 1963, DOI: https://doi.org/10.1098/rspa.1963.0114.

[68] J. Le, Q. Fan, J. Li, and J. Cheng, “Molecular origin of negative component of Helmholtz capacitance at electrified Pt(111)/water interface,” *Science Advances*, vol. 6, no. 41, Oct. 2020, DOI: https://doi.org/10.1126/sciadv.abb1219.

[69] T Pajkossy and D. M. Kolb, “On the origin of the double layer capacitance maximum of Pt(111) single crystal electrodes,” *Electrochemistry Communications*, vol. 5, no. 4, pp. 283–285, Apr. 2003, DOI: https://doi.org/10.1016/s1388-2481(03)00046-8.

[70] T. Pajkossy and D. M. Kolb, “Double layer capacitance of Pt(111) single crystal electrodes,” *Electrochimica Acta*, vol. 46, no. 20–21, pp. 3063–3071, Jul. 2001, DOI: https://doi.org/10.1016/s0013-4686(01)00597-7.

[71] K. Ojha, K. Doblhoff-Dier, and M. T. M. Koper, “Double-layer structure of the Pt(111)–aqueous electrolyte interface,” *Proceedings of the National Academy of Sciences*, vol. 119, no. 3, Jan. 2022, DOI: https://doi.org/10.1073/pnas.2116016119.

[72] K. J. Aoki, “Frequency-dependence of electric double layer capacitance without faradaic reactions,” *Journal of Electroanalytical Chemistry*, vol. 779, pp. 117–125, Oct. 2016, DOI: https://doi.org/10.1016/j.jelechem.2016.04.026.

[73] J. Newman, “Frequency Dispersion in Capacity Measurements at a Disk Electrode,” *Journal of The Electrochemical Society*, vol. 117, no. 2, pp. 198–198, Jan. 1970, DOI: https://doi.org/10.1149/1.2407464.

[74] R. D. Armstrong and W. P. Race, “Capacitance dispersion at the mercury-glycerol interphase,” *Journal of electroanalytical chemistry and interfacial electrochemistry*, vol. 34, no. 1, pp. 244–246, Jan. 1972, DOI: https://doi.org/10.1016/s0022-0728(72)80522-9.

[75] W. Scheider, “Theory of the frequency dispersion of electrode polarization. Topology of networks with fractional power frequency dependence,” *The Journal of Physical Chemistry*, vol. 79, no. 2, pp. 127–136, Jan. 1975, DOI: https://doi.org/10.1021/j100569a008.

[76] R. Leek and N. A. Hampson, “The dispersion of double-layer capacitance with frequency I. Smooth solid electrodes,” *Surface Technology*, Jul. 1978, DOI:

https://doi.org/10.1016/0376-4583(78)90008-0.

[77] L. Nyikos and T. Pajkossy, “Fractal dimension and fractional power frequency-dependent impedance of blocking electrodes,” *Electrochimica Acta*, vol. 30, no. 11, pp. 1533–1540, Nov. 1985, DOI: https://doi.org/10.1016/0013-4686(85)80016-5.

[78] Andrzej Lasia, *Electrochemical impedance spectroscopy and its applications*. New York Etc.: Springer, Cop, 2014.

[79] H. Fricke, “*The Theory of Electrolytic polarization,*” *The London, Edinburgh and Dublin philosophical magazine and journal of science*, vol. 14, no. 90, pp. 310–318, Aug. 1932, DOI: https://doi.org/10.1080/14786443209462064.

[80] G. J. Brug, A. L. G. van den Eeden, M. Sluyters-Rehbach, and J. H. Sluyters, “The analysis of electrode impedances complicated by the presence of a constant phase element,” *Journal of Electroanalytical Chemistry and Interfacial Electrochemistry*, vol. 176, no. 1, pp. 275–295, Sep. 1984, DOI: https://doi.org/10.1016/S0022-0728(84)80324-1.

[81] U. Rammelt and G. Reinhard, “On the applicability of a constant phase element (CPE) to the estimation of roughness of solid metal electrodes,” *Electrochimica Acta*, vol. 35, no. 6, pp. 1045–1049, Jun. 1990, DOI: https://doi.org/10.1016/0013-4686(90)90040-7.

[82] Andrzej Lasia, “The Origin of the Constant Phase Element,” *Jounral of Phydical Chemistry Letter*, vol. 13, no. 2, pp. 580–589, Jan. 2022, DOI: https://doi.org/10.1021/acs.jpclett.1c03782.

[83] J. Ross Macdonald, “Impedance spectroscopy and its use in analyzing the steady-state AC response of solid and liquid electrolytes,” *Materials Sciences and Applications,* vol. 223, no. 1–2, pp. 25–50, May 1987, DOI: https://doi.org/10.1016/0022-0728(87)85249-x.

[84] P. Córdoba-Torres, T. J. Mesquita, O. Devos, B. Tribollet, V. Roche, and R. P. Nogueira, “On the intrinsic coupling between constant-phase element parameters α and Q in electrochemical impedance spectroscopy,” *Electrochimica Acta*, vol. 72, pp. 172–178, Jun. 2012, DOI: https://doi.org/10.1016/j.electacta.2012.04.020.

[85] P. Zoltowski, “On the electrical capacitance of interfaces exhibiting constant phase element behaviour,” *Journal of Electroanalytical Chemistry*,

vol. 443, no. 1, pp. 149–154, Feb. 1998, DOI: https://doi.org/10.1016/s0022-0728(97)00490-7.

[86] T. Pajkossy, T. Wandlowski, and D. M. Kolb, “Impedance aspects of anion adsorption on gold single crystal electrodes,” *Journal of Electroanalytical Chemistry*, vol. 414, no. 2, pp. 209–220, Jan. 1996, DOI: https://doi.org/10.1016/0022-0728(96)04700-6.

[87] K. Aoki, Y. Hou, J. Chen, and Toyohiko Nishiumi, “Resistance associated with measurements of capacitance in electric double layers,” *Journal of Electroanalytical Chemistry*, vol. 689, pp. 124–129, Jan. 2013, DOI: https://doi.org/10.1016/j.jelechem.2012.10.004.

[88] Y. Hou, K. Aoki, J. Chen, and Toyohiko Nishiumi, “Solvent Variables Controlling Electric Double Layer Capacitance at the Metal–Solution Interface,” *Journal of Physical Chemistry C*, vol. 118, no. 19, pp. 10153–10158, May 2014, DOI: https://doi.org/10.1021/jp5018289.

[89] X. Zhao, K. J. Aoki, J. Chen, and T. Nishiumi, “Examination of the Gouy–Chapman theory for double layer capacitance in deionized latex suspensions,” *RSC Adv.*, vol. 4, no. 108, pp. 63171–63181, 2014, DOI: https://doi.org/10.1039/c4ra11258j.

[90] K.J. Aoki, “Dynamic Behavior of Electric Double Layer Impedance,” *Review of Polarography*, vol. 61, no. 1, pp. 33–42, Jan. 2015, DOI: https://doi.org/10.5189/revpolarography.61.33.

[91] Z. Wang, K. J. Aoki, J. Chen, and X. Zeng, “Frequency Dispersion of Double Layer Capacitance of Polyaniline-Coated Electrodes Under the Conducting State,” *International Journal of Chemistry*, vol. 10, no. 2, pp. 25–25, Apr. 2018, DOI: https://doi.org/10.5539/ijc.v10n2p25.

[92] K. J. Aoki, J. Chen, and Z. Wang, “Quantitative Relation of the Frequency Dispersion of Double Layer Capacitances to Surface Roughness,” *Advances in Nanoscience and Nanotechnology*, vol. 2, no. 1, Dec. 2018, DOI: https://doi.org/10.33140/ann/02/01/00003.

[93] H. Wang, K. J. Aoki, J. Chen, T. Nishiumi, X. Zeng, and X. Ma, “Power law for frequency-dependence of double layer capacitance of graphene flakes,” *Journal of Electroanalytical Chemistry*, vol. 741, pp. 114–119, Mar. 2015, DOI: https://doi.org/10.1016/j.jelechem.2015.01.008.

[94] K. J. Aoki, “Molecular interaction model for frequency-dependence of

double layer capacitors," *Electrochimica Acta*, vol. 188, pp. 545–550, Jan. 2016, DOI: https://doi.org/10.1016/j.electacta.2015.12.049.

[95] K. J. Aoki and J. Chen, "Effects of the dipolar double layer on elemental electrode processes at micro- and macro-interfaces," *Faraday Discussions*, vol. 210, pp. 219–234, 2018, DOI: https://doi.org/10.1039/c7fd00212b.

[96] K. J. Aoki and J. Chen, "Scientific hints of developing supercapacitors," *Journal of Solid State Electrochemistry*, vol. 24, no. 9, pp. 2055–2058, Jun. 2020, DOI: https://doi.org/10.1007/s10008-020-04698-9.

[97] Y. Hou, K.J. Aoki, and J. Chen, "Invariance of Double Layer Capacitance to Polarized Potential in Halide Solutions," *Universal Journal of Chemistry*, vol. 1, no. 4, pp. 162–169, Dec. 2013, DOI: https://doi.org/10.13189/ujc.2013.010404.

[98] K. J. Aoki, J. Chen, and P. Tang, "Double Layer Impedance in Mixtures of Acetonitrile and Water," *Electroanalysis*, vol. 30, no. 8, pp. 1634–1641, Mar. 2018, DOI: https://doi.org/10.1002/elan.201800025.

[99] K. Aoki, J. Chen, and R. He, "Potential Step for Double-Layer Capacitances Obeying the Power Law," *ACS omega*, vol. 5, no. 13, pp. 7497–7502, Mar. 2020, DOI: https://doi.org/10.1021/acsomega.0c00301.

[100] R. He, K. J. Aoki, and J. Chen, "Electric Field-Dependence of Double Layer Capacitances by Current-Controlled Charge-Discharge Steps," *Electrochem*, vol. 1, no. 2, pp. 217–225, Jun. 2020, DOI: https://doi.org/10.3390/electrochem1020015.

[101] S. Tan, "Advanced Electrochemical Techniques for Investigating Electron Transfer Kinetics," Thesis, *University of Warwick for a degree of Doctor of Philosophy*, 2017.

[102] E. J. F. Dickinson and A. J. Wain, "The Butler-Volmer equation in electrochemical theory: Origins, value, and practical application," *Journal of Electroanalytical Chemistry*, vol. 872, p. 114145, Sep. 2020, DOI: https://doi.org/10.1016/j.jelechem.2020.114145.

[103] K. J. Aoki, C. Zhang, J. Chen, and T. Nishiumi, "Heterogeneous reaction rate constants by steady-state microelectrode techniques and fast scan voltammetry," *Journal of electroanalytical chemistry*, vol. 706, pp.

40–47, Oct. 2013, DOI: https://doi.org/10.1016/j.jelechem.2013.07.021.

[104] Y. Uchida, E. Kätelhön, and R. G. Compton, “Sweep voltammetry with a semi-circular potential waveform: Electrode kinetics,” *Journal of electroanalytical chemistry (1992)*, vol. 835, pp. 60–66, Feb. 2019, DOI: https://doi.org/10.1016/j.jelechem.2018.12.030.

[105] H. I. Becker, “LOW VOLTAGE ELECTROLYTIC CAPACITOR,” Apr. 14, 1954 Available: https://patents.google.com/patent/US2800616A/en.

[106] B. E. Conway and E. Gileadi, “Kinetic theory of pseudo-capacitance and electrode reactions at appreciable surface coverage,” *Transactions of The Faraday Society*, vol. 58, pp. 2493–2493, Jan. 1962, DOI: https://doi.org/10.1039/tf9625802493.

[107] D. A. Harrington and B. E. Conway, “ac Impedance of faradaic reactions involving electrosorbed intermediates—I. Kinetic theory,” *Electrochimica Acta*, vol. 32, no. 12, pp. 1703–1712, Dec. 1987, DOI: https://doi.org/10.1016/0013-4686(87)80005-1.

[108] A. J. Bard, L. R. Faulkner, and H. S. White, *Electrochemical Methods*, *third edition*. Wiley, 2022.

[109] E. Warburg, “Ueber das Verhalten sogenannter unpolarisirbarer Elektroden gegen Wechselstrom,” *Annalen der Physik*, vol. 303, no. 3, pp. 493–499, Jan. 1899, DOI: https://doi.org/10.1002/andp.18993030302.

[110] D. A. Harrington, “Electrochemical impedance of multistep mechanisms: a general theory,” *Journal of Electroanalytical Chemistry*, vol. 449, no. 1–2, pp. 9–28, Jun. 1998, DOI: https://doi.org/10.1016/s0022-0728(97)00466-x.

[111] K. Ariyoshi *et al.*, “Electrochemical Impedance Spectroscopy Part 1: Fundamentals,” *Electrochemistry*, vol. 90, no. 10, pp. 102007–102007, 2022, DOI: https://doi.org/10.5796/electrochemistry.22-66071.

[112] K. Aoki, J. Chen, and P. Tang, “Capacitive Currents Flowing in the Direction Opposite to Redox Currents,” *Journal of Physical Chemistry C*, vol. 122, no. 29, pp. 16727–16732, Jun. 2018, DOI: https://doi.org/10.1021/acs.jpcc.8b03335.

[113] K. J. Aoki, S. Taniguchi, and J. Chen, “Participation in Negative

Capacitance of Diffusion-Controlled Voltammograms of Hemin," *ACS Omega*, vol. 5, no. 45, pp. 29447–29452, Nov. 2020, DOI: https://doi.org/10.1021/acsomega.0c04384.

[114] P. Tang, K. J. Aoki, and J. Chen, "Reduction Charge Smaller than the Deposited One in Cathodic Stripping Voltammograms of AgCl," *American Journal of Analytical Chemistry*, vol. 10, no. 08, pp. 286–295, 2019, DOI: https://doi.org/10.4236/ajac.2019.108021.

[115] K. J. Aoki, J. Chen, and R. Wang, "Stripped Charge of Ag Less than Deposited one Owing to Negative Capacitance Caused by Redox Reactions," *Electroanalysis*, vol. 31, no. 12, pp. 2303–2310, Jul. 2019, DOI: https://doi.org/10.1002/elan.201800873.

[116] R. Wang, K. J. Aoki, and J. Chen, "Enhancement of the Negative Capacitance Associated with the Dissolution of Silver by Salt Concentrations by Means of Anodic Stripping Voltammetry," *Electrochem*, vol. 3, no. 3, pp. 397–406, Jul. 2022, DOI: https://doi.org/10.3390/electrochem3030027.

Chapter 2

Theory of Measurement of Negative Capacitance

2.1.Fast-scan cyclic voltammetry

We characterize theoretically the property of the negative capacitance using fast-scan cyclic voltammetry. The dynamic variation of the redox charge density σ, which is generated from the faradaic current density, j_F, brings about the negatively capacitive current density, $j_{rx} = d\sigma/dt$. Since the two current densities are in logical conjunction, the inverse of the observed capacitive current density, j_c, is a sum of the inverse of the two:

$$1/j_c = 1/j_F + 1/j_{rx} \qquad (2.1.1)$$

The surface charge density for the oxidized species is followed by the Nernst equation like for the volume concentration at the surface. Therefore, we can write

$$\sigma = \sigma^* /(1 + e^{-\zeta}) \qquad (2.1.2)$$

where σ^* is the sum of the surface charge of the oxidized and the reduced species, and $\zeta = F(E - E^0)/RT$. Then j_{rx} is given by

$$j_{rx} = d\sigma/dt = \sigma^*(Fv/4RT)\,\mathrm{sech}^2(\zeta/2) \qquad (2.1.3)$$

Since the faradaic current here is controlled by diffusion of $FcTMA^+$ by fast-scan cyclic voltammetry, we have

$$j_F = (Fc^*/4)(FDv/\pi RT)^{1/2}\int_{\zeta_{in}}^{\zeta}(\zeta - x)^{-\frac{1}{2}}\,\mathrm{sech}^2\left(\frac{x}{2}\right)dx \qquad (2.1.4)$$

where ζ_{in} is the dimensionless initial potential. Since the observed

current density j is given by j_F - j_c, it is represented by $j = j_F - j_F j_{rx}/(j_F + j_{rx})$. The dimensionless current density into which Eq. (2.1.3) and (2.1.4) are inserted is expressed as

$$\frac{j}{Fc^*}\sqrt{\frac{RT}{FDv}} = \frac{1}{4\sqrt{\pi}}\int_{\zeta_{in}}^{\zeta}(\zeta - x)^{-\frac{1}{2}}\,\mathrm{sech}^2\left(\frac{x}{2}\right)\mathrm{d}x\left\{1 - \frac{1}{1+h(\zeta)}\right\} \qquad (2.1.5)$$

where

$$h(\zeta) = \frac{c^*}{\sqrt{\pi}\sigma^*}\sqrt{\frac{RTFD}{v}}\int_{\zeta_{in}}^{\zeta}(\zeta - x)^{-\frac{1}{2}}\,\mathrm{sech}^2\left(\frac{x}{2}\right)\mathrm{d}x/\mathrm{sech}^2(\zeta/2) \qquad (2.1.6)$$

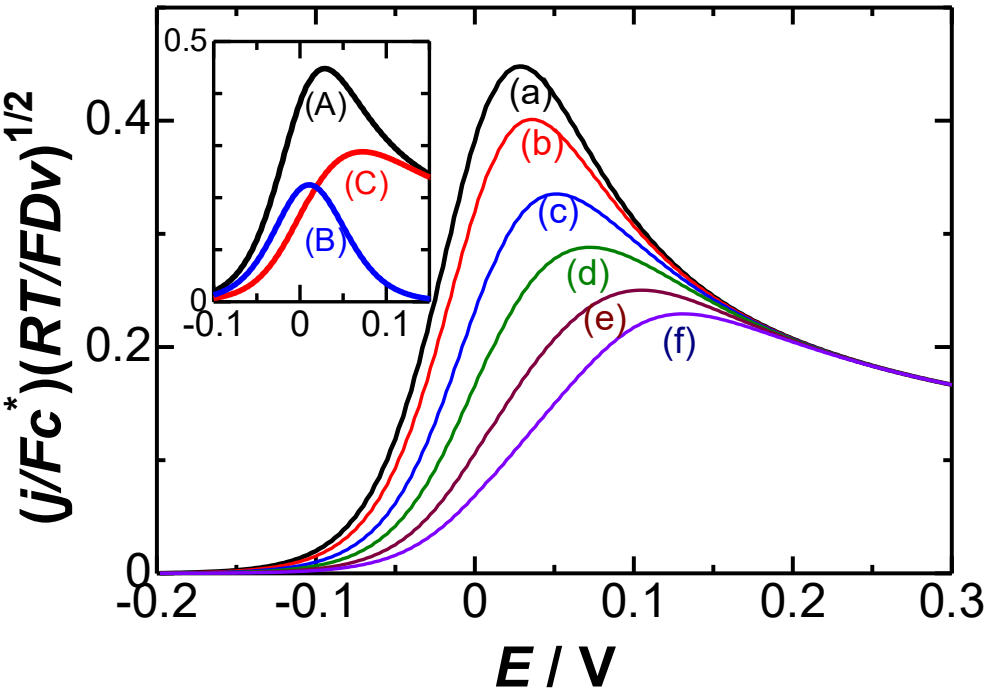

Fig.2.1 Voltammograms calculated from Eq. (2.1.5) for $(\sigma^*/c^*)^2 v/RTFD$ = (a) 0.0, (b) 0.09, (c) 1.0, (d) 4.0, (e) 16.0, and (f) 49.0. The inset shows voltammograms of (A) j_F, (B) j_c, and (C) j, calculated for $(\sigma^*/c^*)^2 v/RTFD$ = 4.

Fig.2.1 shows the dimensionless voltammograms calculated from Eq. (2.1.5) and (2.1.6) for various values of $(\sigma^*/c^*)^2 v/RTFD$. The negative capacitive current makes the observed peak not only decrease by the magnitude $[1+h(\zeta)]^{-1}$ but also shift in the positive direction. The potential shift is caused by the term of $\mathrm{sech}^2(\zeta/2)$ with the bell shape (B), as shown in

the inset of the figure.

Voltammetric peaks of j were detected for various values of $(\sigma^*/c^*)^2 v/RTFD$ by computation of Eq. (2.1.5) and (2.1.6). Fig.2.2 shows the variation of the peak potential with the logarithmic, dimensionless scan rate. The peak potential increases with an increase in $\log[(\sigma^*/c^*)^2 v/RTFD]$, and the plots fall on a line for $\log[(\sigma^*/c^*)^2 v/RTFD] > 3$, expressed by

$$E_p - E^0 = 52 \log[(\sigma^*/c^*)^2 v/RTFD] + 41 \qquad (2.1.7)$$

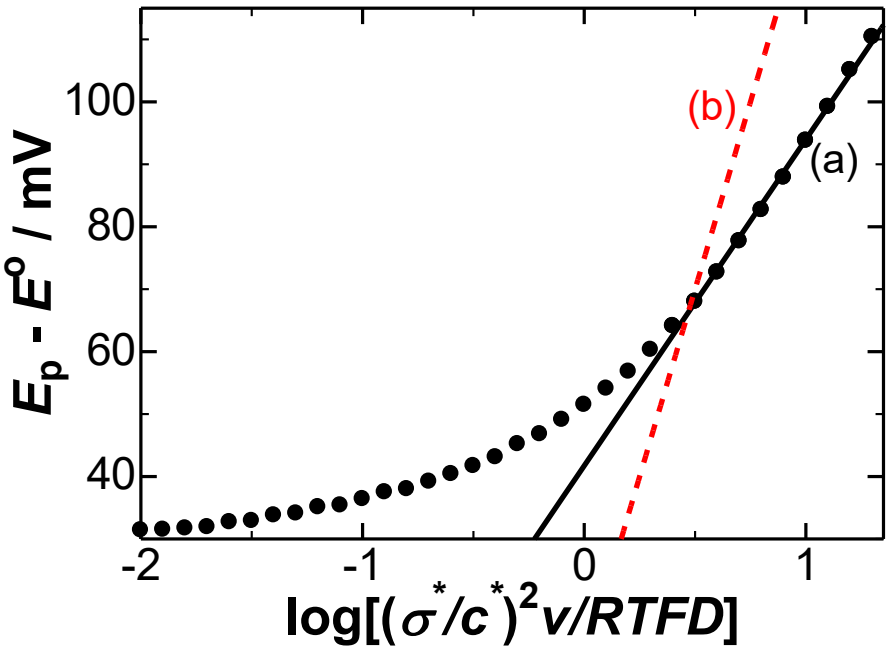

Fig.2.2 Dependence of the peak potential on logarithmic scan rates, calculated from Eq. (2.1.5) and (2.1.6). Lines (a) and (b) have slopes of 52 mV and 120 mV, respectively.

Where units of 52 and 41 are mV. This slope (line (a)) is smaller than that by the BV equation, which is 120 mV at the transfer coefficient of 0.5 (see (b)). It is close to the averaged value of eleven points (53±12) mV with the later type of Fig.3.3. If the voltammogram at the anodic scan is symmetric with that at the cathodic one, the difference in the peak potentials at v = 1 V s^{-1} is represented by

$$E_{pA} - E_{pC} = 104 \log[(\sigma^*/c^*)^2/RTFD] + 82 \quad (2.1.8)$$

The intercept of the plots of E_{pA} and E_{pC} against log v at $v = 1$ V s^{-1} is equivalent to the left term in Eq. (2.1.8). Then we evaluated σ^* to be $(4 \pm 2)\times10^{-5}$ C cm^{-2} for values of $c^* = 1$mM, $D = 0.76\times10^{-5}$ cm^2 s^{-1}. This value of σ^*, corresponding to the surface concentration of the adsorbed species $\sigma^*/F = (4 \pm 2)\times10^{-10}$ C cm^{-2}, might be close to the monolayer-adsorbed density of $FcTMA^+$.

Fig.2.3 shows the dependence of the dimensionless peak current on the square root of the dimensionless scan rate. The peak currents at slow scan rates ($(\sigma^*/c^*)(v/RTFD)^{1/2} < 0.2$) are proportional to $v^{1/2}$, whereas those at high scan rates ($(\sigma^*/c^*)(v/RTFD)^{1/2} > 1$) take a linear relation exhibiting an

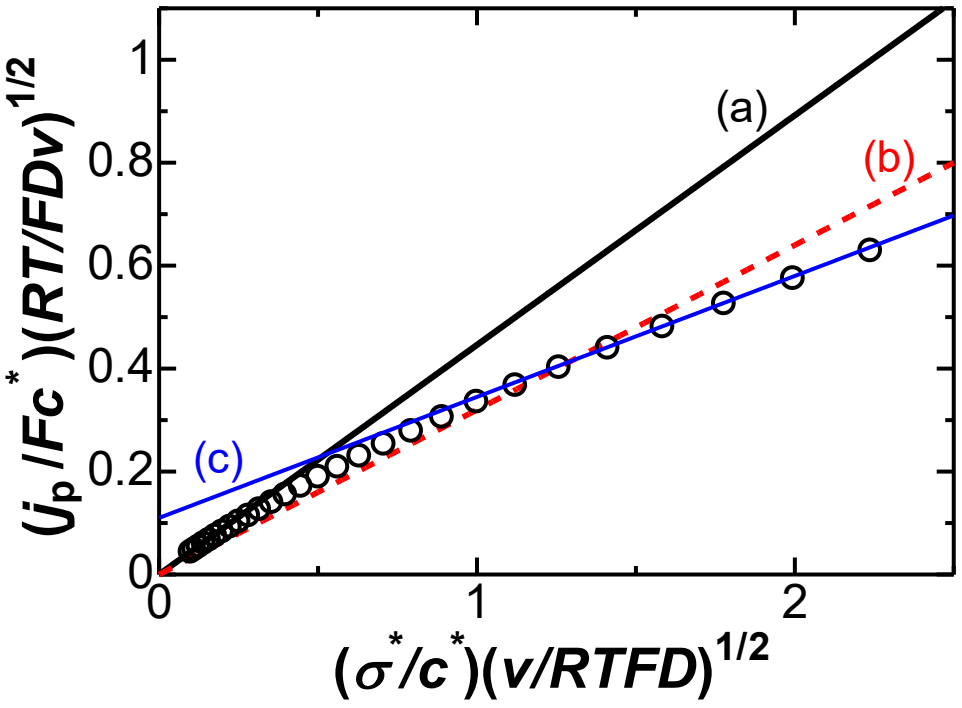

Fig.2.3 Dependence of the dimensionless peak current density on logarithmic scan rates, calculated from Eq. (2.1.5) and (2.1.6). Lines (a) and (b) have slopes of 0.446 and 0.35 (=$0.496\times0.5^{1/2}$) at the transfer coefficient of 0.5, respectively. Line (c) is an extrapolation for $(\sigma^*/c^*)(v/RTFD)^{1/2} > 1.0$.

intercept ((c) in Fig.2.3). The latter variation is different from the BV type in which the current should be proportional (zero intercept) to $v^{1/2}$. The variation is close to the experimental result of Fig.3.2 except for the absence of the current at v = 0. It is unpractical to realize the conditions of $(\sigma^*/c^*)(v/RTFD)^{1/2} > 1$ at conventional experiments.

Amounts of the theoretical peak currents divided by $v^{1/2}$ were plotted against $v^{1/2}$ in Fig.2.4. The variation for $(\sigma^*/c^*)(v/RTFD)^{1/2} < 0.3$ shows a line, expressed by

$$j_p/v^{1/2} = 0.446c^*F(FD/RT)^{1/2} - 0.16\Gamma^*F^2v^{1/2}/RT \qquad (2.1.9)$$

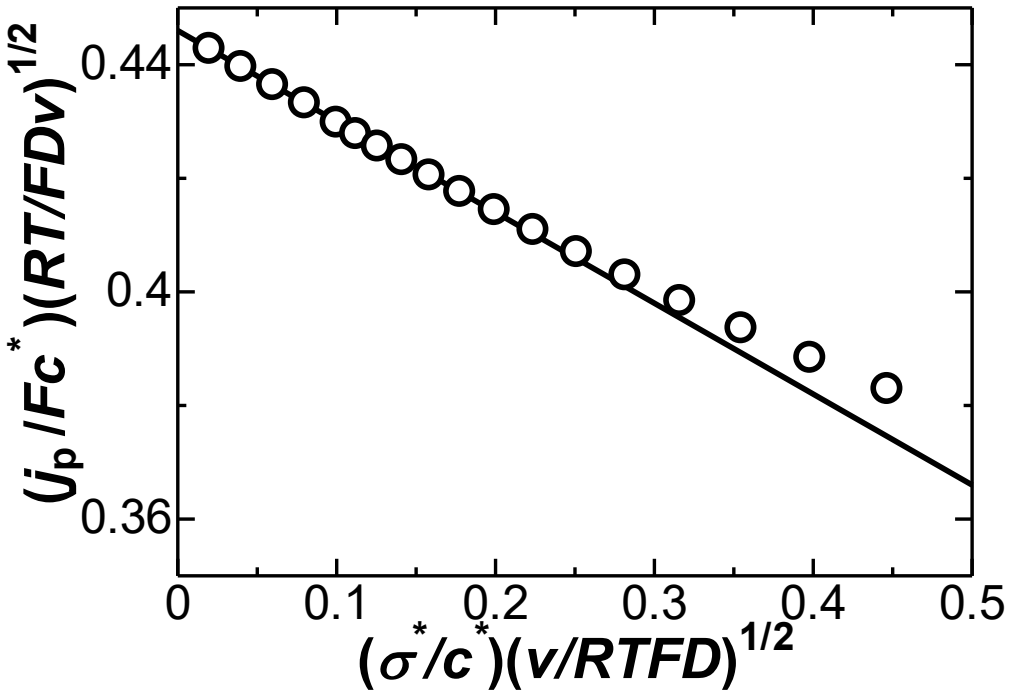

Fig.2.4 Variation of dimensionless $j_pv^{-1/2}$ with $v^{1/2}$, calculated from Eq. (2.1.5) and (2.1.6).

The plot deviates only at very fast scan rates, e.g. 40 V s^{-1} ($(\sigma^*/c^*)(v/RTFD)^{1/2} > 0.2$). Therefore, the plot in Fig.3.4 can be justified. The comparison of Eq.(2.1.9) with the empirical equation (3.3) yields the equality

$$C = 0.16\sigma^* F/RT \equiv C_{pk} \quad (2.1.10)$$

This is the negative capacitance at the reaction peak. A value of σ^* calculated from C_{pk} (64 μF cm^{-2} at c^* = 1 mM) is 1.0×10^{-5} C cm^{-2}, which corresponds to 1.1×10^{-10} mol cm^{-2} if one redox molecule is responsible for one elementary charge. This value is equivalent to (1.3 nm)^2 per area of one redox molecule. $FcTMA^+$ molecules look as if they were adsorbed in mono-molecular form only at the peak potential.

2.2.Chronoamperometry

The concept of the power law of the negative capacitance by chronoamperometry is outlined here. When an oxidation potential is applied to an electrode in a solution containing a redox species, the Nernst equation determines the activity of the redox species on the electrode surface. If the activity is equivalent to a concentration on the electrode, the difference between the surface concentration and bulk concentration causes diffusion, the flux of which is observed as current. The current values are specific to applied potentials. This logic is valid for the assumption of the equivalence of the activity to the concentration. The activity is a measure of such an effective concentration that the energetical balance is formally satisfied via the Nernst equation. In contrast, concentration is the number density of the redox species without considering any energetical concept. It is the concentration rather than the activity that can control diffusion equations.

If the dipole-dipole interaction in solvents, for example, hydrogen

bonding energy, is larger than the standard chemical potential term (the product of the chemical potential times the exchanged charge), the activity value calculated via the Nernst equation is different from concentration.

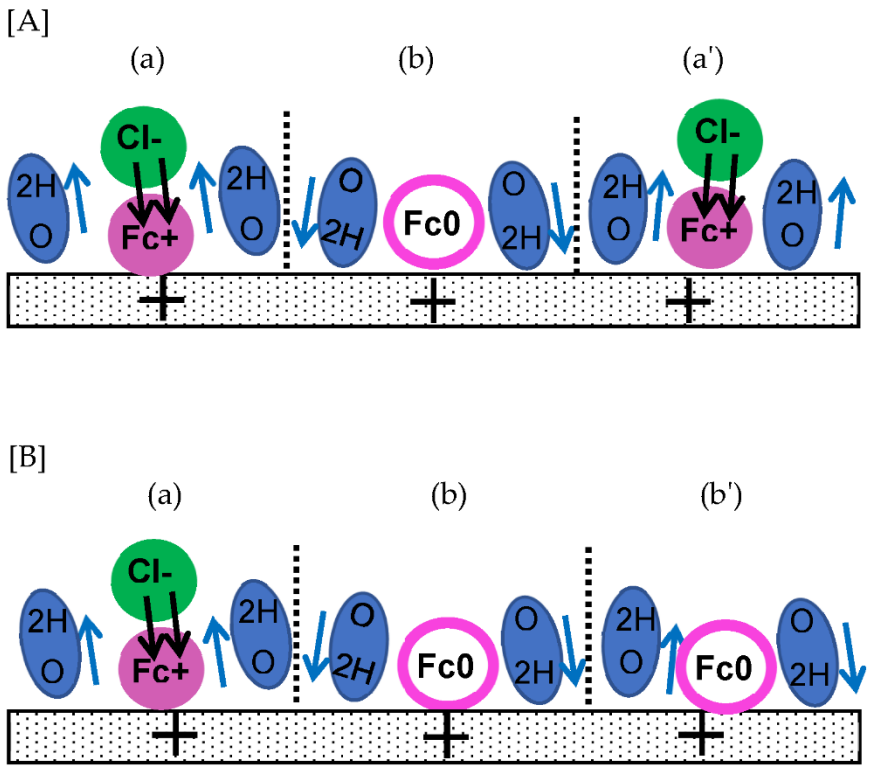

Fig.2.5 Arrangements of redox charge dipoles (black arrows) and solvent dipoles (blue). Since dipole interactions are canceled (**a**,**a′**) with the solvent dipoles, the dipole interaction in (**A**) is the same as (**B**). The activity of (**A**) is the same as in (**B**). Dipoles of (**b**,**b′**) work as EDLC.

Fig.2.5 shows an illustrative example of the difference between when a redox species Fc is partially oxidized compared to Fc^+ by applying an oxidation potential. The oxidation is associated with charge neutrality via a counterion (Cl^-) to form a redox dipole (indicated as two parallel arrows). Water dipoles neighboring Fc^+-Cl^- are oriented in the direction opposite to the orientation of Fc^+-Cl^- (in imaginary cells (a) and (a′)) in order to decrease the dipole–dipole interaction energy. Those next to (a) should be directed

toward the electrode in (b), which can participate in the formation of EDLC. The dipolar structure in (a′) is similar to that in (a). If Fc^+ in (a′) is not oxidized, the neutral form of Fc has no effect on the orientation of the neighboring water diploes in (b′), which may be thermally fluctuated, reaching the sum of the dipoles and the zero dipole moment in (b′). The interaction energy in [A] is the same as that in [B] for dipole-dipole interactions, resulting in the same chemical potential in [A] as in [B]. Consequently, the concentration on the electrode is different from the activity controlled by the Nernst equation, as described in Section. 1.4.

We describe the time dependence of EDLC, which is not only reflected in heterogeneous kinetics but also helpful for subtracting the EDLC components from the observed components. When voltage V is applied in a step form to EDLC, the chronoamperometric current density at $t > 0.3$ ms can be calculated as follows [1]:

$$j_{\mathrm{EDL}} = \lambda V C_{1\mathrm{s}} t^{\lambda-1} \tag{2.2.1}$$

where $C_{1\mathrm{s}}$ is the EDLC per area at $t = 1$ s, and λ is the number close to 0.1, according to previous results [1]. It is not in the form of $\exp(-t/R_{\mathrm{s}}C)$ for a solution resistance, R_{s} and C in the EDL structure, because it largely deviates from an ideal capacitance due to frequency dispersion. Since no point of zero charge has been found on a platinum electrode in various aqueous solutions [2,3], V is the step voltage independent of the formal potential of a redox species. Although the decay speed ($t^{-0.9}$) is larger than the Cottrell's decay value ($t^{-0.5}$), the EDLC current still survives even at 1 s.

This long relaxation caused by the power laws may be involved in the heterogeneous kinetics via dipole interactions.

We consider a faradaic current via a one-electron transferring Nernstian redox couple dissolved in a solution. The mass transport of the redox species is assumed to be controlled by time-dependent one-dimensional diffusion via the diffusion coefficient, D, common to reduced and oxidized species. When a potential is stepped from a fully reduced domain to a given oxidized potential E, a solution of the diffusion equation provides the relationship between the surface concentration, c_s, and the observed current density, j_{ob} [4] as follows:

$$c_s = c^* - F^{-1}(\pi D)^{-\frac{1}{2}} \int_0^t j_{ob}(u)(t-u)^{-\frac{1}{2}} du \tag{2.2.2}$$

where c^* is the bulk concentration of the redox species, and F is the Faraday constant. The observed current density is the result of subtracting the negatively capacitive density, j_{rx}, from Cottrell's current density, j_C:

$$j_{ob}(t) = j_C - j_{rx} \tag{2.2.3}$$

where:

$$j_C = c^* F (D/\pi t)^{1/2} \tag{2.2.4}$$

$$j_{rx} = \mu V C_{rx} t^{\mu-1} \tag{2.2.5}$$

Here, μ is a positive number close to zero because the behavior of μ seems to be similar to that of λ in the mechanisms, and C_{rx} is the capacitance associated with a redox reaction. The functional form of j_{rx} is assumed to be similar to that of EDLC (Equation (2.2.1)) because of the similarity of the current source by the dipole-dipole interaction. Inserting Equation (2.2.3)

into Equation (2.2.2) and carrying out integrations via the Beta function formula Eq.(6.2.1) in [5] We have:

$$c_{\mathrm{s}}(t) = \left((\mu V C_{\mathrm{rx}})/(FD^{1/2})\right)\{\Gamma(\mu)/\Gamma(\mu + 1/2)\}t^{\mu-\frac{1}{2}} \qquad (2.2.6)$$

where Γ is the gamma function. This equation states that the surface concentration decreases with $t^{\mu-1/2}$ dependence. Although sufficiently oxidized electrical potential is applied to the electrode, the concentration of the reduced species may not instantaneously reduce to zero. The observed currents lower than the Cottrell's current mean that the concentration values on the electrode are detectable.

Observed currents always include the EDLC current, i.e., $I_{\mathrm{C}} - I_{\mathrm{rx}} + I_{\mathrm{EDL}}$. Each contribution is examined here in order to find which current contributes the most to c_{s}. Chronoamperometric curves were calculated using Equations (2.2.1), (2.2.4), and (2.2.5) for our experimental values of c^*, D, λ and μ, where the gamma functions were evaluated with the use of the approximate Eq. (6.1.35) in [5]. They are shown in Fig.2.6.A, and the Cottrell plots (I vs. $t^{-1/2}$) are shown in Fig.2.6.B. The lower deviation of the current, $I_{\mathrm{C}} - I_{\mathrm{rx}}$, from the Cottrell equation is noticeable at a time shorter than 0.1 s ($t^{-1/2} > 3$ in Fig.2.6.B) and is a kinetic effect. The time-dependent current must include the DLC current (c). The observed current, $I_{\mathrm{C}} - I_{\mathrm{rx}} + I_{\mathrm{EDL}}$, is predicted to be curved (d), which is close to the Cottrell equation without the capacitive current. When c^* is less than 0.1 mM, values of $I_{\mathrm{C}} - I_{\mathrm{rx}}$ are close to those of I_{EDL}. Thus, pulse voltammetric currents for low redox concentrations always suffer from capacitive currents [6,7,8].

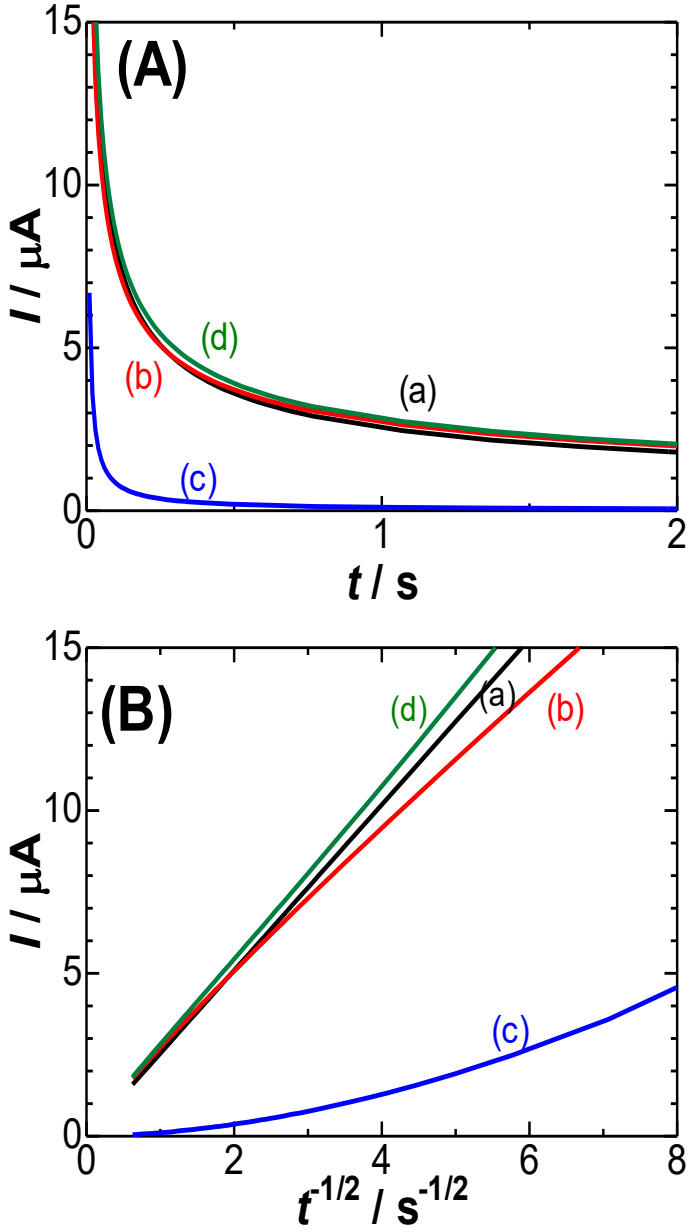

Fig.2.6 Chronoamperometric curves (**A**) and their variations with $t^{-1/2}$ (**B**) for (a) I_C, (b) $I_C - I_{rx}$, (c) I_{EDL}, (d) $I_C - I_{rx} + I_{EDL}$, calculated from Equations (1), (4) and (5) at c^* = 1 mM, $D = 0.7\times10^{-5}$ cm^2 s^{-1}, $\mu = 0.1$, $\lambda = 0.1$, $V = 0.2$ V, $C_{1s} = 30$ μF cm^{-2}, $C_{rx} = 70$ μF cm^{-2} and the electrode area 1.77 mm^2.

It is interesting to compare negative capacitance with Butler-Volmer kinetics, which is expressed in chronoamperometry as [9,10] :

$$j_{BV} = c^* F D^{1/2} \Lambda \exp(\Lambda^2 t)\,\mathrm{erfc}\left(\Lambda t^{\frac{1}{2}}\right) \qquad (2.2.7)$$

where,

$$\Lambda = k_0 D^{-1/2}\{\exp[\beta(E_{\mathrm{dc}} - E^0 F/RT)] + \exp[-\alpha(E_{\mathrm{dc}} - E^0 F/RT)]\} \quad (2.2.8)$$

Here, k^0 is the standard rate constant for the charge transfer reaction, and α and β are the cathodic and anodic transfer coefficients, respectively. Fig.2.7 shows (A) Cottrell plots and (B) their logarithmic plots calculated using Equation (2.2.3) and BV kinetics for three values of $E_{\mathrm{dc}} - E^0$. The Cottrell plots for BV kinetics exhibit a nonlinear shape for $E_{\mathrm{dc}} - E^0 < 0.10$ V, while those for negative capacitance fall on each line with almost zero intercepts. These two kinds of kinetics can be distinguished from the logarithmic plots more clearly than from the Cottrell plots at the two points: (i) the plotted lines for negative capacitance are shown, and (ii) the slopes of the lines are independent of E_{dc}.

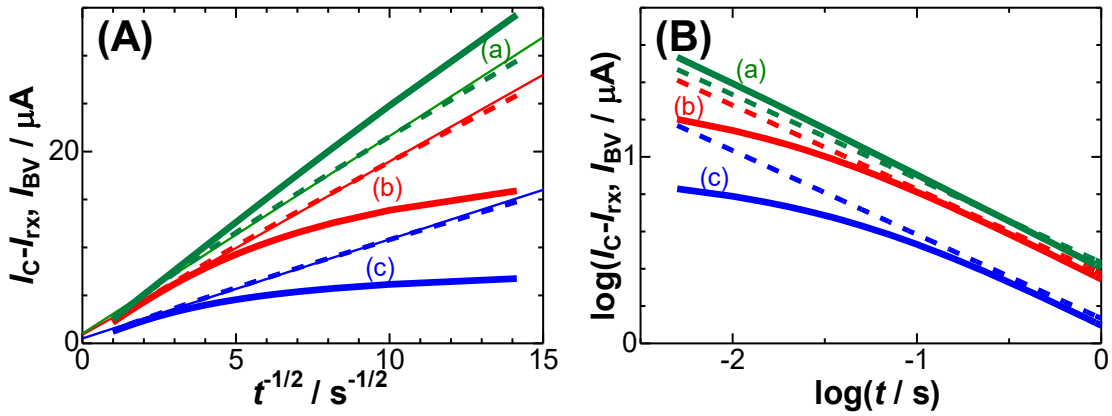

Fig.2.7 Variations of (**A**) I_{BV} (bold solid curves) and $I_{\mathrm{C}} - I_{\mathrm{rx}}$ (dashed curves) with $t^{-1/2}$ for $E_{\mathrm{dc}} - E^0$ = (a) 0.15, (b) 0.05 and (c) 0.0 V, and (**B**) their logarithmic plots when k_0 = 0.005 cm s^{-1}, $\alpha = \beta = 0.5$.

Chapter 3

A Single Faradaic Reaction as the Oxidation of $FcTMA^+$ by Fast-Scan Cyclic Voltammetry Method

3.1 Motivation

A fundamental parameter in faradaic impedance, R_{ct}, represents the resistance to electron transfer at the electrode|solution interface and serves as an indicator of the rate of heterogeneous reactions, k_0, as mentioned in Chapter 1. Theoretical estimates of k_0 can be derived by analyzing Nyquist plots showing faradaic responses at high frequencies, where the plot typically exhibits a semi-circle [11,12,13]. The diameter of this semi-circle can be used to calculate the value of k_0. However, experimental results for species undergoing extremely fast electron transfers did not display a semi-circle [14,15], indicating that the AC impedance method has limitations in assessing k_0. Hence, considering alternative electrochemical measurement methods is necessary.

Fast-scan cyclic voltammetry allows for rapid response measurements of current within ms and is employed to determine rates of heterogeneous reactions [16,17,18,19,20] and to detect intermediates involved in electrode kinetics [21]. As the scan rate v increases, so does the voltammetric current, because both the diffusion current and adsorption current are proportional to

$v^{1/2}$ and v, respectively. The fast-scan voltammograms obtained at very high scan rates are complex and may include:

A) Slow charge transfer reaction rates, B) Peak potential shifts caused by solution resistance, C) Delays in electrochemical equipment, and D) EDL currents. This research work conducts a qualitative study based on the dependencies of peak current, I_p, and peak potential, E_p on v, addressing the aforementioned factors.

For A), Professor Matsuda previously derived mathematical expressions for charge transfer kinetics [22]. When the mass transfer coefficient is 0.5, the kinetically controlled current decreases, and the peak potential changes linearly with log$v$.

For B), the solution resistance, R_s, causes deviations in peak potential due to ohmic drops, significantly reducing the time-correspondent, I_pR_s/v, resulting in I_p derivated from the proportional curve with $v^{1/2}$. Subsequently, the peak current empirically correlates linearly with E_p [23].

For C), An instrumental delay is revealed in the depression of observed currents at a short time, which can be estimated using virtual electric circuits.

For D), EDL current is always involved in the observed current and is generally proportional to the v. As the increase in v, the rapid rise in EDL current blurs the peak shape. This effect is opposite to those of A) and B). In summary, (B) and (C) underestimate the observed currents, whereas (D) overestimates. (A) is not necessary to be earnestly considered unless a rate constant can be obtained by ultramicroelectrode voltammetry. However, the effect of heterogeneous reactions is important historically.

As observed in the faradaic currents of ferrocene compounds [15], anodic [24] and cathodic stripping voltammetry [25]results for adsorbed silver ions show that capacitive currents are suppressed due to the rapid formation of redox dipoles, known as the NC effect [26], which is similar to effects A), B), and C). Considering short time scales as equivalent to high scan rates and differentiating these factors by measuring diffusion-controlled ferrocene derivative species at high scan rates, it is predicted that the observed current at high scan rates should be less than the theoretical diffusion-controlled current. Specifically, using fine-wire microelectrodes not only reduces the current to a few microamperes but also prevents floating capacitance at the boundary of an electrode and an insulation wall. Finally, the measured results are compared with BV kinetic outcomes to elucidate the reasons for limitations in assessing k_0.

3.2 Experimental

The electrochemical solution here had varying concentrations of (ferrocenylmethyl)trimethyl ammonium ($FcTMA^+$) and 0.1 M (M= mol dm^{-3}) KCl. All of the chemicals were analytical grade, and the water was distilled and deionized.

A delay of the potentiostat, Compactstat by Ivium (Netherlands), was investigated by employing a dummy cell with a carbon resistance of 1 kΩ and applying cyclic voltammetry in the voltage domain of 1 V. The maximum variation in current between the forward and reverse scans was 3% at 8 kV s^{-1}. Our voltammetry for $FcTMA^+$ was performed at scan rates

of less than 7 kV s^{-1}.

The working electrode was a 30 μm platinum wire in diameter. The tip was put into the solution about 1 mm. The precise length was determined using an optical microscope. The electrode was processed by immersing it in a mixture of 0.26 M acetic acid, 0.33 M nitric acid, and 0.73 M phosphoric acid for 1 minute. The reference and the counter electrodes were Ag|AgCl(1 M KCl) and platinum coil, respectively. The normal-sized Pt electrode (1.6 mm in diameter) was used for fast scan voltammetry by activating the positive feedback at selected values of the variable resistance. The resistance values not only altered peak currents and peak potentials but also deformed the voltammograms. Therefore, the *IR*-compensation was not useful for the present work.

3.3 Results and Discussion

Cyclic voltammograms at several scan rates have been displayed in Fig. 3.1 in the aqueous solution of 1.0 mM $FcTMA^+$ (M = mol dm^{-3}) + 0.1 M KCl at the thin wire platinum electrode. Since the solution resistance was at least 50 Ω based on ac-impedance techniques, the *IR*-drop (< 0.1 mV) for all peak currents of less than 2 μA could be ignored. The voltammograms at slow scan rates are close to the steady-state or sigmoidal (a) in Fig.3.1), characterizing the cylindrically diffusion-controlled voltammogram [27]. Peak potential changed at slow rates in the backward direction ((a) to (b)) as a result of increasing scan rates, and at fast scan rates in the forward direction ((b) to (d)). The former shift is in accord with the theoretical estimation [27],

whereas the latter is close to the behavior of the heterogeneous kinetic control. The background current (c') has no effect obviously on the redox components (c).

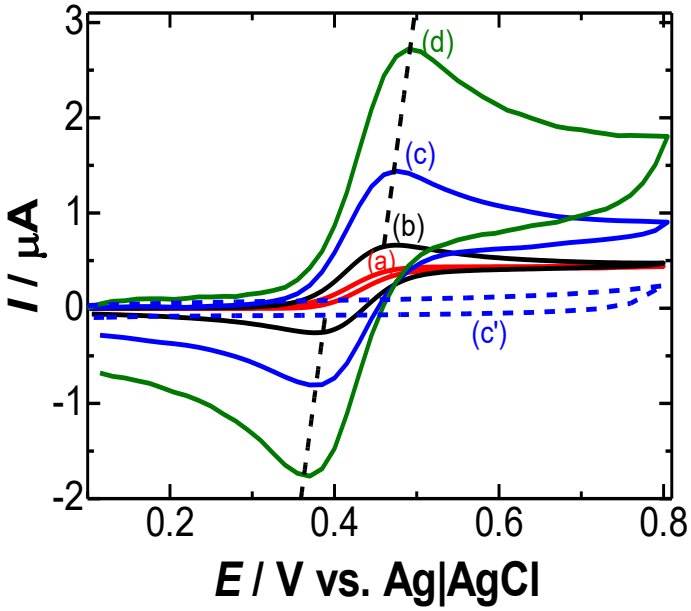

Fig.3.1 Voltammograms in 1.0 mM $FcTMA^+$ + 0.1 M KCl at the Pt wire 30 μm in diameter 1 mm in length at scan rates of (a) 0.01, (b) 0.1, (c) 1.0 and (d) 4.0 V s^{-1}. (c') is the background voltammogram for (c).

Fig.3.2 shows a variation of the peak currents with $v^{1/2}$, exhibiting a line-like convex curve without passing through the origin. This variation is different from the diffusion-controlled peak current at a planar electrode, which is proportional to $v^{1/2}$ (passing through the origin). We shall take into account the presence of the extrapolated line's intercept in addition to the convex curve. The expression for the peak current at a cylindrical electrode is given by Ref. [27]:

$$I_p = (AFc^*D/a)[0.446(Fv/RTD)^{1/2}a + 0.335(Fv/RTD)^{0.075}a^{0.15}] \quad (3.1)$$

where A is the geometrical area of the wire electrode, c^* is the bulk concentration of the redox species, F is Faraday's constant, R is the gas constant, T is the temperature, and a is the radius of the cylindrical electrode. Under our experimental conditions, the dimensionless peak current, $I_p/(AFc^*Da^{-1})$, as calculated from Eq. (3.1) has an essentially linear relationship on $v^{1/2}$ for values of a and D, as shown in the inset of Fig. 3.2. Along the plots of the experimental data at the lower scan rates, we draw an extrapolated line, the intercept of which is designated as I_{p0}. The intercept should be apparent due to the visual extrapolation and may tend to zero current at quite slow scan rates, as can be seen in the inset. The physical appearance of the convex form is what interests us, not the intercept.

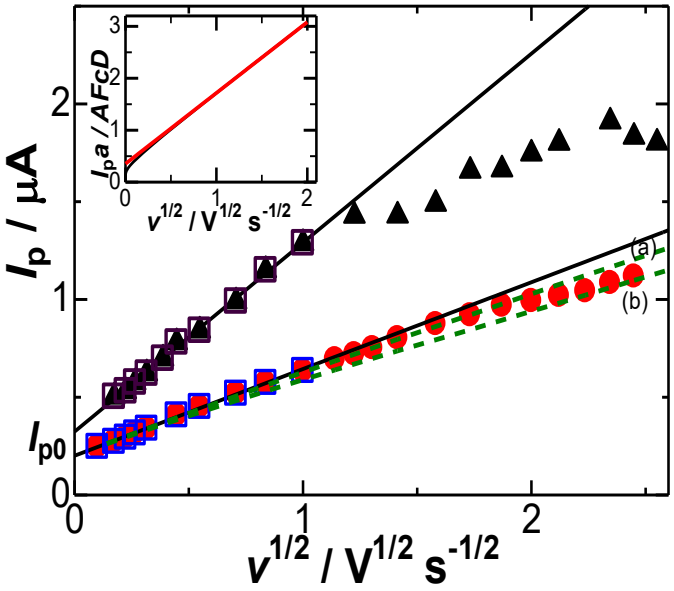

Fig.3.2 Variation of the peak currents with $v^{1/2}$ at the cylindrical Pt electrode 1 mm in length in the aqueous solution of (●) 1 mM $FcTMA^+$ + 0.1 M KCl and (▲) 2 mM $FcTMA^+$ + 0.1 M KCl. Lines were drawn for the square-marked points. The dimensionless currents in the inset was calculated from Eq. (3.1) for $2a$ = 30 μm, c^* = 1 mM, $D = 10^{-5}$ cm^2 s^{-1}. Dashed curves are theoretical ones calculated [28] for k_0 = (a) 0.05 cm s^{-1} and (b) 0.01 cm s^{-1}, respectively, and the transfer coefficient α = 0.5.

Interestingly, the BV-type kinetics causes the downward deviation from the proportionality of I_p vs. $v^{1/2}$ with an increase in v [22]. Additionally, I_p vs. $v^{1/2}$ curves for values of the heterogeneous rate constants, k_0 that comprise the experimental values for 1 mM $FcTMA^+$ are shown in Fig.3.2, which are covered by using the analytical equation [28] at the transfer coefficient, α of 0.5.

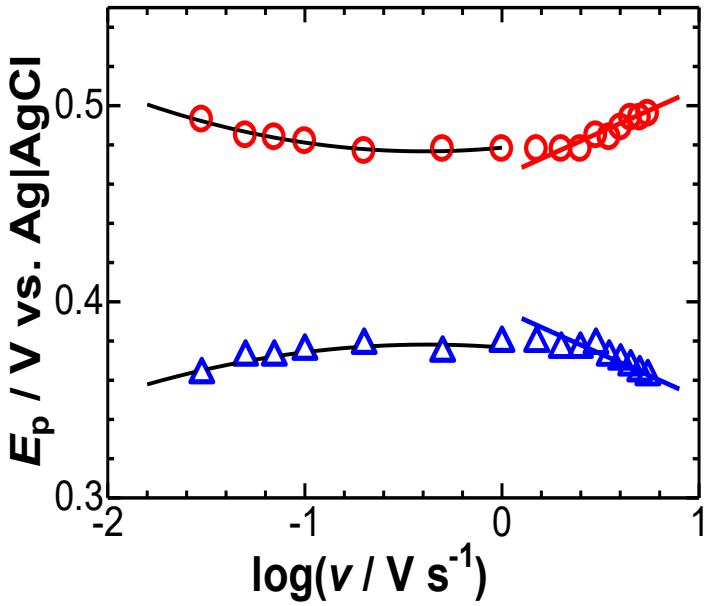

Fig.3.3 Dependence of the peak potentials under the conditions in Fig.3.2 for c^* = 1 mM on the logarithms of the scan rates for (○) the oxidation and (△) the reduction.

The experimental variation of I_p (circles) with $v^{1/2}$ is different from the theoretical one in that the disagreement of I_p at fast scan rates was found for any value of the rate constants. The plots for high concentration (triangles) also cannot be fitted to any theoretical curve. The charge transfer reaction rate constant at 1 nm electrode is larger than 10 cm s^{-1}, which corresponds to v = 21 MV s^{-1} at a large electrode [29], as we have demonstrated based on the invariance of the half-wave potential shift of steady-state voltammograms of $FcTMA^+$ to radii of nanodisk electrodes [29]. Thus, the

convex curve in Fig.3.2 cannot be caused by the charge transfer kinetics.

Examining the relationship between the peak potential and scan rates will yield more convincing proof. Fig.3.3 shows variations of the anodic and the cathodic peak potentials, E_p, with the logarithms of the scan rates. The peak potentials at $v < 30$ mV s^{-1} ($\log(v$ /V $s^{-1}) < -1.5$) were vague because of the steady state-like wave form. The difference between the anodic and the cathodic potentials decreased with an increase in v until 1 V s^{-1} owing to the contribution of cylindrical diffusion [27]. For both the reduction and the oxidation waves, a further rise in v shows linear relationships in E_p vs log v. Values of the slopes for the oxidation and the reduction were (55 ± 15) mV and (−52 ± 13) mV, respectively. These are close to the frequently observed potential shift, ± 2.3RT/F (= 60 mV). The slopes for the oxidation and reduction, where α is the transfer coefficient, should be 2.3$RT/\alpha F$ and −2.3$RT/(1-\alpha)F$, respectively, if the slope were brought on by a slow heterogeneous rate. These values are 60 mV and −60 mV, respectively, for the transfer coefficient 0.5. However, the BV heterogeneous kinetics provides the values of the transfer coefficient are diverse. It can be proved the peak potential shift is not caused by the heterogeneous kinetics (effect (A)) from the viewpoint of the kinetic potential shift.

The potential shift by the *IR*-drop (effect (B)), which causes a downward deviation of the peak current from the predicted diffusion current, can be neglected owing to the peak currents as low as 1 μA. The delay of the potentiostat (effect (C)) has demonstrated not to influence the lower deviation of the currents by seeing the experimental section.

The other possibility of the downward deviation is the contribution of the NC associated with the redox reaction [14,15,24,25]. It is based on the concept of the formation of NC, as the Chapter 1,2 of this thesis. It is primitively assumed that the cylindrical diffusion current for $v > 10$ mV s^{-1} can be approximated as a sum of the linear diffusion current and a constant, I_{p0}, empirically supported by experimental results (Fig.3.2). Since the observed peak current includes the NC current, it is represented by

$$I_p = I_{diff} + I_{p0} - I_{rx} = 0.446AFc^*D(Fv/RTD)^{1/2} + I_{p0} - C_{rx}v \quad (3.2)$$

where $-C_{rx}$ is the NC and the detail of the subscript rx in C_{rx} means a source of the redox reaction such as $FcTMA^+|FcTMA^{2+}$. Then, Eq. (3.2) can be rewritten as:

$$(I_p - I_{p0})\, v^{-1/2} = 0.446AFc^*D(F/RTD)^{1/2} + C_{rx}v^{1/2} \quad (3.3)$$

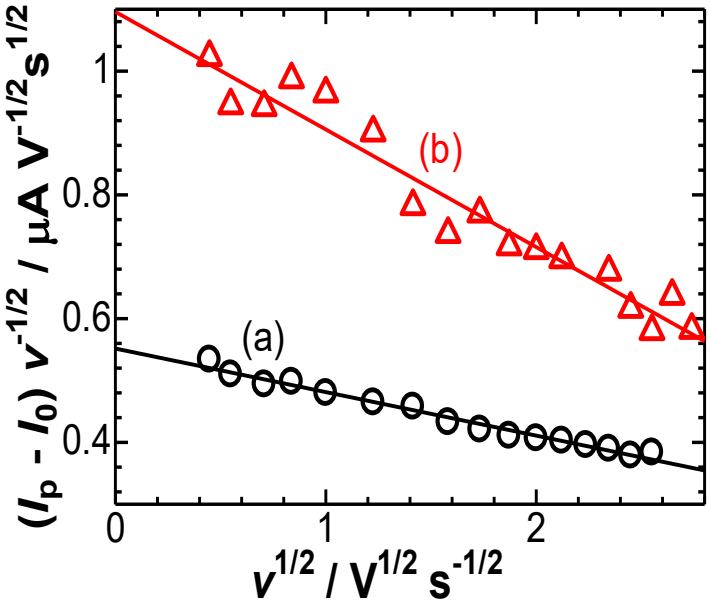

Fig.3.4 Variation of $(I_p - I_{p0})\, v^{-1/2}$ with $v^{1/2}$ (a) for [$FcTMA^+$]= 1 mM and (b) 2 mM in 0.1 M KCl solution.

The plots of $(I - I_{p0})\, v^{-1/2}$ against $v^{1/2}$ are displayed in Fig.3.4, where a

line that was expected from Eq (3.3) was seen. It is implied by the negative slope that a NC is appropriate. Values of $-C_{rx}$ were determined for some areas (0.1-0.3 mm^2) of cylindrical electrodes to be $-$ (64 ± 8) μF cm^{-2} for c^* = 1 mM, where the error is the standard deviation. The average negative value is twice the EDLC at platinum electrodes in aqueous solutions [2,3]. As such, its magnitude is greater than that of traditional EDLCs.

Values of the NC were roughly linear to concentrations of $FcTMA^+$ in the domain from 1 mM to 3 mM, as shown in Fig.3.5. This variation has been demonstrated for the capacitance values by AC-impedance techniques [15]. The linearity indicates that NC should be caused by the redox reaction. No capacitance value at c^* = 0.5 mM was determined unequivocally. The appearance of the intercept in Fig.3.5 indicates that EDLC by solvent dipoles

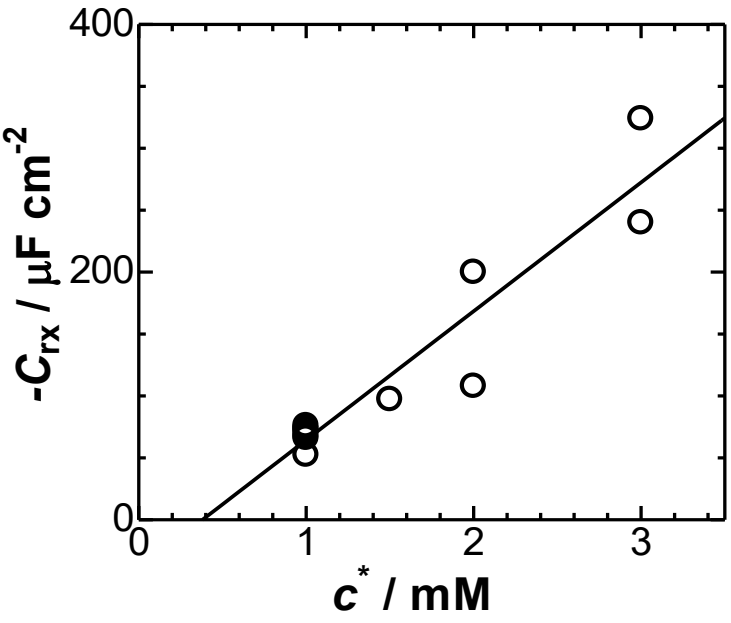

Fig.3.5 Variation of the NC with the concentrations of $FcTMA^+$.

is predominant to the redox capacitance.

3.4 Conclusive and Remarks

The peak currents in the cyclic voltammograms for the redox couple, $FcTMA^{+}|FcTMA^{2+}$, showed a linear relationship with the square of the scan rate in the low scan rate domain, indicating that the current is diffusion-controlled. At higher scan rates, the peak currents were less than the theoretical ones. Additionally, the peak potential shifted and showed a linear relationship with the logarithm of the scan rate, which was not caused by solution-resistance effects. This can be explained by the NC currents rather than heterogenous charge transfer kinetics.

Capacitive currents result from the dynamic formation of redox charges, which inhibits the faradaic reaction as if suppressing the external electric field. This behavior is inconsistent with the conventional concept of the independence between the capacitance and faradaic reactions, but is consistent with the thermodynamic rule of evolution towards the lowest energy state. Ultimately, the observed capacitive values caused by the faradaic reaction are contrary to the EDLCs, which are suppressed by the orientation of solvent dipoles to inhibit the electric field.

Chapter 4

Reduction of Hydrogen Ions by means of Fast-Scan Cyclic Voltammetry

4.1 Motivation

The electrochemical evolution of hydrogen gas is a key technique for replacing fossil-based transportation fuels [30,31,32]. It offers economic advantages such as (a) producing pure hydrogen, (b) portability when combined with solar cells, and (c) on-demand generation capabilities. However, the reaction is complex due to kinetic barriers associated with activation, and its heterogeneous rate depends on the electrode materials [33,34]and catalysts used [35,36]. The activation involved is equivalent to the irreversibility of the reaction:

$$2H^+ + 2e^- \leftrightarrow H_2 \qquad (4.1)$$

The key steps reported in the process are [37,38,39,40,41,42]:

$H_2O + e^- \leftrightarrow H_{ad} + OH^-$ (Volmer step)

$2H_{ad} \leftrightarrow H_2$ (Tafel step)

$H_{ad} + H_2O + e^- \leftrightarrow H_2 + OH^-$ (Heyrovsky step)

Here, H_{ad} represents the hydrogen atom adsorbed on an electrode. Currently, there is some disagreement in the literature regarding the proposed mechanisms [43,44,45,46]. These models are primarily based on the analysis

of almost steady-state current-voltage curves [43,47,48,49,50], which fortunately block electrode reactions due to the formation of gas phases. To circumvent the blocking effect, it is essential to measure currents at a short time before the formation of the gas phase. Short-time responses have complicated the voltammetric studies on the reduction of H^+ [44,51]and the oxidation of H_2 [52], due to their involvement in capacitive effects.

Adsorption can be detected and analyzed using fast-scan cyclic voltammetry by leveraging the proportionality of the absorbed current to scan rates. However, it faces drawbacks such as the deformation of voltammograms caused by solution resistance at enhanced currents and by capacitive currents of EDL. There is another source of capacitive current caused by faradaic reactions, which suppresses the faradaic current [14,15115,25]. We address these drawbacks individually. *IR* drop can be minimized by reducing observed currents to less than 10 μA using microelectrodes even at fast scan rates. A boundary between a micro-electrode and an insulator can cause large floating capacitance, interfering with accurate measurements of faradaic currents during short-time responses. Since a thin wire electrode has no boundary with an insulator, it does not suffer from capacitive currents at high scan rates. This enables us to conduct fast-scan cyclic voltammetry of H^+ without *IR* drop or floating capacitive currents, as evidenced by previous work at scan rates over 1 V s^{-1}.[53,54] Here, we perform fast-scan cyclic voltammetry of reduction of H^+ at a Pt wire electrode 30 μA in diameter for scan rates ranging from 0.01 to 8 V s^{-1} in solutions with various concentrations of HCl less than 5 mM. A key

objective is to identify adsorption species and evaluate their amounts in the context of NC. The observed behaviors may be valuable for the development of industrial hydrogen gas generation and/or fuel cells.

4.2 Experimental

The test solution comprised various concentrations of hydrochloric acid and 0.5 M (M = mol dm^{-3}) KCl. A commercially concentration-calibrated HCl solution (Fuji Film, Osaka) was used. All the chemicals were of analytical grade, and water was distilled and deionized. The diluted concentration of HCl was confirmed to agree almost with the measured value of pH.

The performance of the potentiostat, Compactstat by Ivium (Netherlands), especially a delay was examined by using a carbon resistance of 1 kΩ for a dummy cell, to which cyclic voltammetry was applied in the voltage domain of 1 V. The maximum difference in the currents at the forward and the reverse scan was 3% at 8 V s^{-1}.

The working electrode was a platinum wire 30 μm in diameter. The tip was inserted into the solution by a given length (1 mm) of which value was measured with an optical microscope. This length had no effect on complications at the wire|solution|air interface. The active area of the electrode was 0.095 mm^2. The electrode was pretreated by being soaked in the mixed acid (0.26 M acetic acid + 0.33 M nitric acid + 0.73 M phosphoric acid) for 1 min. The reference and the counter electrodes were Ag|AgCl (sat. KCl) and platinum coil, respectively. The potential scale of the

voltammograms presented here was represented as a standard of NHE. A commercially available platinum disk electrode 1.6 mm in diameter (BAS, Tokyo) was used for steady-state voltammetry.

The solution resistance was evaluated using ACimpedance to be ca. 250 Ω. This value was negligible in terms of its impact on the voltammograms distortion from the viewpoint of the *IR* drop when currents were below 8 μA in magnitude.

4.3 Results and Discussion

Fig.4.1 shows voltammograms of the deaerated solution of 1.0 mM HCl at the 1.6 mm Pt disk electrode for several scan rates, v, with the scan staring at 0.40 V vs. Ag|AgCl. The voltammogram at v = 0.01 V s^{-1} exhibited the

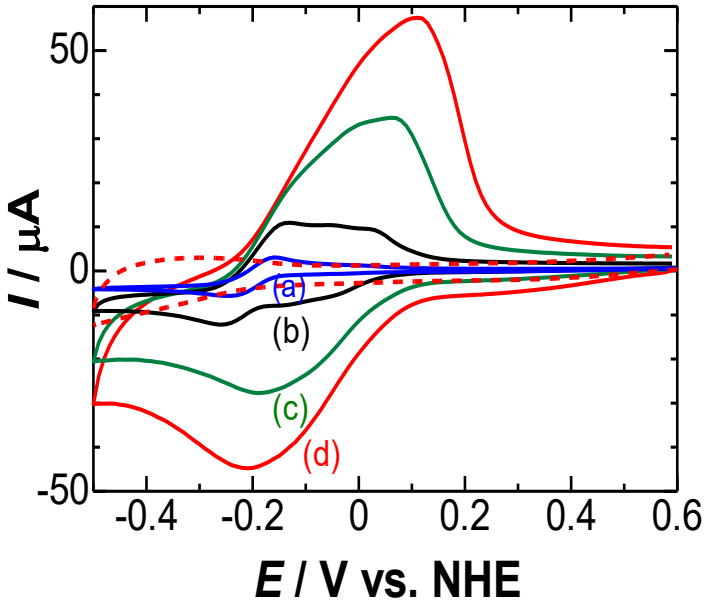

Fig.4.1 Voltammograms of 1.0 mM HCl + 0.5 M KCl solution at the Pt disk electrode 1.6 mm in diameter for v = (a) 0.01, (b) 0.1, (c) 0.5 and (d) 1.0 V s^{-1}. The dotted wave is in 0.5 M KCl solution at v = 1.0 V s^{-1}.

reduction peak at −0.23 V vs. NHE and the oxidation peak at −0.16V. Since

the mid potential, −0.19 V, is close to {0 + 0.06 log[HCl]} V = −0.18 V vs. NHE, and hence the waves may be attributed to Reaction (4.1). In contrast, scan rates higher than 0.1 V s^{-1} made the voltammograms be complicated with waves at more positive potentials. Peak currents at v > 1.0 V s^{-1} were over 50 μA, resulting in potential shifted owing to the *IR*-drop. Therefore, we used a thin wire electrode 30 μm in diameter in order to ignore the *IR*-drop effect. Two peaks of voltammograms reported so far at highly acidic concentrations correspond to the voltammograms in Fig.4.1 (a) or (b). There is no effect of chloride ion on the redox reactions, as shown for the dotted wave of Fig.4.1 in only 0.5 M KCl solution.

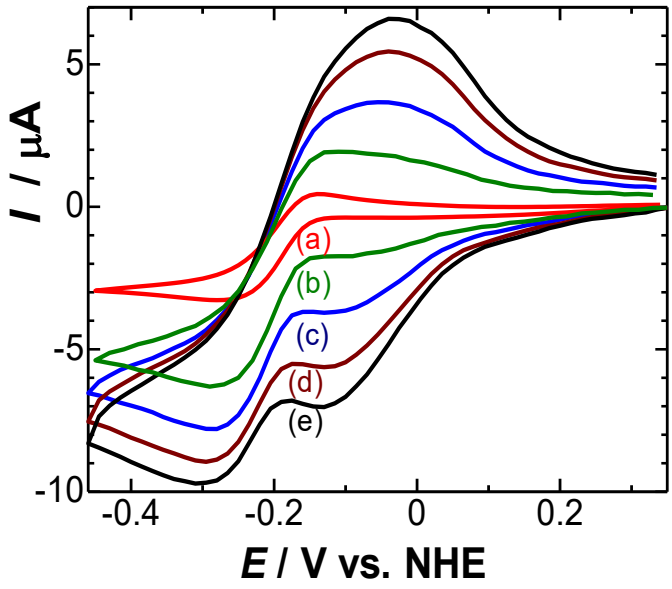

Fig.4.2 Voltammograms of 1.37 mM HCl + 0.5 M KCl solution at the Pt wire electrode for v = (a) 0.1, (b) 2, (c) 4, (d) 6 and (e) 8 V s^{-1}.

Voltammograms at several scan rates at the Pt wire electrode are displayed in Fig.4.2. Since the maximum peak current at v < 8 V s^{-1} was less than 10 μA in magnitude, the *IR* drop distortion of the voltammograms can

be disregarded. There appeared two reduction waves at $v > 1$ V s^{-1} and one oxidation wave for any scan rate. The first reduction wave was not clearly defined for $v < 0.2$ V s^{-1}. However, it was identified for $v > 1$ V s^{-1}. A diffusion tail-like drawn out of the second wave was seen. In contrast, the oxidation wave peaked and then became less intense as the voltage increased.

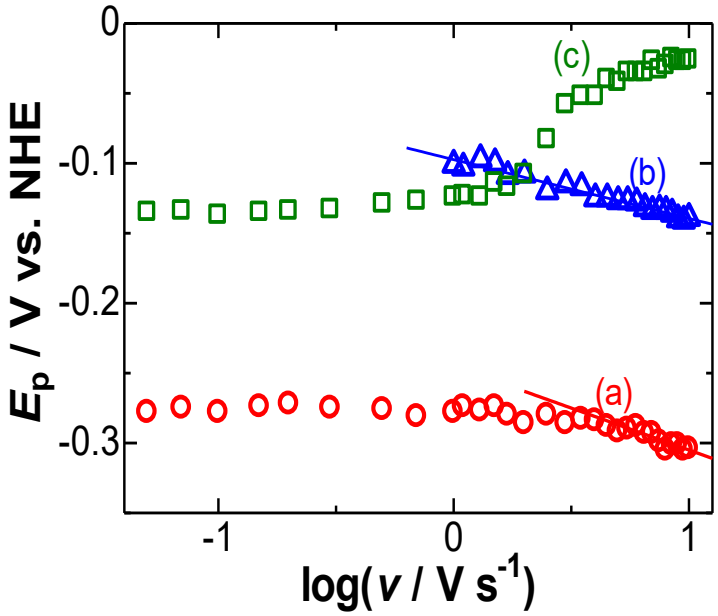

Fig.4.3 Scan rate dependence of the peak potentials of (b) the first and (a) the second reduction waves and (c) the oxidation wave at the 30 μm wire electrode.

A plot of the peak potentials, E_p, versus logarithmic scan rates, as seen in Fig.4.3, which are used to specify a voltammetric characteristic. The values of E_p both for the reduction of the oxidation waves remain constant for $v < 2$ V s^{-1}, indicating the lack of kinetic complications. For $v < 1$ V s^{-1}, no peak of the first reduction wave (b) was observed. E_p of the second reduction peaks (a) was shifted linearly with log v for $v > 3$ V s^{-1}, exhibiting the slope, −60 mV, which will be covered subsequently concerning the NC

later. The shift of the oxidation (c) for $v > 2$ V s^{-1} is caused by the participation in the reaction relevant to the first reduction wave. Confirmation of the rate-determining step needs quantitative analysis of variations of peak currents with the scan rates.

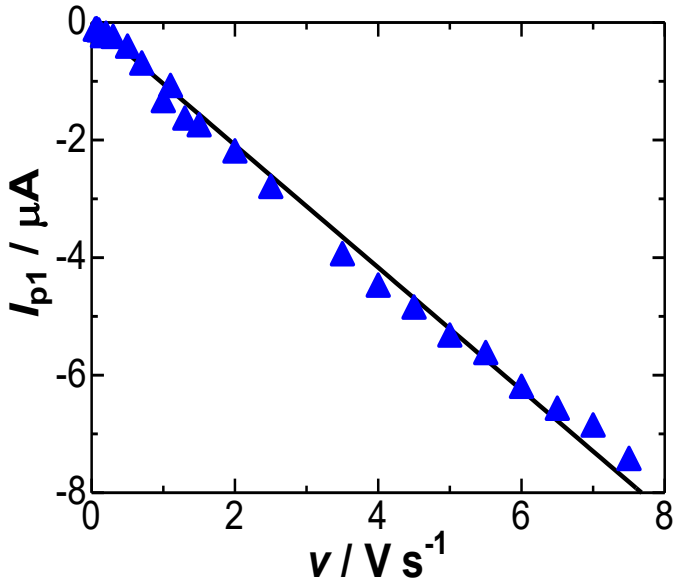

Fig.4.4 Scan rate dependence of I_{p1}(wire) at the wire electrode in 1.46 mM HCl + 0.5 M KCl solution.

Here we denoted the reduction peak currents for the Pt wire electrode at the first and the second wave as I_{p1} and I_{p2}, respectively. Fig.4.4 shows the variation of I_{p1}(wire) with v, exhibiting the proportionality. Therefore, the first reduction wave should be attributed to the reduction of adsorbed species. Since the peak current was independent of HCl concentrations above 1 mM, it may be caused by the saturation of the adsorbate. Assuming no interaction among the adsorbates, the peak current density is expressed by $j_p = F^2\Gamma v/4RT$, where Γ is the surface concentration, F is the Faraday constant, R is the rate constant and T is the room temperature. The proportionality constant from

the plot of j_p versus v yields $\Gamma = 1.2\times10^{-9}$ mol cm^{-2} or (0.38 nm)^2 per adsorbate, which is close to the density for monolayer adsorption. Since this value includes the charge by the NC as has been observed for adsorbed species at stripping voltammetry [24,25], the net redox charge should be less than this value. When the species to be reduced is adsorbed before the voltage scan to the negative, the adsorbate should be hydrogen ion, H_{ad}^+, rather than H_{ad}. Although our detection appears similar to the Volmer Step ($H^+ + e^- \leftrightarrow H_{ad}$), the difference lies in the charged state (H_{ad}^+) of the adsorbate.

By letting the hydrogen ion in the solution take the form of a hydronium ion (H_3O^+), the reduction involving the adsorption is written as:

$$H_3O^+ \rightarrow H_2O + H_{ad}^+,\ H_{ad}^+ + e^- \rightarrow H_{ad} \qquad (4.3.2)$$

Since H_{ad}^+ is saturated on the electrode as demonstrated by the invariance of the peak currents to the bulk concentration of H^+ (c_b), [H_{ad}^+] is much higher than c_b. The Nernst equation describes that the reduction potential of H_{ad}^+ is shifted in the positive direction by 0.059 log([H_{ad}^+]) V. The potential shift of the first wave from the second one, −0.14−(−0.28) V in Fig.4.3, may be caused by the enhancement of [H_{ad}^+]. Therefore, we have

$$-0.14 - (-0.28)\ \text{V} = 0.059\ \log([H_{ad}^+]/c_b)\ \text{V} \qquad (4.3.3)$$

Then we can estimate [H_{ad}^+] = 0.34 M. This value is equivalent to 1×10^{-10} mol cm^{-2} or (1.7 nm)^2 per H_{ad}^+ on the electrode. This surface concentration smaller by one order in Fig.4.4 can be attributed to the drawn-out peak of the first wave (in Fig.4.2) owing to the adsorption of the reaction (4.3.2). A question is which chemical step H_{ad} can take after the reaction (4.3.2).

According to the Tafel step, two H_{ad} would be dimerized on an electrode to yield a hydrogen molecule. Since the generated H_2 is dispersed to the solution, H^+ should be supplied back from the solution by diffusion. As a result, the observed current should be diffusion control rather than adsorption-control. This logic is inconsistent with the experimental result of the absence of diffusion control at the first reduction. Therefore, the Tafel step in the Motivation as Section 4.1 does not occur at an electrode.

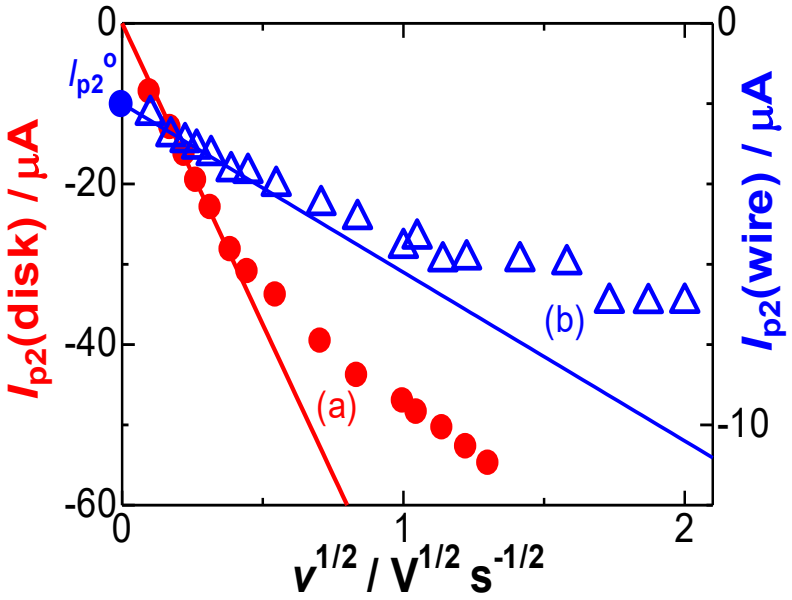

Fig.4.5 Variations of the peak currents, I_{p2}, at (a) the 1.6 mm disk and (b) the 30 μm wire electrode with $v^{1/2}$ in the solution of 1.37 mM HCl.

The dependence of I_{p2}(disk) at the 1.6 mm disk electrode on $v^{1/2}$ for slow scan rates is shown in Fig.4.5(a). The peak currents (a) were proportional to $v^{1/2}$ for $v < 0.15$ V s^{-1}, indicating a diffusion-controlled step. The slope was consistent with the value of $0.465F^{3/2}c^*(D/RT)^{1/2}$ for the diffusion current of the one-electron transfer reaction at $D = 9.3\times10^{-5}$ cm^2 s^{-1}, as predicted from reaction (4.1) per H^+. The lower deviation from the proportionality at $v >$

0.15 V s^{-1} may be ascribed to a contribution of the NC [53,54], which diminished I_{p2}(disk) at v = 1 V s^{-1} by 40%.

The peak current, $-I_{p2}$(wire), increased with $v^{1/2}$, as shown in Fig.4.4(b), but deviated below the line drawn for slow scans, exhibiting an intercept. The intercept, $I_{p2,0}$, should be caused by cylindrical diffusion under the quasi-steady state [27]. The lower deviation from the linearity can be attributed to the NC. Then the peak current is represented as [53]:

$$I_{p2} - I_{p2,0} = k_1 v^{1/2} + k_2 v \tag{4.3.4}$$

where k_1 is the contribution of linear diffusion, and k_2 is of the NC as $-C_{rx}$.

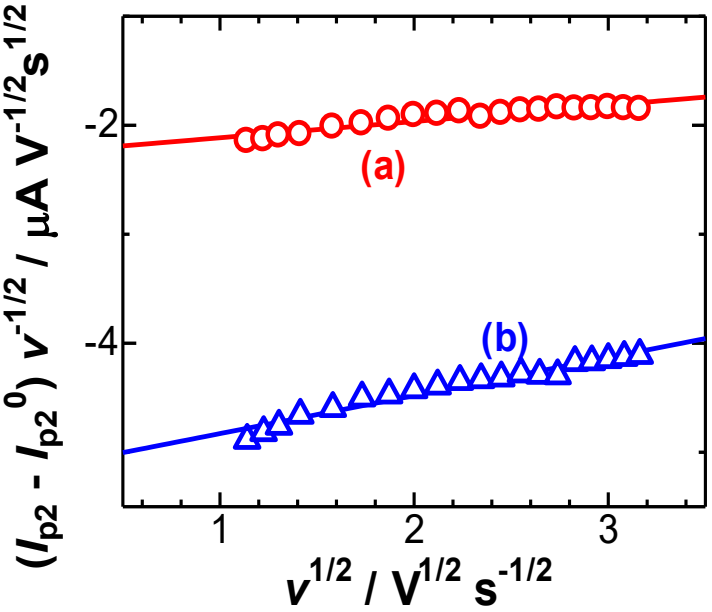

Fig.4.6 Variations of $(I_{p2}-I_{p2}^{o})v^{-1/2}$ with $v^{1/2}$ for (a) 1.0 mM and (b) 2.0 mM HCl solutions.

The plot of $(I_{p2}-I_{p2,0})v^{-1/2}$ against $v^{1/2}$ showed a linear relation, as demonstrated in Fig.4.6. Since the slope has a positive sign, the term k_2v ($=-C_{rx}v$) makes the negative values of the diffusion-controlled current large, where the subscript rx in C_{rx} means a source of the redox reaction. The value of k_2

at c_b = 1 mM is twice that at 2 mM. Twice the slope indicates that the NC should be associated with the reduction of H^+.

In terms of the dimension of $-C_{rx}v$, which is equal to the current, the physical meaning of $-C_{rx}$ is undoubtedly a NC. The capacitive current works as suppressing the redox current so that $I_{p2}C_{rx} > 0$. As seen in Fig.4.7(A), the dipole moment, $\boldsymbol{P}_s$ of a solvent molecule is oriented so that an applied electric field, $\boldsymbol{E}_1$ may decrease because of the amount proportional $\boldsymbol{P}_s$ when $\boldsymbol{E}_1$ is applied externally to an electrode|solution interface. Then, it is noticed that the measured capacitance rises by the permittivity amount or that the field intensity decreases by the inverse of the relative permittivity. When a field $\boldsymbol{E}_2$ large enough to cause an electrode reaction is applied to the interface, a charge at the electrode is transferred to the solution in an ionic form, as shown in Fig.4.7(B). The redox dipole moment $\boldsymbol{P}_r$ associated with a counterion is generated by the ion. Since the ion contacts the electrode at its moment of generation, the dipole is oriented in the same direction as $\boldsymbol{E}_2$. The observed field intensity is then enhanced by the amount linear to the $\boldsymbol{P}_r$. As a result, the construction of $\boldsymbol{P}_r$ reduced the EDLCs, making it appear as though a conventional EDLC would take a negative value. A hydrogen ion is accompanied by a counterion to form $\boldsymbol{P}_r$ to keep electric neutrality and reach the electrode just before the reduction in Fig.4.7(C). The difference between the two fields is $k\boldsymbol{P}_r$ ($k = 1/\varepsilon_o$), which is the same as the difference between (A) and (B), as the $\boldsymbol{P}_r$ is extinguished after the reduction (D).

The $\boldsymbol{P}_r$ is exhibited as a result of the charge transferred to the solution

to make the energetic gradient smooth. The smoothing is brought about generally by entropic dissipation. Therefore, the suppression of faradaic

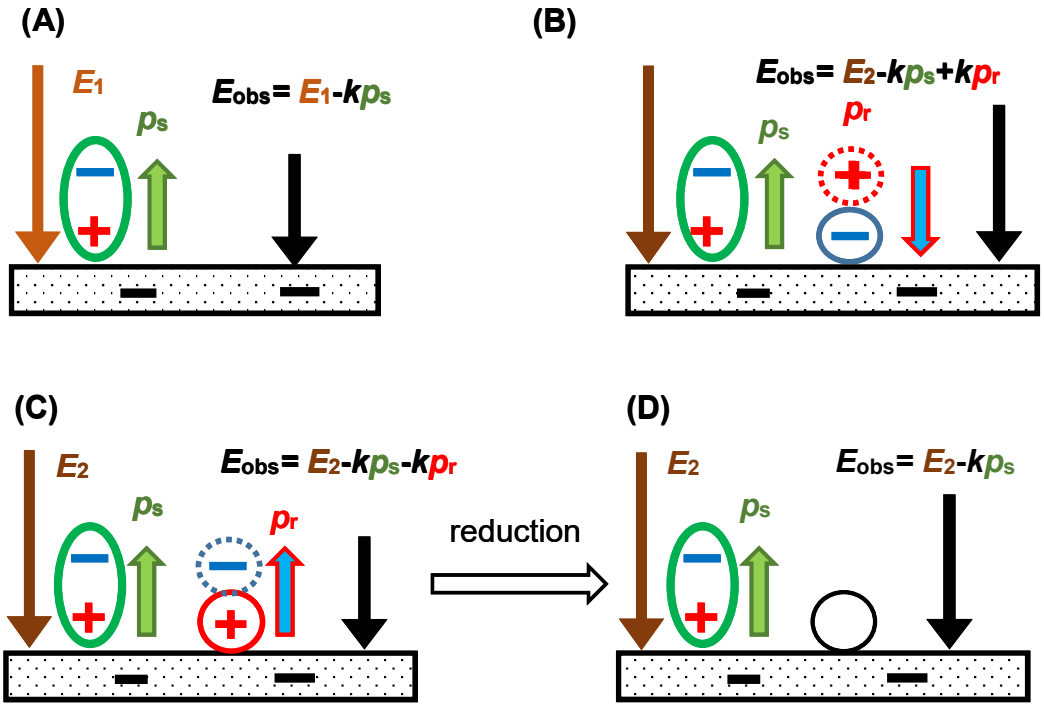

Fig.4.7 Illustration of the contribution of dipole moments of redox species to the effectively electric field (A) without redox reaction, (B) with the reduction, (C) with a hydrogen ion coupled with a counterion, and (D) after the reduction, where $k = 1/\varepsilon_0$.

currents by the NC is based on the thermodynamic principle. Since $k\boldsymbol{P}_r$ includes the electrode potential, its value may be proportional to $\log(c_b)$ as well as the logarithmic reduction current, as predicted from the Nernst equation. Then, the effective field, $\boldsymbol{E}_2 - k\boldsymbol{P}_s - \boldsymbol{P}_r$, in Fig.4.7(C) has been observed to be shifted logarithmically with v in Fig.4.3(a).

To verify if $-C_{rx}$ originates from reaction (4.3.1) or not, we assessed C_{rx} across various c_b values at the wire electrode. The voltammetric

characteristics observed were consistent with those shown in Fig.4.1 and 4.2. Variations of I_{p2} with $v^{1/2}$ were similar to those in Fig.4.5 and Fig.4.6. Fig.4.8 displays the dependence of C_{rx} thus obtained on c_b, indicating that C_{rx} should be caused by the reduction of H^+. This behavior has also been found in the last Chapter in (ferrocenylmethyl)trimethyl ammonium (denoted as $FcTMA^+$), as shown in Fig.4.8. The twice the value of slope H^+ species could be attributed to the variance in dipole intensity between H^+-Cl^- and Fc^+-Cl^-. Since the NC arises from the charge transfer reaction, it is not directly linked to a degree of adsorption. The slope value, 150 μF cm^{-2} mM $(H^+)^{-1}$ significantly exceeds the conventional EDLC values (ca. 30 μF cm^{-2}). Comparing these values without considering unit differences is not meaningful. The hydrogen bond exhibits the energy ten times larger than the field-orientation energy of water dipoles in EDLs. Therefore, only a small part of water dipoles can participate in the EDLCs. In contrast, all the reacting hydrogen ions on the electrode cause the NC with a minor effect on the hydrogen bond. The NC, akin to pseudocapacitance, is associated with faradaic reactions. However, as capacitive current inhibits faradaic currents, it is impractical for the development of energy storage.

There are some reports [55,56]on NC related to EDLs. A necessary condition of a NC is an enhancement of the applied field rather than a relaxation of the field. Since electrostatic interaction-driven adsorption serves as the relaxation, it fails to produce the NC. Potential origins of the NC include charge generation by faradaic reactions, by electromagnetic waves, by adsorption through chemical bonds, and also by turbulence flow.

We considered in this Chapter not only thermodynamics but also the kinetics effect of the reduction of hydrogen ions. Simply, although BV kinetics also deviates theoretically from the linearity of peak currents with $v^{1/2}$ and provides a linear potential shift with log(v) [4], it is not valid for real

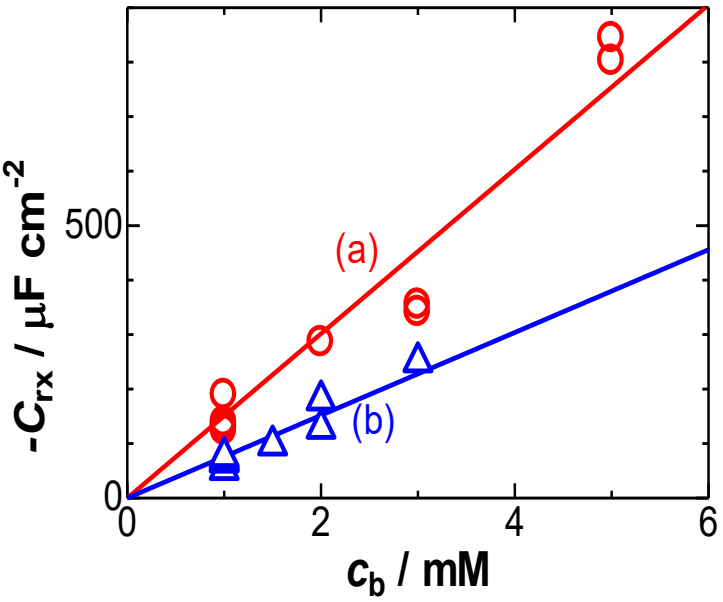

Fig.4.8 Variation of C_{rx} with bulk concentrations of (a) HCl and (b) FcTMA.

electrochemical reactions [57,58]. Our experimental results in Fig.4.3, 4.6, and 4.8 are inconsistent with the behavior complicated by the BV kinetics.

It is interesting to examine whether the present data are satisfied with the Heyrovsky step ($H_{ad} + H^+ + e^- \leftrightarrow H_2$) or not. The Heyrovsky step does not apply at the first reduction potential, as H_2 is not yet generated at this potential. If H_{ad} is alive at the second reduction potential, H^+ in the solution may react at the electrode to yield H_2 without inconsistency through the Heyrovsky step. However, at the second reduction potential, if H_{ad} persists, H^+ from the solution could feasibly react at the electrode to form H_2 via the Heyrovsky step without contradiction. A required condition is to keep the

generation of H_{ad} through reaction (4.2) during the formation of H_2. Given the high concentration of H_{ad} (0.34 M), the Heyrovsky step is likely to proceed readily, making it a plausible mechanism.

The oxidation of H_2 does not simply reverse the reduction of H^+, as suggested by the asymmetric voltammograms in Fig.4.1 and 4.2. The difference in peak potentials between the oxidation and reduction shown in Fig.4.3 indicates that oxidation does not proceed via a two-electron transfer step. Since the oxidation peak aligns closely with the potential of the first reduction peak for $H^+ + e^- \rightarrow H_{ad}$, the oxidation process involves the step of $H_{ad}\text{-}H_{ad} \rightarrow H_{ad}\text{-}H_{ad}^+ + e^-$. When H_{ad}^+ gets high enough density for the saturation density, it is desorbed into the solution, facilitating further oxidation of the remaining H_{ad}. Since a loss of H_{ad}^+ is compensated by diffusion from the solution, it can be used to explain why the oxidation peak currents were roughly proportional to $v^{1/2}$ at lower scan rates. The peak potential for $v > 2$ V s^{-1} was shifted positively with increasing in v as shown in Fig.4.3. This may be attributed to the kinetics of the desorption relevant to interaction among H_{ad}^+. It is difficult to analyze the oxidation voltammograms, partly because the certain concentration of reactant, H_2, depends on the reduction process and partly because a gas state of H_2, whether as bubbles or hydrated, remains unclear.

4.4 Conclusive and Remarks

The reduction peak current of H^+ to H_2 is composed of the diffusion

current proportional to $v^{1/2}$ and of the NC proportional to v. The observed current is smaller than the diffusion-controlled current by the capacitive contribution. Since the capacitance values are proportional to the concentration of H^+, they should be brought about with the redox reaction. They are twice the NC values of $FcTMA^+$. The NC causes the potential shift with v. Only the Heyrovsky step of the three suggested steps can be realized voltammetrically. This conclusion has not resulted from ambiguous potential shifts complicated by adsorption but has been done from the dependence of the peak currents on the scan rates. The reduction of H^+ to H_2 occurs as the second wave at the one-electron transfer reaction under the diffusion-control through the Heyrovsky step. In contrast, the adsorbed species H_{ad}^+ is reduced at the potential more positive than the equilibrium potential for H^+/H_2 because of adsorbed concentrations as high as 0.3 M of H_{ad}^+.

Chapter 5

Irreversible Oxidation of Hydroxide Ion in Light of Negative Capacitance

5.1 Motivation

Electrocatalytic water splitting is accompanied by the classical oxygen evolution reaction [59,60,61]. In alkaline solutions, dioxygen has been recognized as being a product of the reaction $4OH^- \rightarrow O_2 + 2H_2O + 4e^-$ [62,63]. The four-electrode transfer indicates that various steps involving unknown intermediates present some complications. On the other hand, there are occurrences of sluggish kinetics which consequently limit the overall rate of of oxygen generation. The complications can be partially overcome by the use of catalysts of Co_3O_4 [63] RuO_2 [64,65,66], and IrO_2.[67,68,69] in the structures of perovskite [70,71], spinel [72,73] and layers [74,75,76]. In contrast, a common dissolved intermediate like hydrogen peroxide [77,78], which may take other forms of radicals or anions, has been identified both spectroscopically and voltammetrically [79,80]. It suggests that the four-electron oxidation of hydroxide ions should be considered a highly significant overall reaction.

Intermediates can be detected or estimated electrochemically by analyzing rapid responses in cyclic voltammetry, often appearing as a new wave in a reverse scan [81]. However, electrochemical responses recorded

in a short time present certain challenges. These include rounded-off voltammograms due to delays of the potentiostat and contributions from EDLC currents and *IR*-drop. Unlike exponential decay, the EDLC currents are proportional to t^{-v} for $0.9 < v < 1$ [1,3,26], while faradaic currents relate to t^{-v} for $0 < v < 0.5$ [53]. Thus, the shorter time responses may lose accuracy in determining faradaic currents. Additionally, the enhancement of current at a short time can cause a potential shift due to solution resistance, affecting the control over the applied voltage.

The capacitive current arises not only from the EDLC but also from the formation of dipoles generated by faradaic reactions along with counterions. It has been mentioned in Chapter 1. Since its magnitude is greater than that of the EDLC currents, the observed current is less than the predicted faradaic current by the amount of the NC current. NC has been assessed using AC impedance techniques [14,25,54] and linear sweep voltammetry [53,54].

This work aims at obtaining a rate-determining step of the oxidation of OH^- in the context of NC using fast-scan cyclic voltammetry. Accurately detecting intermediates requires overcoming the aforementioned challenges, which are mentioned above. The *IR*-drop can be addressed by using microelectrodes or a high concentration of supporting electrolyte. An electrode shielded with an insulator often exhibits unstable floating capacitance due to the crevice between the electrode and the insulator. To avoid floating capacitance, we will employ a thin wire electrode without any shield for fast-scan cyclic voltammetry [53,82].

5.2 Experimental

A stock solution of sodium hydroxide, NaOH with ca. 10 mM (M = mol dm^{-3}) was prepared by dissolving a given amount of solid NaOH. The concentration was determined with a pH meter and titration of a known concentration of hydrochloric acid, HCl (Fuji Film, Osaka). Hydrogen peroxide, H_2O_2 (30 wt% in H_2O) was purchased from Fuji Film, Osaka. All the chemicals were of analytical grade, and water was distilled and deionized.

A delay of the potentiostat, Compactstat by Ivium (Netherlands), for fast scans was examined by using a carbon resistance 1 kΩ for a dummy cell by applying the voltage with a 1 V span. The maximum difference in the currents at the forward and the reverse scan was 3% at 8 V s^{-1}.

The working electrode was a platinum wire 30 μm in diameter, of which a tip was inserted into the solution by approximately 1 mm deep. The accurately inserted length was determined with an optical microscope. The electrode was pretreated by being soaked in the mixed acid (0.26 M acetic acid + 0.33 M nitric acid + 0.73 M phosphoric acid) for 1 min and washed with distilled water. The reference electrodes were a commercially available Ag|AgCl (sat. KCl) and the $Ag|Ag_xO$ which was prepared by oxidizing a Ag wire. The latter was used in case of avoiding leakage of chloride ions from the former. The counter electrode was a platinum coil. A commercially available platinum disk electrode 1.6 mm and a microdisk 10 μm in diameter (BAS, Tokyo) were used for low-scan voltammetry to examine redox effects of other than oxidation of hydroxide ion.

The solution resistance was evaluated by AC impedance to be ca. 250

Ω, which had negligible effects on the deformation of voltammograms from a viewpoint of the *IR* drop when currents were less than 8 μA in magnitude.

5.3 Results and Discussion

The oxidation potential of OH^- is slightly more cathodic than the oxidation potential of the chloride ion, Cl^-. It was shifted positively with addition of Cl^- to the solution, and hence the oxidized products may interact with Cl^-. We used $NaNO_3$ as an electrolyte instead of KCl to avoid the interaction. Reference electrodes often contain Cl^-, which leaks to test solutions, to vary ionic conductivity during measurements [83]. Effects of Cl^- on oxidation of OH^- were examined by use of a commercially available Ag|AgCl (sat. KCl) and a surface-oxidized Ag-wire called Ag_xO. Voltammograms obtained at the Ag_xO were more stable in long experimental runs than those at the Ag|AgCl (sat. KCl), probably because of leakage of Cl^- from the reference electrode. However, they varied with pH values. Open circuit voltages of the Ag_xO were measured with respect to the Ag|AgCl (sat. KCl) in some concentrations of deaerated NaOH solutions. Here we used the Ag|AgCl (sat. KCl) for most voltammograms in which the effects of Cl^- were examined to be negligible by use of the Ag_xO.

Fig.5.1 shows voltammograms in 0.42 mM NaOH solution at the Pt thin wire electrode for some potential scan rates, v. The oxidation wave rose at 1.05 V, and exhibited a limiting current for $E > 1.2$ V. Since the limiting current was proportional to concentrations of NaOH in the domain from 0.4 mM to 3.0 mM, the wave should be caused by the oxidation of OH^-. The

one-electron transfer of OH^- would yield an unstable hydroxyl radical. Although the oxidation can be expressed by several reaction mechanisms in overall steps, an elementary step may lie in the one-electron transfer.

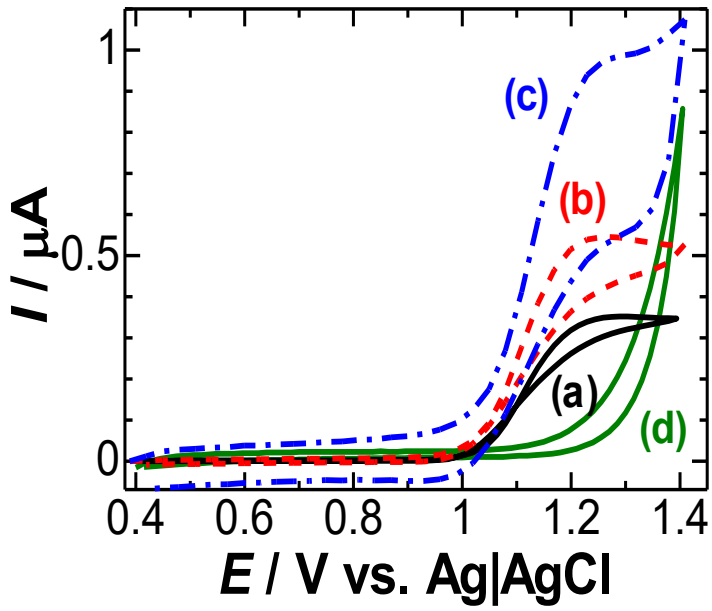

Fig.5.1 Voltammograms at the Pt wire electrode in 0.42 mM NaOH + 0.5 M $NaNO_3$ for v = (a) 0.01, (b) 0.1 and (c) 0.7 V s^{-1}, and (d) in 0.5 M $NaNO_3$ for v = 0.1 V s^{-1}.

The voltammogram at the lowest scan rate in Fig.5.1 takes almost the steady state like observed at microdisk electrodes. This is due to the cylindrical diffusion, exhibiting the quasi-steady state current [52]. With an increase in the scan rates, the voltammograms get hysteresis by linear diffusion. A notable point is a loss of any reduction wave indicating that the electrochemically oxidized product should be unstable through some following chemical reactions. The voltammogram at the platinum disk electrode 10 μm in diameter ($2a$) showed almost a steady state. The value of the limiting current, I_L, given by $4FcDa$, yielded the diffusion coefficient, D = (8.3±1.0)×10^{-5} cm^2 s^{-1} for the bulk concentration c = 0.42 mM of NaOH.

This is close to that of hydrogen ions [84], and is eight times larger than that of water. The closeness inspires us to imagine that the diffusion is caused by H^+ via the Grotthus mechanism combined with the equilibrium of H^+ and OH^-. A possible mechanism is illustrated in Fig.5.2, in which H^+ dissociated from H_2O diffuses toward OH^- to form a new H_2O molecule. Under the equilibrium of OH^- with H^+, diffusion of OH^- cannot be discerned from that of H^+ except for the opposite directions of diffusion. The fastest of the two diffusing species ought to be observed, and hence diffusion of H^+ be a rate-determining step of the oxidation of OH^- [85].

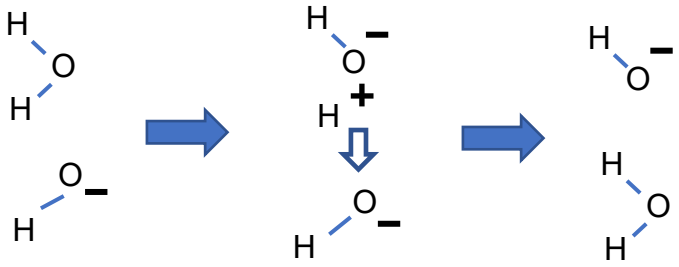

Fig.5.2 Grotthus mechanism of diffusion of OH^-, combined with the equilibrium of H^+ and OH^-.

An oxidized, stabilized product of OH^- has been reported to be H_2O_2 rather than O_2, according to the spectroscopic study [80]. In order to confirm the presence of H_2O_2, we attempted to reduce the oxidized product in the cathodic potential domain. Fig.5.3(b) shows the reverse voltammogram after the formation of the product at 1.3 V, exhibiting a cathodic peak at –0.25 V. The negligible change in iterative voltammograms indicates that the decomposition of H_2O_2 during the voltammetry could be insignificant. The peak potential was close to that of the cathodic wave of H_2O_2 (Fig.5.3(a)).

The peak current at −0.25 V in the NaOH solution was proportional to v rather than $v^{1/2}$, as shown in the inset of Fig.5.3.

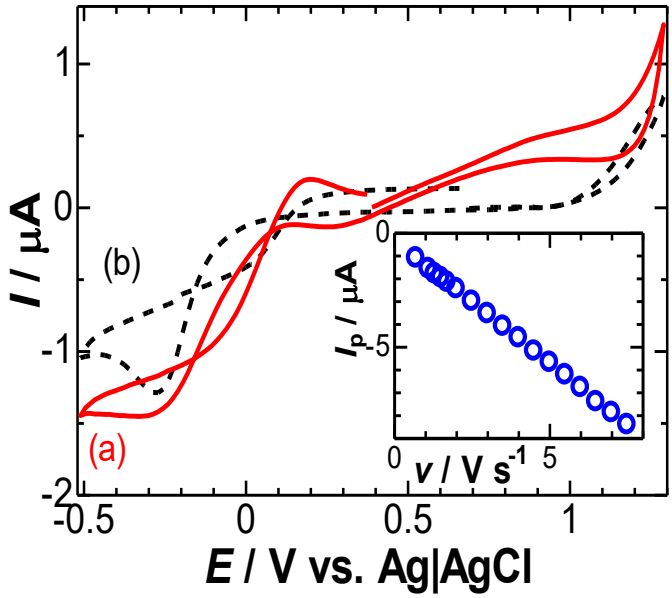

Fig.5.3 Cyclic voltammograms of (a) 0.5 mM H_2O_2 (b) 0.42 mM NaOH including 0.5 M $NaNO_3$ solutions for v = 0.1 V s^{-1}. The inset is the variation of the peak current of (b) at −0.25 V with v.

Furthermore, the value of the peak current at v = 1 V s^{-1} was ten times larger than that theoretically calculated from the diffusion-controlled equation. As a result, the reduction wave was due to the adsorbed H_2O_2, which was oxidized from OH^-. The adsorption behavior was examined as to whether it would be observed in H_2O_2 bulk solution or not. The cathodic peak current in the H_2O_2 solution without NaOH was proportional to $v^{1/2}$ for v < 1 V s^{-1}, as shown in Fig.5.4(a), whereas it deviated from the $v^{1/2}$-linearity to v-linearity for v > 1.5 V s^{-1}, as was seen from the plot of $I_p v^{-1/2}$ vs $v^{-1/2}$ on the right ordinate. The proportional constant in Fig.5.4(a) was ten times larger than the theoretically diffusion-controlled one. This extra-supply of H_2O_2 over the diffusion is evidence of the adsorption of H_2O_2 generated from the

oxidation of OH^- in Fig.5.3(b).

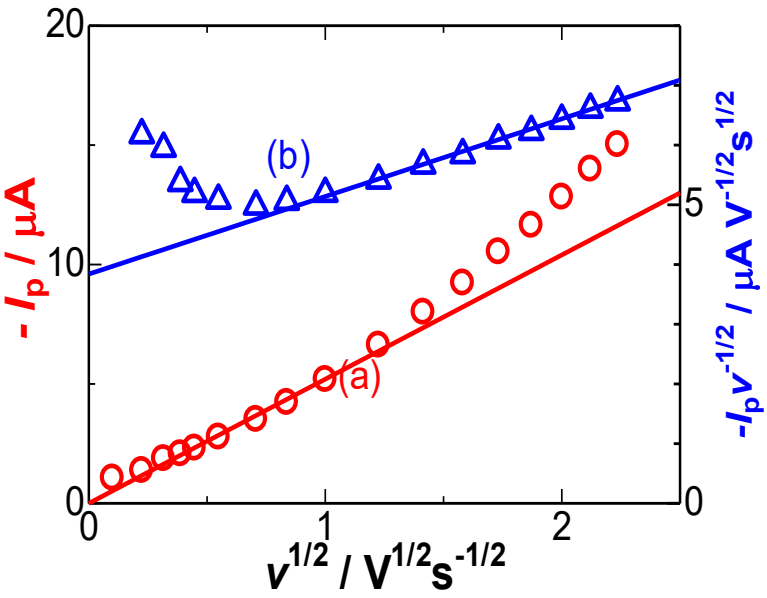

Fig.5.4 Variations of (a) the peak current, I_p, at −0.25 V and (b) $I_p v^{-1/2}$ with $v^{1/2}$ for the cathodic scan reversed at 1.0 V in 0.5 mM H_2O_2 including 0.5 M $NaNO_3$ solution for v = 0.1 V s^{-1}.

The peak potential of the oxidation wave of OH^- was almost independent of the scan rates for 0.1 < v < 2 V s^{-1} (shown later). If a product immediately after the oxidation was decomposed through the first-order reaction, the peak potential should be shifted linearly with log v with the 30 mV slope [86]. The following chemical reaction should obey mechanisms other than the first-order decomposition. The limiting or peak currents of the oxidation of OH^- were plotted against $v^{1/2}$ in Fig.5.5 in expectation of the diffusion-control of OH^-. The currents for v < 0.5 V s^{-1} were linear to $v^{1/2}$. The plot showed an intercept, I_{p0}, under the quasi-steady state, which should be caused by cylindrical diffusion at thin wire electrodes [52].

A slope of the line fitting to I_p for v < 0.5 V s^{-1} agreed with the theoretical diffusion-controlled current calculated for given concentrations of NaOH,

the diffusion coefficient obtained above, and the geometrical surface area of the thin wire electrode. The lower deviation of the plot from the line may be ascribed to the BV charge transfer kinetics, especially the transition from the reversible reaction at slow scan rates to the irreversible one at high scan ones. We attempted to evaluate the variations of the I_p with v for various combinations of transfer coefficients and standard rate constants so that they may fit the experimental variations in Fig.5.5 (triangles).

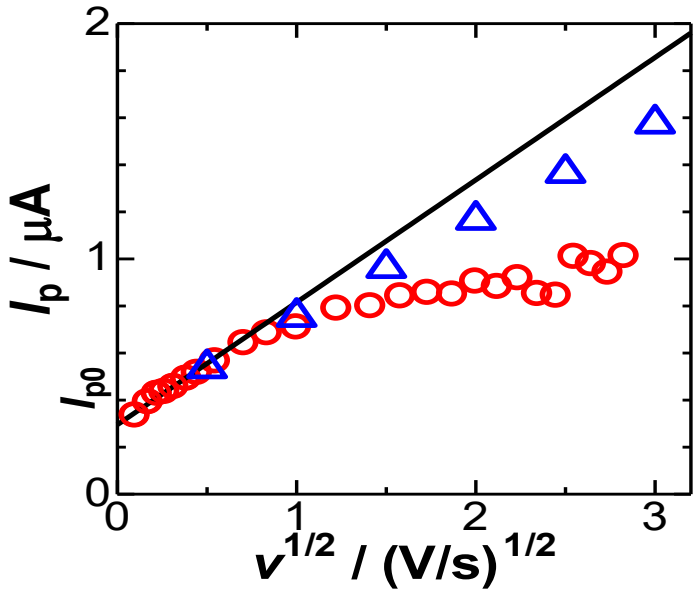

Fig.5.5 Variation of the limiting or peak currents with the square root of the scan rates observed at Pt wire electrode in 0.42 mM NaOH + 0.5 M $NaNO_3$. Triangles are from the electrode kinetics for the transfer coefficient 0.5 and the transfer rate constant 0.01 cm s^{-1}.

The effect of the charge transfer kinetics disagreed with the experimental results for any values of the kinetic parameters. Voltammetric features of the oxidation of OH^- depend not only on time scales but also on concentrations of OH^- and materials of electrodes. For example, cobalt oxide electrodes at high concentrations of OH^- showed adsorption currents at catalytically low potentials [87,88]. Therefore, the results in Fig.5.5 are not

universal behavior.

A possible reason for the lower deviation from the line is the NC as described previously, which is remarkable at high scan rates because it is proportional to v. It is assumed that the observed current density is the sum of the diffusion-controlled current density of OH^- and the capacitive one [53,54,82]:

$$j_p = j_{p0} + 0.446Fc\,(DF/RT)^{1/2}v^{1/2} + C_{rx}v \qquad (5.1)$$

where c is the bulk concentration of OH^-, and C_{rx} is the NC associated with the faradaic reaction. Eq. (5.1) suggests the linearity for the plot of $(j_p\text{-}j_{p0})v^{-1/2}$ with $v^{1/2}$.

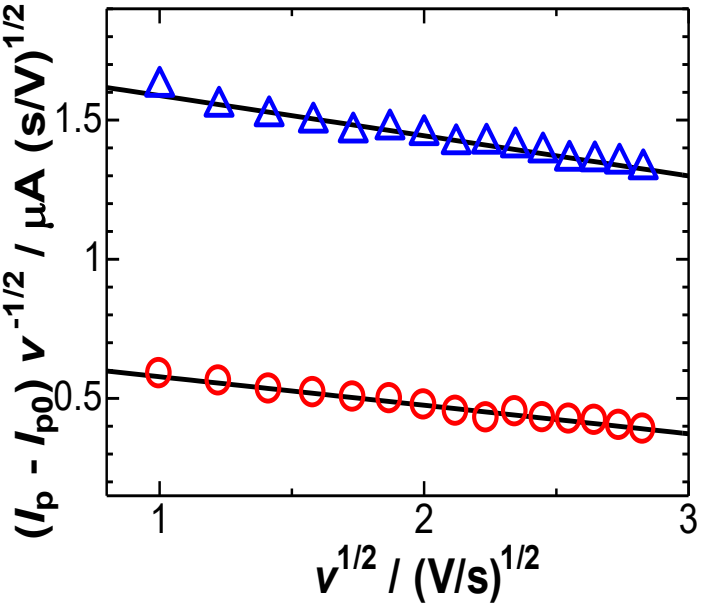

Fig.5.6 Plots for separating two components of the v-dependence and $v^{1/2}$-one in (circles) 0.66 mM and (triangles) 1.32 mM NaOH including 0.5 M $NaNO_3$ solutions.

Fig.5.6 shows the plots at two concentrations, exhibiting each line. The slope, being a negative value, should be C_{rx}, values of which were 100 μF cm^{-2} and 150 μF cm^{-2} for the 0.66 mM and 1.32 mM OH^- solutions,

respectively. The values of C_{rx} were a few times larger than those of the EDLCs (ca. 30 μF cm^{-2}).

The NC is expected to be brought about through the following steps. An OH^- to be oxidized comes in contact with the electrode for the charge transfer reaction. The oxidation energy should be minimized electrostatically so that

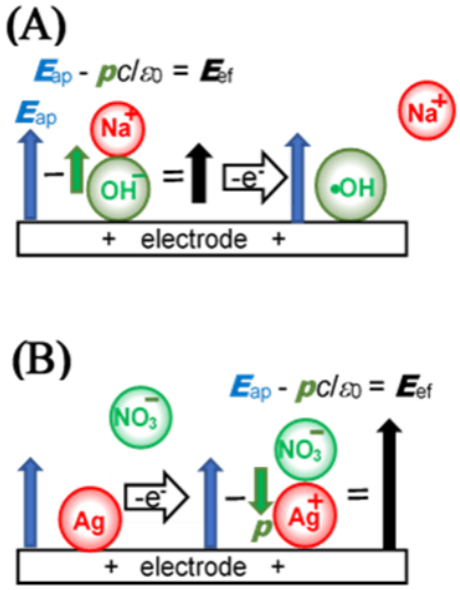

Fig.5.7 Illustrations of the formation of (A) Na^+- OH^- and (B) Ag^+- NO_3^- dipoles [24]caused by the oxidation.

a cation Na^+ may approach the OH^- up to the closest separation, forming a Na^+ - OH^- dipole as illustrated in Fig.5.7(A). The dipole moment, $\boldsymbol{p}$, with the surface concentration of OH^-, c, decreases the applied electric field $\boldsymbol{E}_{ap}$ by $\boldsymbol{p}c/\varepsilon_0$ to yield the effective field, $\boldsymbol{E}_{ef} = \boldsymbol{E}_{ap} - \boldsymbol{p}c/\varepsilon_0$ [89], where ε_0 is the permittivity of the vacuum. The electrochemical oxidation varies the field from $\boldsymbol{E}_{ef}$ to $\boldsymbol{E}_{ap}$ to acquire the difference, $\Delta\boldsymbol{E} = \boldsymbol{E}_{ap} - (\boldsymbol{E}_{ap} - \boldsymbol{p}c/\varepsilon_0) = \boldsymbol{p}c/\varepsilon_0$. This difference is the same as for the metal oxidation, with the distinction between the initial and the final stages, as shown in Fig.5.7(B). The potential scan causes the capacitive current, the direction of which is opposite to the

faradaic current as well as the EDLC current.

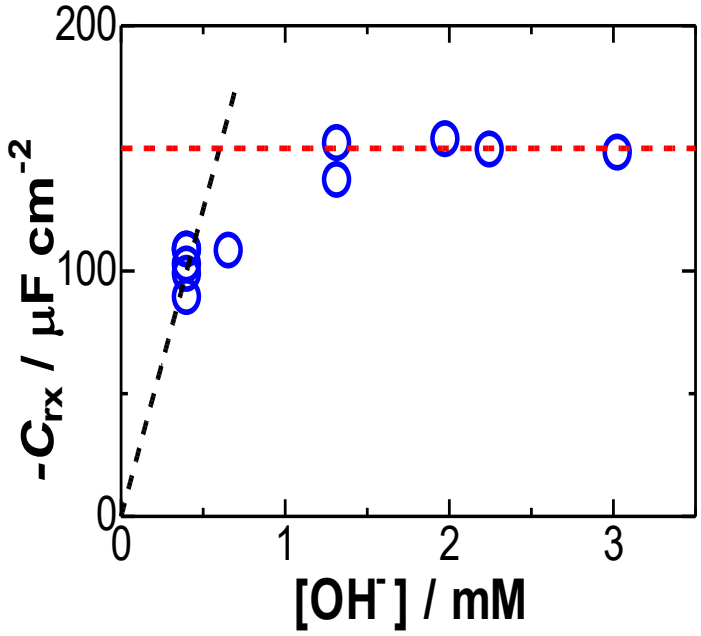

Fig.5.8 Variation of the NC with concentrations of OH^-.

In order to confirm whether C_{rx} is caused by the oxidation of OH^- or not, we evaluated C_{rx} at several concentrations of NaOH with the expectation that C_{rx} would be proportional to the concentrations. The dependence of $(I_p - I_{p0})v^{-1/2}$ on $v^{1/2}$ for the other concentrations was linear as shown in Fig.5.6. Fig.5.8 shows the variation of C_{rx} with $[OH^-]$, exhibiting invariance to concentrations higher than 1.5 mM. This result indicated that the effect of NC currents on the oxidation of OH^- was very small even at high concentrations of hydroxide ions. The loss of energy remains constant at a certain value of applied voltage, which was more favorable for the development of energy storage. The proportionality of C_{rx} to the concentrations for H^+ [82], FcTMA [53], and hemin [54] has demonstrated that the NCs have been caused by the faradaic reactions, irrespective of

EDLCs. However, the oxidation of OH^- was different from the redox reaction mechanisms reported so far.

We discuss here possible reaction mechanisms in detail. They may be revealed in variations of peak potentials and currents with scan rates and concentrations. Fig.5.9 shows assembly of voltammograms at several scan rates in (A) low and (B) high concentrations. The cathodic peak-shift at (A) the low concentration with a decrease in v suggests participation in the following chemical reaction. An inverse variation was found for the high concentration (B), indicating that products by the following chemical reaction should be oxidized at potentials more anodic than those of OH^-. In order to confirm the potential shift by the concentrations, we showed in Fig.5. 9(C) dependence of the voltammograms normalized with the peak currents at v = 0.1 V s^{-1} on concentrations. Since an increase in the concentrations causes the anodic potential shift, there may be the formation of new redox species at a more positive potential. This prediction suggests the following example of reaction mechanisms:

$$OH^- \rightarrow \bullet OH + e^- \quad (5.2a)$$

$$OH^- + 2\bullet OH \rightarrow HO_2^- + H_2O \quad (5.2b)$$

$$HO_2^- + H_2O \rightarrow 3/2\ H_2O_2 + e^- \quad (5.2c)$$

where $\bullet OH$ and HO_2^- are hydroxyl radical and hydroperoxyl anion, respectively, which can be replaced by others. The determination of the mechanism will be further explained using the concept of Lewis Structures, which is displayed in the Appendix Information. Since the addition through $\{2\times(2a)+(2b)+(2c)\}/3$ yields $OH^- \rightarrow (1//2)H_2O_2 + e^-$, both $\bullet OH$ and HO_2^-

are intermediates. Dipoles of OH^--Na^+ and HO_2^--Na^+, which are required to decrease the oxidation energy, generate the NC. Thus, the magnitude of C_{rx} should increase with an increase in the oxidation currents or concentrations

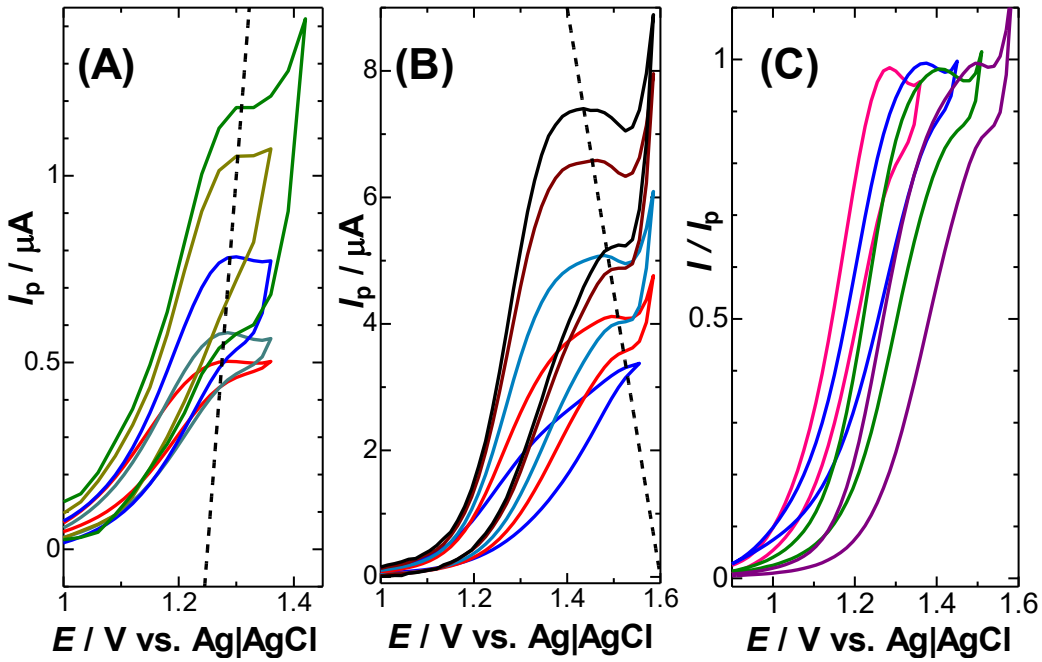

Fig.5.9 Voltammograms in (A) 0.66 and (B) 3.03 mM [OH^-] solutions for v = 0.01, 0.1, 0.3, 1.0 and 1.5 V s^{-1} from smaller to larger ones, and (C) voltammograms normalized by peak currents for concentrations of 0.66, 1.21, 1.98 and 3.03 mM from the left to the right for v = 0.1 V s^{-1}. Dashed lines are connections for peaks.

of OH^- in the mechanism (5.2). However, this prediction is inconsistent with the concentration-dependence of C_{rx} in Fig.5.8.

The inconsistency can be explained in terms of two ways (i) compensation of C_{rx} with the EDLC of H_2O_2 and (ii) destruction of stable dipoles. (i) If H_2O_2, a product of the oxidation of OH^-, is adsorbed and oriented in such a direction that the external field may be relaxed, like the behavior of solvent dipoles for conventional EDLCs, it would partially cancel C_{rx}. We evaluated the EDLC in 1 mM H_2O_2 solution in the polarized

potential domain from 0.1 to 0.4 V by AC impedance and cyclic voltammetry. The values were independent of $[H_2O_2]$ to have ca. 80 μF cm^{-2}. The independence cannot break the predicted proportionality of C_{rx} to $[H_2O_2]$. Furthermore, the value is too small to compensate C_{rx}. Therefore, it is reasonable to consider case (ii). A series of reactions (5.2) includes the generation of the hydroxyl radical, the free energy of which is too high to keep the dipoles unoriented. Then, values of C_{rx} may be determined by fluctuation of orientation agitated by the radical.

5.4 Conclusive and Remarks

A product of the anodic oxidation of OH^- at a platinum electrode is hydrogen peroxide in the adsorbed state, which is further decomposed spontaneously to dioxide. This is consistent with the conventional four-electron transfer oxidation of OH^-. The oxidation current is controlled by diffusion of OH^- in solution without any participation in heterogeneous kinetics. The truly diffusing species is H^+ rather than OH^- because of the equilibrium of OH^- and H^+ in the discussion of values of the diffusion coefficients. The oxidation is followed by the decomposition involving radical reaction, which is not of the first-order reaction of OH^- so that the peak potential is almost invariant to the scan rates and varies with $[OH^-]$. The radical reactions may deteriorate membranes and electrodes for long use in applications of water electrolysis.

The peak current obeys a linear relation to $v^{1/2}$ at low scan rates, whereas does to v at high ones. The latter can be responsible for the capacitive current,

the values of which are negative. The NC is theoretically caused by the formation of dipole, OH^--Na^+, during the oxidation of OH^-. However, hydroxyl radical may make the life time of the dipole too short to observe the capacitance. As a result, it causes the values of the NC to be nonlinear to $[OH^-]$ or be constant. The NC currents may have a minor effect in highly alkaline solutions.

5.5 Appendix Information

When considering whether or not to produce $H_2O_2^-$ ions in the second reaction step (5.2(b)) or not, the Lewis structure of $H_2O_2^-$ ion is drawn. Each hydrogen atom has one valence electron, and each oxygen atom has six ones. It results in a total of 15 valence electrons for the $H_2O_2^-$ ion. Upon verifying the "octet rule" for the two hydrogen atoms and two oxygen atoms, it is observed that both hydrogen atoms have two electrons, and the oxygen atoms also satisfy the octet rule, maintaining stability. There is no apparent arrangement for the fifteenth electron in the current Lewis structure for $H_2O_2^-$ ion, as shown in Figure below. It indicates that the $H_2O_2^-$ ions cannot be produced in the second step of oxidation of OH^-.

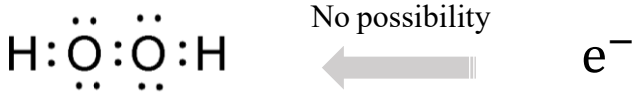

Regarding another reaction, the oxidation of OH^- can be represented as follows:

$OH^- \rightarrow OH_0 + e^-$,

$OH^- + 2OH_0 \rightarrow HO^{2-} + H_2O$.

The HO^{2-} ion contains a total of 14 valence electrons. Calculating the formal charges, an O atom in the HO^{2-} ion carries a formal charge of −1. The possible products following the second step are the HO^{2-} ion and water. The arrangement for the electron of each molecule and molecule ions to reach the

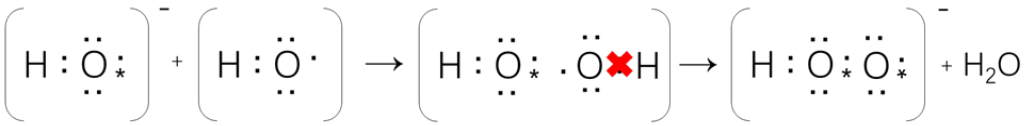

Octets rule in the Lewis structure is shown in Figure below. Subsequently, HO^{2-} ions react with H_2O to form H_2O_2.

Chapter 6

What is the essence of Negative Capacitance?

6.1 Motivation

EDLC is characterized by frequency dispersion, a phenomenon where the actual capacitance deviates from the ideal due to the dielectric response of polarized structures [90,91]. This dispersion is quantified using the constant phase element [92,93,94,95,96] and power laws [1,2,3,26], revealing a wide observable frequency range from 0.01 Hz to 10 kHz [97]. Such dispersion is not solely due to dipole inversion from an external field, but rather, it may involve complex interactions among a huge number of dipoles, termed cooperative phenomena [98,99].

When an external voltage is applied to the electrode|solution interface, solvent dipoles are oriented by an electric field to decrease electrostatic energy. However, the interaction energy of hydrogen bonds at the electrode surface is significantly stronger than field-oriented energy [100], causing alternating orientations for neighboring solvent dipoles. The parts of dipoles oriented by the field, and thus overcoming thermal fluctuations, can participate in the EDLC, where the time domain is as long as 1 s. A redox charge dipole is generated through faradaic reactions. It is oriented in the direction opposite to the field-oriented solvent dipoles [101]. Thus, it works to suppress the EDLC and lead to observed capacitance as a negative value [14,15,24,25,26,53,54,82,102]. Since suppressing the EDLC takes an unpre-

dictably long time to establish the stable, macroscopic, two-dimensional structure of oriented dipoles, faradaic reactions may have a behavior similar to the delay of EDLCs.

The kinetics of these reactions, including the delay in reaching Nernst equilibrium, is typically described using the Tafel equation or BV equations, which highlight the exponential dependence of reaction rates on an applied voltage. Exponential dependence refers to the rate-determining step, which involves a transfer of electrons through an electric field, studied via transition state theory [103,104,105], without any influence of alterations of charge neutrallization, solvation, chemical complications, or adsorption. These influences have been incorporated by integrating reorganization energy into reaction-free energy curves [106,107]. However, evaluated charge transfer rate constants depend on practical conditions, such as measurement techniques [108], curve-fitting methods [109], and sometimes research groups. In contrast, real-world measurements and theoretical models indicate that other factors like solvent dynamics [110], hydrodynamic radius [111], and viscosity [112] significantly influence these rates. Since the various effects, ie, dipole arrangement, are significantly slower than the motion of electrons through an electric field, the exponential dependence of reaction rates mentioned previously is unlikely to present actual rates. One approach that can be attempted is to control the overall rate through a pre-exponential factor preceding the transient state. This method may aid in proposing a new form of heterogeneous kinetics, incorporating time variables rather than solely voltage-dependent exponential dependence as in the BV equation.

It is essential to recognize that the analysis of faradaic reactions on the EDL structure incorporates both the EDLCs and the charge transfer reactions. Both of them participate in dipole-dipole interactions. The former is characterized by frequency dispersion or power law, while the latter is assessed using NC. To explore potential similarities in their interactions, we employed chronoamperometry to measure a ferrocenyl derivative. Here, we derive equations for the chronoamperometric curves and design a suitable potential step experiment. We also attempt to separate EDLCs and NCs through data processing and by setting experimental conditions.

6.2 Experimental

The potentiostat used for the cyclic voltammetry and chronoamperometry was a Compactstat (Ivium, The Netherlands). The working electrode was a platinum wire 0.5 mm in diameter, the 1 mm long tip of which was inserted into the solution. This structure has the advantage of an exposed electrode area that is unaffected by floating capacitance caused by a crevice between the electrode and its insulator during area control [53]

The accurate length was controlled using a Z-stage with the help of an optical microscope. The counter electrode was a platinum wire with an area 100 times larger than that of the working electrode, and the reference electrode was Ag|AgCl in saturated KCl solution. The test solutions were dearerated for 15 min before each experimental measurement.

All the chemicals were of analytical grade. Aqueous solutions of 1 mM (mM = 10^{-3} mol dm^{-3}) (ferrocenylmethyl)trimethyl ammonium ($FcTMA^{+}$)

and 0.5 M KCl were prepared in distilled and then ion-exchanged water using an ultrapure water system, CPW-100 (Advance, Tokyo, Japan). All the measurements were recorded at room temperature.

6.3 Results and Discussion

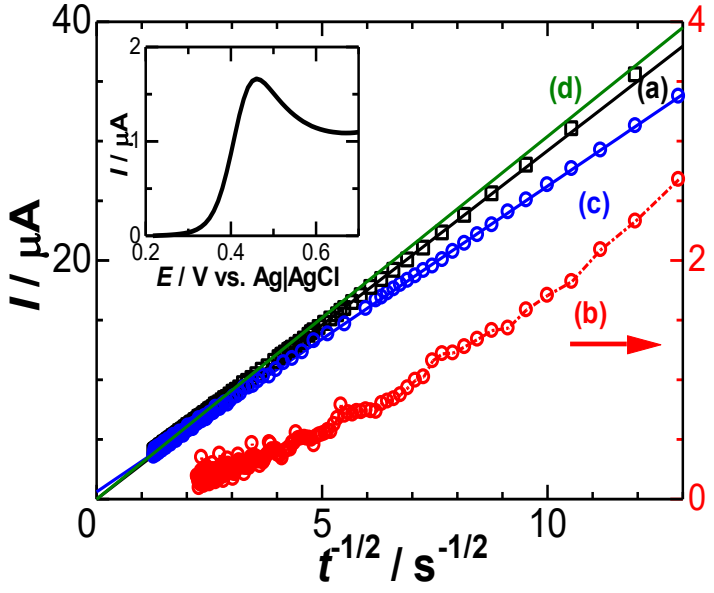

Fig.6.1 Cottrell plots of the observed chronoamperograms in the solution of 0.5 M KCl (a) with and (b) without 1 mM $FcTMA^+$ for the potential stepped from 0.26 V to 0.489 V and for (d) the calculated potential of $D = 0.7 \times 10^{-5}$ cm^2 s^{-1}. Plots for the subtracted current against $t^{-1/2}$ are shown in (c). The inset shows the current-voltage curve in the solution of 1 mM FcTMA and 0.5 M KCl at a scan rate of 0.015 Vs^{-1}. The arrow means that plots (b) follow the right ordinate.

Fig.6.1 shows Cottrell plots for the observed chronoamperometric curves in solutions (a) with and (b) without $FcTMA^+$ when the potential was stepped from the reduced domain (0.26 V) to the limiting domain (E_{dc} = 0.489 V). The cyclic voltammogram is shown in the inset to specify the potential domain. The difference in the currents of the sweep voltammogram and the chronoamperogram is caused by the large difference in the time scale.

The solution resistance was evaluated using Nyquist plots via AC impedance and was found to be 100 Ω. If 4 mV of *IR*-drop is added to the applied voltage, the effectively maximum current, 40 μA, corresponds to the chronoamperometric time 0.006 s according to the Cottrell equation for $D = 0.7\times10^{-5}$ cm^2 s^{-1}. On the other hand, the longest and most efficient time deviation from the Cottrell equation is the incidence time for cylindrical diffusion. The current at a cylindrical electrode of radius a is approximately expressed as $a(\pi Dt)^{-1/2} + 0.422$ [113]. If 3% errors are allowed to be involved in the current, the longest time, t_L, satisfying $a(\pi Dt_L)^{-1/2} > 0.422 \times 0.03$ is $t_L < 0.2$ s. Consequently, the time domain for the analysis is 0.006 s $< t <$ 0.2 s.

The observed chronoamperometric current in the Cottrell plots exhibited a linear relationship with passing through the origin (a). Since the EDLC current (b) was as much as 1/10 of the observed current (a), it was subtracted from the observed current and is shown (c) in Fig.6.1. The subtracted current shows a still linearity with $t^{-1/2}$. The Cottrell plot theoretically calculated for $c^* = 1$ mM and $D = 0.7 \times 10^{-5}$ cm s^{-1} is shown in Fig.6.1(d). The EDLC-included current (a) is ironically close to the Cottrell current (d), indicating that the contribution of kinetics should be numerically similar to the EDLC current. The difference between (d) and (c) seems to lie in the contribution of the NC. This resembles the deviation of the plots of the peak current against the square root of potential scan rates in cyclic voltammetry [53].

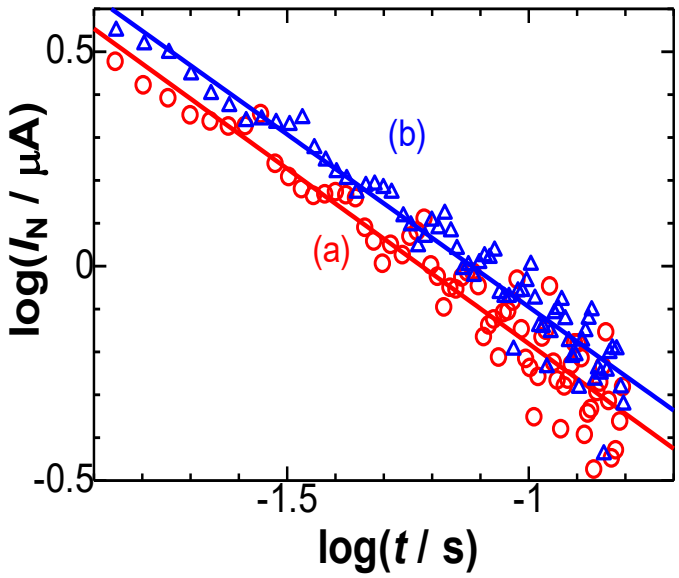

Fig.6.2 Logarithmic plots of the NC current against time for the current–time curves observed at the stepped potential from 0.26 V to E_{dc} = (a) 0.440 and (b) 0.489 V.

Eq. (2.2.5) described in Chapter 2 predicts that the negatively capacitive current, which can be evaluated from $I_N = I_C + I_{EDL} - I_{ob}$, has $t^{\mu-1}$ dependence. In order to examine the power law in I_N, we logarithmically plotted I_N against t for two values of E, as shown in Fig.6.2. All the points at each E fell on each line, of which slopes were common and determined to be μ = 0.1. Values of VC_{rx} were obtained from the intercept, as shown in Fig.6.2, and were plotted against E, as shown in Fig.6.3. They fell on a line, the slope of which represents C_{rx}, according to Equation (2.2.5). The value was C_{rx} = 67 μF cm^{-2}, which is close to 64 μF cm^{-2} [15] and was obtained via AC impedance and 60 μF cm^{-2} [53] using fast-scan cyclic voltammetry.

We numerically evaluated c_s using Equation (2.2.6) for the determined values of μ and C_{rx} at c^* = 1 mM. Fig.6.4 shows the calculated time variation in c_s and a dotted line averaged over $t < 0.2$. The value of c_s might be almost

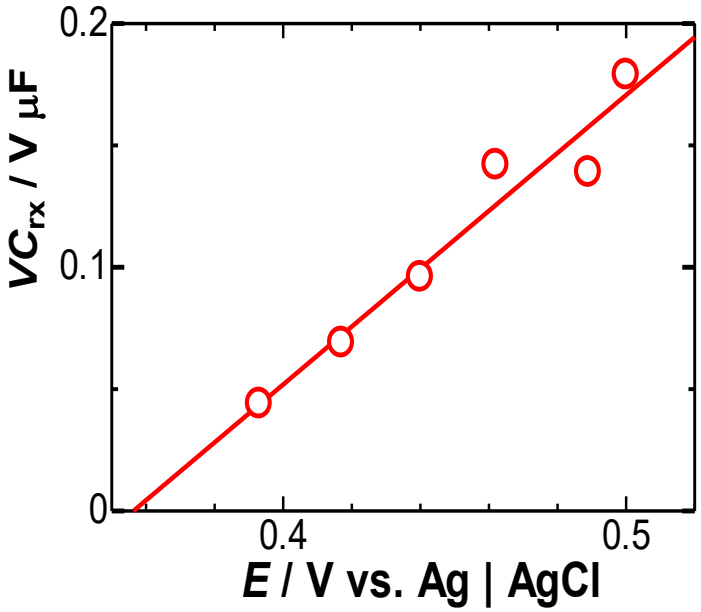

Fig.6.3 Variations in VC_{rx} with E, obtained from the intercept of the plots shown in Fig.6.2.

zero without any interaction.

The average concentration is 0.1 mM, suggesting that it is ineffective in oxidation. Although the potential is in the limiting current domain, the concentration of the reduced species on the electrode is not zero, as illustrated in Fig1.24. Oxidation energy is consumed by decreasing the dipole-dipole interaction on the electrode until the interaction becomes stable. This interaction is also a source of NC, and hence the non-zero surface concentration is equivalent to NC. The times at which the concentration at the surface becomes 5% and 2% of the bulk concentration are 0.5 s and 5 s, respectively. This slow relaxation is close to the frequency dispersion of the EDLCs.

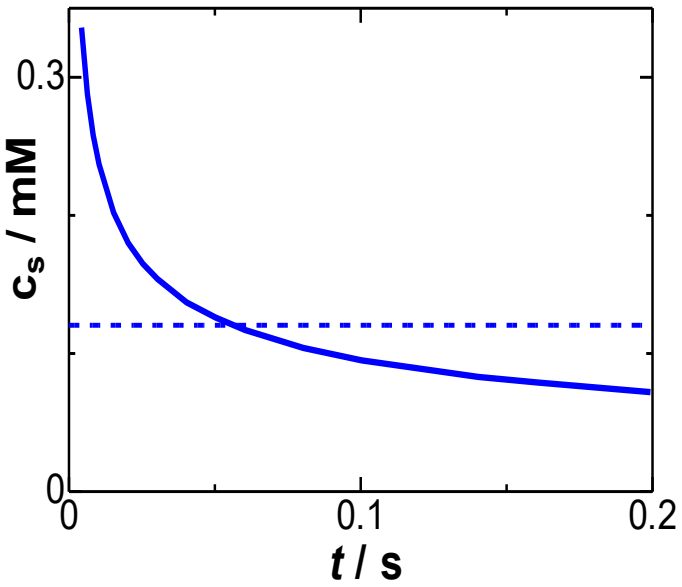

Fig.6.4 Time variation of the concentration on the electrode surface, calculated using Equation (2.2.6) for $\mu = 0.1$, $C_{rx} = 67$ μF cm$^{-2,}$ and $D = 0.7 \times 10^{-5}$ cm^2 s^{-1} at $E_{dc} =$ 0.489 V vs. Ag|AgCl. The dashed line is the average concentration for $0 < t < 0.2$ s.

6.4 Conclusive and Remarks

The level of depression in the current caused by the Cottrell current, being proportional to the power of the time, corresponds to the NC current brought about by the redox reaction in the physical experiment. It exhibited almost the same form as EDLC caused by solvent dipole-dipole interaction. This similarity indicates that kinetics should be ascribed to the dipole-dipole interactions activated by the generation of the redox dipole, whereas EDLC is activated by the applied electric field. Since dipole interactions on the electrode widely vary and thermally fluctuate, it takes a macroscopic time rather than a microscopic inversion time of one dipole to establish a stable structure both for the kinetics and EDLC. Therefore, both the faradaic reaction and EDLC have a similar power law of the time.

Chapter 7

Conclusions

This thesis is devoted to the time dependence of the diffusion-controlled faradaic reactions on the EDL structure by fast-scan cyclic voltammetry and chronoamperometry. My experimental evidence has verified the concept of the NC to yield the interpretation at the molecular-level with time dependence close to the frequency dispersion of the EDLC.

Fast-scan cyclic voltammetry was applied to reactions of $FcTMA^+$, H^+, and OH^- to exhibit a decrease in the theoretical diffusion-controlled peak currents at a short time domain. The decrease can be attributed to the NC currents. The data analysis has provided me the additional information such as the adsorbed species of uncharged H^0 and OH radicals, associated with potential shifts.

My molecular perspective is that the thermal fluctuation of solvent dipoles in the Helmholtz layer suppresses the EDLC by faradaic reactions up to negative values, called the NC. This suppression occurs until the interaction energy among the dipoles may attain the lowest energy state in the EDLC. Since dipole interactions on the electrode widely vary and thermally fluctuate, it takes a macroscopic time rather than a microscopic inversion time of one dipole to establish a stable structure both for the kinetics and EDLC. The determination of macroscopic time is achieved by chronoamperometry.

The observed chronoamperometric NC current was proportional to time to the power of -0.1. The power law for the NC is similar to that of the EDLC. This similarity indicates that NC should be ascribed to the dipole-dipole interactions activated by the generation of the redox dipole, which can be equivalent to a new kind of heterogeneous kinetic. The prophet concluded that the EDLC is activated by the applied electric field. We can see that the NC is different from the EDLC in a trigger, comparing the NC and the EDLC.

The values of NC obtained for the reduction of H^+ were twice that for oxidation of $FcTMA^+$. Both values of the two reactions were linear to the concentration of the species. However, the NC for the oxidation of hydroxide ions was not linear with hydroxide ions and even remained constant. The difference in the former can be attributed to the variance in dipole strength between H^+-Cl^- and $FcTMA^+$-Cl^-. The latter involves the generation of radicals.

Verifying the NC with fast-scan cyclic voltammetry for three different redox species was highly successful. Determination of complex reaction mechanisms can also be achieved by fast-scan cyclic voltammetry, it was determined that through electrochemical analysis, for example: 1) Adsorbed hydrogen ions were identified as reaction intermediates, contradicting the conclusion of H_{ad}^0 in the Volmer step; 2) H^+ reduction to H_2 occurs as a second step through a Heyrovsky step controlled by single-electron transfer under diffusion control; 3) The calculated concentration of adsorbed hydrogen ions reached up to 0.3 M, causing a potential deviation from the more correct potential of H^+/H_2.

The four-electron reaction of OH^- was difficult to detect from the peak shape. The voltammogram of hydroxide ion oxidation observed was irreversible, and the peak potential was almost invariant with the scan rate. According to the relationship between peak current and the square of scan rate, the calculated diffusion coefficient for hydroxide ions was balanced with that of hydrogen ions. This indicates that the true diffusion substance for the faradaic reaction is H^+ not OH^-. The product of the anodic oxidation of hydroxide ions on a platinum electrode is adsorbed hydrogen peroxide, which further spontaneously decomposes into dioxide. The instability of radicals affected the determination of peak shape and NC.

References

[1] K. J. Aoki, J. Chen, and R. He, "Potential Step for Double-Layer Capacitances Obeying the Power Law," *ACS omega*, vol. 5, no. 13, pp. 7497–7502, Mar. 2020, DOI: https://doi.org/10.1021/acsomega.0c00301.

[2] K. J. Aoki, Y. Hou, J. Chen, and T. Nishiumi, "Resistance associated with measurements of capacitance in electric double layers," *Journal of Electroanalytical Chemistry*, vol. 689, pp. 124–129, Jan. 2013, DOI: https://doi.org/10.1016/j.jelechem.2012.10.004.

[3] Y. Hou, K. J. Aoki, and J. Chen, "Invariance of Double Layer Capacitance to Polarized Potential in Halide Solutions," *Universal journal of chemistry*, vol. 1, no. 4, pp. 162–169, Dec. 2013, DOI: https://doi.org/10.13189/ujc.2013.010404.

[4] Matsuda H, Ayabe Y, "The theory of the cathode-ray polarography of Randles-Sevcik," *Z. Elektrochmie*, 59, pp 494-503,1955.

[5] M. Abramowitz and I. A. Stegun, Handbook of mathematical functions, National Bureau of Standards. In *Applied Mathematics Series—55*; Tenth Printing, *National Institute of Informatics: Tokyo, Japan*, 1972, p. 257.

[6] R. A. Osteryoung and J. Osteryoung, "Pulse voltammetric methods of analysis," *Philosophical transactions of the Royal Society of London*, vol. 302, no. 1468, pp. 315–326, Sep. 1981, DOI: https://doi.org/10.1098/rsta.1981.0170.

[7] M. Lovrić and J. Osteryoung, "Theory of differential normal pulse voltammetry," *Electrochimica Acta*, vol. 27, no. 7, pp. 963–968, Jul. 1982, DOI: https://doi.org/10.1016/0013-4686(82)80220-x.

[8] Z. Stojek, "Pulse Voltammetry," *Springer eBooks*, pp. 99–110, Jan. 2005, DOI: https://doi.org/10.1007/978-3-662-04757-6_5.

[9] A. J. Bard and L. R. Faulkner, *Electrochemical Methods: Fundamentals and Applications, 2nd Edition*. Wiley Global Education, 2000.

[10] A. J. Bard, L. R. Faulkner, and H. S. White, *Electrochemical Methods, third edition*. Wiley, 2022.

[11] A. Ch. Lazanas and M. I. Prodromidis, "Electrochemical Impedance Spectroscopy─A Tutorial," *ACS Measurement Science Au*, vol. 3, no. 3,

Mar. 2023, DOI: https://doi.org/10.1021/acsmeasuresciau.2c00070.

[12] A. Lasia, "Electrochemical Impedance Spectroscopy and its Applications," *Modern Aspects of Electrochemistry*, pp. 143–248, DOI: https://doi.org/10.1007/0-306-46916-2_2.

[13] B.A. Mei, O. Munteshari, J. Lau, B. Dunn, and L. Pilon, "Physical Interpretations of Nyquist Plots for EDLC Electrodes and Devices," *The Journal of Physical Chemistry C*, vol. 122, no. 1, pp. 194–206, Dec. 2017, DOI: https://doi.org/10.1021/acs.jpcc.7b10582.

[14] K. J. Aoki, J. Chen, X. Zeng, and Z. Wang, "Decrease in the double layer capacitance by faradaic current," *RSC Advances*, vol. 7, no. 36, pp. 22501–22509, Jan. 2017, DOI: https://doi.org/10.1039/c7ra01770g.

[15] K. J. Aoki, J. Chen, and P. Tang, "Capacitive Currents Flowing in the Direction Opposite to Redox Currents," *Journal of Physical Chemistry C*, vol. 122, no. 29, pp. 16727–16732, Jun. 2018, DOI: https://doi.org/10.1021/acs.jpcc.8b03335.

[16] D. O. Wipf, E. W. Kristensen, M. R. Deakin, and R. Mark. Wightman, "Fast-scan cyclic voltammetry as a method to measure rapid heterogeneous electron-transfer kinetics," *Analytical Chemistry*, vol. 60, no. 4, pp. 306–310, Feb. 1988, DOI: https://doi.org/10.1021/ac00155a006.

[17] S. J. Percival and B. Zhang, "Fast-Scan Cyclic Voltammetry Allows Determination of Electron-Transfer Kinetic Constants in Single Nanoparticle Collision," *Journal of Physical Chemistry. C./Journal of physical chemistry. C*, vol. 120, no. 37, pp. 20536–20546, Apr. 2016, DOI: https://doi.org/10.1021/acs.jpcc.5b11330.

[18] P. R. Birkin and S. Silva-Martinez, "Determination of Heterogeneous Electron Transfer Kinetics in the Presence of Ultrasound at Microelectrodes Employing Sampled Voltammetry," *Analytical Chemistry*, vol. 69, no. 11, pp. 2055–2062, Jun. 1997, DOI: https://doi.org/10.1021/ac961128v.

[19] C. P. Andrieux, P. Hapiot, and J. M. Saveant, "Fast chemical steps coupled with outer-sphere electron transfers: application of fast scan voltammetry at ultramicroelectrodes to the cleavage of aromatic halide anion radials in the microsecond lifetime range," *Journal of Physical Chemistry*, vol. 92, no. 21, pp. 5987–5992, Oct. 1988, DOI: https://doi.org/10.1021/j100332a030.

[20] N. V. Rees, O. V. Klymenko, B. A. Coles, and R. G. Compton, “Fast scan linear sweep voltammetry at a high-speed wall-tube electrode,” *Journal of electroanalytical chemistry*, vol. 557, pp. 99–107, Oct. 2003, DOI: https://doi.org/10.1016/s0022-0728(03)00352-8.

[21] J. Hirst and F. A. Armstrong, “Fast-Scan Cyclic Voltammetry of Protein Films on Pyrolytic Graphite Edge Electrodes: Characteristics of Electron Exchange,” *Anal. Chem*, vol. 70, no. 23, pp. 5062–5071, Oct. 1998, DOI: https://doi.org/10.1021/ac9805571.

[22] H. Matsuda and Y. Ayabe, “The theory of the cathode-ray polarography of Randles-Sevcik,” *Zeitschrift fuer Elektrochmie and Angewandte Physikalische Chemie*, 1955,59, 494-503.

[23] K. J. Aoki and J. Chen, “Tips of Voltammetry,” *Voltammetry*, Jun. 2019, DOI: https://doi.org/10.5772/intechopen.81341.

[24] K. J. Aoki, J. Chen, and R. Wang, “Stripped Charge of Ag Less than Deposited one Owing to Negative Capacitance Caused by Redox Reactions,” *Electroanalysis*, vol. 31, no. 12, pp. 2303–2310, Jul. 2019, DOI: https://doi.org/10.1002/elan.201800873.

[25] P. Tang, K. J. Aoki, and J. Chen, “Reduction Charge Smaller than the Deposited One in Cathodic Stripping Voltammograms of AgCl,” *American Journal of Analytical Chemistry*, vol. 10, no. 08, pp. 286–295, 2019, DOI: https://doi.org/10.4236/ajac.2019.108021.

[26] K. J. Aoki and J. Chen, “Effects of the dipolar double layer on elemental electrode processes at micro- and macro-interfaces,” *Faraday Discussions*, vol. 210, pp. 219–234, 2018, DOI: https://doi.org/10.1039/c7fd00212b.

[27] K. Aoki, K. Honda, K. Tokuda, and H. Matsuda, “Voltammetry at microcylinder electrodes,” *Journal of electroanalytical chemistry and interfacial electrochemistry*, vol. 182, no. 2, pp. 267–279, Jan. 1985, DOI: https://doi.org/10.1016/0368-1874(85)87005-2.

[28] K. Aoki and H. Kaneko, “Theory of irreversible cyclic voltammograms at microcylinder electrodes,” *Journal of Electroanalytical Chemistry and Interfacial Electrochemistry*, vol. 247, no. 1–2, pp. 17–27, Jun. 1988, DOI: https://doi.org/10.1016/0022-0728(88)80127-x.

[29] K. J. Aoki, C. Zhang, J. Chen, and T. Nishiumi, “Heterogeneous

reaction rate constants by steady-state microelectrode techniques and fast scan voltammetry," *Journal of electroanalytical chemistry*, vol. 706, pp. 40–47, Oct. 2013, DOI: https://doi.org/10.1016/j.jelechem.2013.07.021.

[30] B. E. Logan *et al.*, "Microbial Fuel Cells: Methodology and Technology†," *Environmental Science & Technology*, vol. 40, no. 17, pp. 5181–5192, Sep. 2006, DOI: https://doi.org/10.1021/es0605016.

[31] T. Mei, C. Cong, Q. Huang, T. Song, and J. Xie, "Effect of 3D Carbon Electrodes with Different Pores on Solid-Phase Microbial Fuel Cell," *Energy & fuels*, vol. 34, no. 12, pp. 16765–16771, Dec. 2020, DOI: https://doi.org/10.1021/acs.energyfuels.0c03591.

[32] C. W. Anson and S. S. Stahl, "Mediated Fuel Cells: Soluble Redox Mediators and Their Applications to Electrochemical Reduction of O2 and Oxidation of H2, Alcohols, Biomass, and Complex Fuels," *Chemical Reviews*, vol. 120, no. 8, pp. 3749–3786, Mar. 2020, DOI: https://doi.org/10.1021/acs.chemrev.9b00717.

[33] John O'm Bockris, B. E. Conway, E. B. Yeager, R. E. White, and Supramaniam Srinivasan, *Comprehensive treatise of electrochemistry*. New York: Plenum Press, 1981.

[34] R. Subbaraman, D. Tripkovic, D. Strmcnik, K-C. Chang, M. Uchimura, A. Paulikas, V. Stamenkovic, N.M. Markovic, "Enhancing Hydrogen Evolution Activity in Water Splitting by Tailoring Li + -Ni(OH) 2 -Pt Interfaces," *Science*, vol. 334, no. 6060, pp. 1256–1260, Dec. 2011, DOI: https://doi.org/10.1126/science.1211934.

[35] S. Wang, A. Lu, and C.-J. Zhong, "Hydrogen production from water electrolysis: role of catalysts," *Nano Convergence*, vol. 8, no. 1, Feb. 2021, DOI: https://doi.org/10.1186/s40580-021-00254-x.

[36] R. M. Bullock, A. M. Appel, and M. L. Helm, "Production of hydrogen by electrocatalysis: making the H–H bond by combining protons and hydrides," *Chemical Communications*, vol. 50, no. 24, pp. 3125–3143, Feb. 2014, DOI: https://doi.org/10.1039/C3CC46135A.

[37] S. Dunn, "Hydrogen futures: toward a sustainable energy system," *International Journal of Hydrogen Energy*, vol. 27, no. 3, pp. 235–264, Mar. 2002, DOI: https://doi.org/10.1016/s0360-3199(01)00131-8.

[38] S. Trasatti, "Work function, electronegativity, and electrochemical

behaviour of metals," *Journal of Electroanalytical Chemistry and Interfacial Electrochemistry*, vol. 33, no. 2, pp. 351–378, Dec. 1971, DOI: https://doi.org/10.1016/s0022-0728(71)80123-7.

[39] D. M. F. Santos, C. A. C. Sequeira, and J. L. Figueiredo, "Hydrogen production by alkaline water electrolysis," *Química Nova*, vol. 36, no. 8, pp. 1176–1193, 2013, DOI: https://doi.org/10.1590/s0100-40422013000800017.

[40] J. D. Benck, T. R. Hellstern, J. Kibsgaard, P. Chakthranont, and T. F. Jaramillo, "Catalyzing the Hydrogen Evolution Reaction (HER) with Molybdenum Sulfide Nanomaterials," *ACS Catalysis*, vol. 4, no. 11, pp. 3957–3971, Oct. 2014, DOI: https://doi.org/10.1021/cs500923c.

[41] A. Kahyarian, A. Schumacher, and S. Nesic, "Mechanistic Investigation of Hydrogen Evolution Reaction from Multiple Proton Donors: The Case of Mildly Acidic Solutions Containing Weak Acids," *Journal of the Electrochemical Society*, vol. 166, no. 8, pp. H320–H330, Jan. 2019, DOI: https://doi.org/10.1149/2.0411908jes.

[42] K. Krischer and E. R. Savinova, "Fundamentals of Electrocatalysis," *Handbook of Heterogeneous Catalysis*, pp. 1873–1905, Feb. 2008, DOI: https://doi.org/10.1002/9783527610044.hetcat0101.

[43] L. A. Khanova and L. I. Krishtalik, "Kinetics of the hydrogen evolution reaction on gold electrode. A new case of the barrierless discharge," *Journal of Electroanalytical Chemistry*, vol. 660, no. 2, pp. 224–229, Sep. 2011, DOI: https://doi.org/10.1016/j.jelechem.2011.01.016.

[44] G. J. Brug, M. S. Rehbach, J. H. Sluyters, and A. Hemelin, "The kinetics of the reduction of protons at polycrystalline and monocrystalline gold electrodes," *Journal of electroanalytical chemistry and interfacial electrochemistry*, vol. 181, no. 1–2, pp. 245–266, Dec. 1984, DOI: https://doi.org/10.1016/0368-1874(84)83633-3.

[45] B. E. Conway and L. Bai, "State of adsorption and coverage by overpotential-deposited H in the H2 evolution reaction at Au and Pt," *Electrochimica acta*, vol. 31, no. 8, pp. 1013–1024, Aug. 1986, DOI: https://doi.org/10.1016/0013-4686(86)80017-2.

[46] R. Parsons, G. Picq, and P. Vennereau, "Comparison between the protonation of atomic hydrogen resulting in hydrogen evolution and in the

protonic trapping of photoemitted electrons on gold electrodes," *Journal of electroanalytical chemistry and interfacial electrochemistry*, vol. 181, no. 1–2, pp. 281–287, Dec. 1984, DOI: https://doi.org/10.1016/0368-1874(84)83635-7.

[47] E. Santos, A. Lundin, K. Pötting, P. Quaino, and W. Schmickler, "Model for the electrocatalysis of hydrogen evolution," *Physical review. B, Condensed matter and materials physics*, vol. 79, no. 23, Jun. 2009, DOI: https://doi.org/10.1103/physrevb.79.235436.

[48] M. Jafarian, M. Behazin, I. Danaee, and F. Gobal, "Kinetic Investigations of the Hydrogen evolution reaction on Hg electrode: Impedance Spectroscopy studies," *Research Journal of Chemical Sciences*, vol. 3, no. 10, pp. 56–63, Oct. 2013, Accessed: Apr. 16, 2024. [Online]. Available: https://www.isca.me/rjcs/Archives/v3/i10/9.ISCA-RJCS-2013-150.pdf.

[49] F. Safizadeh, E. Ghali, and G. Houlachi, "Electrocatalysis developments for hydrogen evolution reaction in alkaline solutions – A Review," *International Journal of Hydrogen Energy*, vol. 40, no. 1, pp. 256–274, Jan. 2015, DOI: https://doi.org/10.1016/j.ijhydene.2014.10.109.

[50] M. Videa, D. Crespo, G. Casillas, and G. Zavala, "Electrodeposition of nickel-molybdenum nanoparticles for their use as electrocatalyst for the hydrogen evolution reaction," *Journal of New Materials for Electrochemical Systems*, vol. 13, no. 3, pp. 239–244, Feb. 2010, DOI: https://doi.org/10.14447/jnmes.v13i3.165.

[51] H. Zhang, K. Aoki, J. Chen, T. Nishiumi, H. Toda, and E. Torita, "Voltammetric Determination of Both Concentration and Diffusion Coefficient by Combinational Use of Regular and Microelectrodes," *Electroanalysis*, vol. 23, no. 4, pp. 947–952, Mar. 2011, DOI: https://doi.org/10.1002/elan.200900603.

[52] K. Aoki, H. Toda, J. Yamamoto, J. Chen, and T. Nishiumi, "Is hydrogen gas in water present as bubbles or hydrated form?," *Journal of Electroanalytical Chemistry*, vol. 668, pp. 83–89, Mar. 2012, DOI: https://doi.org/10.1016/j.jelechem.2012.01.013.

[53] K. J. Aoki, J. Chen, Y. Liu, and B. Jia, "Peak potential shift of fast cyclic voltammograms owing to capacitance of redox reactions," *Journal of Electroanalytical Chemistry*, vol. 856, p. 113609, Jan. 2020, DOI:

https://doi.org/10.1016/j.jelechem.2019.113609.

[54] K. J. Aoki, S. Taniguchi, and J. Chen, “Participation in Negative Capacitance of Diffusion-Controlled Voltammograms of Hemin,” *ACS Omega*, vol. 5, no. 45, pp. 29447–29452, Nov. 2020, DOI: https://doi.org/10.1021/acsomega.0c04384.

[55] J. Huang, T. Zhou, J. Zhang, and M. Eikerling, “Double layer of platinum electrodes: Non-monotonic surface charging phenomena and negative double layer capacitance,” *Journal of Chemical Physics*, vol. 148, no. 4, Jan. 2018, DOI: https://doi.org/10.1063/1.5010999.

[56] J.-B. Le, Q.-Y. Fan, J.-Q. Li, and J. Cheng, “Molecular origin of negative component of Helmholtz capacitance at electrified Pt(111)/water interface,” *Science Advances*, vol. 6, no. 41, Oct. 2020, DOI: https://doi.org/10.1126/sciadv.abb1219.

[57] K. J. Aoki, “Voltammetry at a single nano-electrode by varying electrode diameters: Review,” *Journal of Electroanalytical Chemistry*, vol. 779, pp. 7–17, Oct. 2016, DOI: https://doi.org/10.1016/j.jelechem.2016.03.029.

[58] K. Aoki, J. Chen, and Z. Hua, “Comparison of fast scan voltammetry with microelectrode voltammetry of reduction of 1,4-benzoquinone,” *Journal of electroanalytical chemistry*, vol. 610, no. 2, pp. 211–217, Dec. 2007, DOI: https://doi.org/10.1016/j.jelechem.2007.07.021.

[59] N.-T. Suen, S.-F. Hung, Q. Quan, N. Zhang, Y.-J. Xu, and H. M. Chen, “Electrocatalysis for the oxygen evolution reaction: recent development and future perspectives,” *Chemical Society Reviews*, vol. 46, no. 2, pp. 337–365, 2017, DOI: https://doi.org/10.1039/c6cs00328a.

[60] J. Song *et al.*, “A review on fundamentals for designing oxygen evolution electrocatalysts,” *Chemical Society Reviews*, vol. 49, no. 7, pp. 2196–2214, 2020, DOI: https://doi.org/10.1039/c9cs00607a.

[61] G.-F. Li, M. Divinagracia, M. F. Labata, J. D. Ocon, and P.-Y. A. Chuang, “Electrolyte-Dependent Oxygen Evolution Reactions in Alkaline Media: Electrical Double Layer and Interfacial Interactions,” *ACS applied materials & interfaces*, vol. 11, no. 37, pp. 33748–33758, Aug. 2019, DOI: https://doi.org/10.1021/acsami.9b06889.

[62] Y. Liang, Y. Li, H. Wang, J. Zhou, J. Wang, T. Regier, H. Dai, “Co3O4

nanocrystals on graphene as a synergistic catalyst for oxygen reduction reaction," *Nature Materials*, vol. 10, no. 10, pp. 780–786, Aug. 2011, DOI: https://doi.org/10.1038/nmat3087.

[63] L. Xu, Q. Jiang, Z. Xiao, X. Li, J. Huo, S. Wang, L. Dai, "Plasma-Engraved Co_3 O_4 Nanosheets with Oxygen Vacancies and High Surface Area for the Oxygen Evolution Reaction," *Angewandte Chemie International Edition*, vol. 55, no. 17, pp. 5277–5281, Mar. 2016, DOI: https://doi.org/10.1002/anie.201600687.

[64] R. Frydendal *et al.*, "Benchmarking the Stability of Oxygen Evolution Reaction Catalysts: The Importance of Monitoring Mass Losses," *ChemElectroChem*, vol. 1, no. 12, pp. 2075–2081, Oct. 2014, DOI: https://doi.org/10.1002/celc.201402262.

[65] Y. Lee, J. Suntivich, K. J. May, E. E. Perry, and Y. Shao-Horn, "Synthesis and Activities of Rutile IrO2 and RuO2 Nanoparticles for Oxygen Evolution in Acid and Alkaline Solutions," *The Journal of Physical Chemistry Letters*, vol. 3, no. 3, pp. 399–404, Jan. 2012, DOI: https://doi.org/10.1021/jz2016507.

[66] T. Reier, M. Oezaslan, and P. Strasser, "Electrocatalytic Oxygen Evolution Reaction (OER) on Ru, Ir, and Pt Catalysts: A Comparative Study of Nanoparticles and Bulk Materials," *ACS Catalysis*, vol. 2, no. 8, pp. 1765–1772, Jul. 2012, DOI: https://doi.org/10.1021/cs3003098.

[67] E. Antolini, "Iridium As Catalyst and Cocatalyst for Oxygen Evolution/Reduction in Acidic Polymer Electrolyte Membrane Electrolyzers and Fuel Cells," *ACS Catalysis*, vol. 4, no. 5, pp. 1426–1440, Apr. 2014, DOI: https://doi.org/10.1021/cs4011875.

[68] R. Kötz, H. Neff, and S. Stucki, "Anodic Iridium Oxide Films: XPS-Studies of Oxidation State Changes and," *Journal of The Electrochemical Society*, vol. 131, no. 1, pp. 72–77, Jan. 1984, DOI: https://doi.org/10.1149/1.2115548.

[69] S. Cherevko, S. Geiger, O. Kasian, N. Kulyk, J.-P. Grote, A. Savan, B. R. Shrestha, S. Merzlikin, B. Breitbach, A. Ludwig, K. J. J. Mayrhofer, "Oxygen and hydrogen evolution reactions on Ru, RuO 2 , Ir, and IrO 2 thin film electrodes in acidic and alkaline electrolytes: A comparative study on activity and stability," *Catalysis Today*, vol. 262, pp. 170–180, Mar.

2016, DOI: https://doi.org/10.1016/j.cattod.2015.08.014.

[70] Y. Matsumoto, S. Yamada, T. Nishida, and E. Sato, “Oxygen Evolution on La1 − x Sr x Fe1 − y Co y O 3 Series Oxides,” *Journal of The Electrochemical Society*, vol. 127, no. 11, pp. 2360–2364, Nov. 1980, DOI: https://doi.org/10.1149/1.2129415.

[71] J. O’M. Bockris and T. Otagawa, “The Electrocatalysis of Oxygen Evolution on Perovskites,” *Journal of The Electrochemical Society*, vol. 131, no. 2, pp. 290–302, Feb. 1984, DOI: https://doi.org/10.1149/1.2115565.

[72] A. Kabbabi, F. Gloaguen, F. Andolfatto, and R. Durand, “Particle size effect for oxygen reduction and methanol oxidation on Pt/C inside a proton exchange membrane,” *Journal of Electroanalytical Chemistry*, vol. 373, no. 1–2, pp. 251–254, Aug. 1994, DOI: https://doi.org/10.1016/0022-0728(94)03503-2.

[73] I. Nikolov, R. Darkaoui, E. Zhecheva, R. Stoyanova, N. Dimitrov, and T. Vitanov, “Electrocatalytic activity of spinel related cobalties MxCo3−xO4 (M = Li, Ni, Cu) in the oxygen evolution reaction,” *Journal of Electroanalytical Chemistry*, vol. 429, no. 1–2, pp. 157–168, May 1997, DOI: https://doi.org/10.1016/s0022-0728(96)05013-9.

[74] R. Subbaraman, D. Tripkovic, K.-C. Chang, D. Strmcnik, A. P. Paulikas, P. Hirunsit, M. Chan, J. Greeley, V. Stamenkovic, N. M. Markovic, “Trends in activity for the water electrolyser reactions on 3d M(Ni,Co,Fe,Mn) hydr(oxy)oxide catalysts,” *Nature Materials*, vol. 11, no. 6, pp. 550–557, May 2012, DOI: https://doi.org/10.1038/nmat3313.

[75] H. Liang, F. Meng, M. Caba´n-Acevedo, L. Li, A. Forticaux, L. Xiu, Z. Wang, S. Jin, “Hydrothermal Continuous Flow Synthesis and Exfoliation of NiCo Layered Double Hydroxide Nanosheets for Enhanced Oxygen Evolution Catalysis,” *Nano Letters*, vol. 15, no. 2, pp. 1421–1427, Feb. 2015, doi: https://doi.org/10.1021/nl504872s.

[76] Z. Lu, H. Wang, D. Kong, K. Yan, P.-C. Hsu, G. Zheng, H. Yao, Z. Liang, X. Sun, Y. Cui, “Electrochemical tuning of layered lithium transition metal oxides for improvement of oxygen evolution reaction,” *Nature Communications*, vol. 5, no. 1, Jul. 2014, DOI: https://doi.org/10.1038/ncomms5345.

[77] K. Shimizu, L. Sepunaru, and R. G. Compton, “Innovative catalyst design for the oxygen reduction reaction for fuel cells,” *Chemical Science*, vol. 7, no. 5, pp. 3364–3369, 2016, DOI: https://doi.org/10.1039/c6sc00139d.

[78] R. Rozada, J. R. Paredes, S. Villar-Rodil, A. Martínez-Alonso, and J. M. D. Tascón, “Towards full repair of defects in reduced graphene oxide films by two-step graphitization,” *Nano Research*, vol. 6, no. 3, pp. 216–233, Feb. 2013, DOI: https://doi.org/10.1007/s12274-013-0298-6.

[79] S. Mavrikis, S. C. Perry, P. K. Leung, L. Wang, and C. Ponce de León, “Recent Advances in Electrochemical Water Oxidation to Produce Hydrogen Peroxide: A Mechanistic Perspective,” *ACS Sustainable Chemistry & Engineering*, vol. 9, no. 1, pp. 76–91, Dec. 2020, DOI: https://doi.org/10.1021/acssuschemeng.0c07263.

[80] R.-C. Xie, M. Volokhova, A. Boldin, L. Seinberg, M. Tsujimoto, M. Yang, B. Rasche, R.G. Compton, “Electrocatalytic Oxidation of Hydroxide Ions by Co_3O_4 and Co_3O_4@SiO_2 Nanoparticles Both at Particle Ensembles and at the Single Particle Level,” *ChemElectroChem*, vol. 7, no. 5, pp. 1261–1276, Mar. 2020, DOI: https://doi.org/10.1002/celc.202000230.

[81] B. J. Venton and Q. Cao, “Fundamentals of fast-scan cyclic voltammetry for dopamine detection,” *The Analyst*, vol. 145, no. 4, pp. 1158–1168, 2020, DOI: https://doi.org/10.1039/c9an01586h.

[82] Y. Liu, K. J. Aoki, and J. Chen, “A Loss of Charge at Reduction of Hydrogen Ion by Fast Scan Voltammetry,” *Journal of The Electrochemical Society*, vol. 169, no. 3, p. 036510, Mar. 2022, DOI: https://doi.org/10.1149/1945-7111/ac593d.

[83] K. Aoki, C. Li, T. Nishiumi, and J. Chen, “Self-dispersion of mercury metal into aqueous solutions,” *Journal of electroanalytical chemistry*, vol. 682, pp. 66–71, Aug. 2012, DOI: https://doi.org/10.1016/j.jelechem.2012.07.003.

[84] L. Liu, K. J. Aoki, and J. Chen, “Electric Migration of Hydrogen Ion in Pore-Voltammetry Suppressed by Nafion Film,” *Electrochem*, vol. 1, no. 4, pp. 400–409, Nov. 2020, DOI: https://doi.org/10.3390/electrochem1040027.

[85] T. Miyake and M. Rolandi, “Grotthuss mechanisms: from proton

transport in proton wires to bioprotonic devices," *Journal of Physics: Condensed Matter*, vol. 28, no. 2, p. 023001, Dec. 2015, DOI: https://doi.org/10.1088/0953-8984/28/2/023001.

[86] R. S. Nicholson and Irving. Shain, "Theory of Stationary Electrode Polarography. Single Scan and Cyclic Methods Applied to Reversible, Irreversible, and Kinetic Systems.," *Analytical Chemistry*, vol. 36, no. 4, pp. 706–723, Apr. 1964, DOI: https://doi.org/10.1021/ac60210a007.

[87] S. Liu, L. Kang, J. Zhang, E. Jung, S. Lee, and S. C. Jun, "Structural engineering and surface modification of MOF-derived cobalt-based hybrid nanosheets for flexible solid-state supercapacitors," *Energy Storage Materials*, vol. 32, pp. 167–177, Nov. 2020, DOI: https://doi.org/10.1016/j.ensm.2020.07.017.

[88] L. Kang, M. Zhang, J. Zhang, S. Liu, N. Zhang, W. Yao, Y. Ye, C. Luo, Z. Gong, C. Wang, X. Zhou, X. Wu, S.C. Jun, "Dual-defect surface engineering of bimetallic sulfide nanotubes towards flexible asymmetric solid-state supercapacitors," *Journal of materials chemistry. A, Materials for energy and sustainability*, vol. 8, no. 45, pp. 24053–24064, Jan. 2020, DOI: https://doi.org/10.1039/d0ta08979f.

[89] D. J. Griffiths, *Introduction to electrodynamics*. Cambridge I Pozostałe: Cambridge University Press, 2018.

[90] R. A. Gerhardt, "Impedance Spectroscopy and Mobility Spectra," *Elsevier eBooks*, pp. 350–363, Jan. 2005, DOI: https://doi.org/10.1016/b0-12-369401-9/00685-9.

[91] D. S. Frolov and V. I. Zubkov, "Frequency dispersion of capacitance–voltage characteristics in wide bandgap semiconductor-electrolyte junctions," *Semiconductor science and technology*, vol. 31, no. 12, pp. 125013–125013, Nov. 2016, DOI: https://doi.org/10.1088/0268-1242/31/12/125013.

[92] R. E. White, E. Conway, J. O. Bockris, and J. O'm, *Modern aspects of electrochemistry. No. 32*. New York: Plenum Press, 1999.

[93] G. J. Brug, A. L. G. van den Eeden, M. Sluyters-Rehbach, and J. H. Sluyters, "The analysis of electrode impedances complicated by the presence of a constant phase element," *Journal of Electroanalytical Chemistry and Interfacial Electrochemistry*, vol. 176, no. 1, pp. 275–295,

Sep. 1984, DOI: https://doi.org/10.1016/S0022-0728(84)80324-1.

[94] L. Nyikos and T. Pajkossy, “Fractal dimension and fractional power frequency-dependent impedance of blocking electrodes,” *Electrochimica Acta*, vol. 30, no. 11, pp. 1533–1540, Nov. 1985, DOI: https://doi.org/10.1016/0013-4686(85)80016-5.

[95] P. Zoltowski, “On the electrical capacitance of interfaces exhibiting constant phase element behaviour,” *Journal of Electroanalytical Chemistry*, vol. 443, no. 1, pp. 149–154, Feb. 1998, DOI: https://doi.org/10.1016/s0022-0728(97)00490-7.

[96] M. Schalenbach, Y. E. Durmus, S. A. Robinson, H. Tempel, H. Kungl, and R.-A. Eichel, “Physicochemical Mechanisms of the Double-Layer Capacitance Dispersion and Dynamics: An Impedance Analysis,” *Journal of physical chemistry. C*, vol. 125, no. 10, pp. 5870–5879, Mar. 2021, DOI: https://doi.org/10.1021/acs.jpcc.0c11335.

[97] M. Schalenbach, Y. E. Durmus, H. Tempel, H. Kungl, and R. Eichel, “Double layer capacitances analysed with impedance spectroscopy and cyclic voltammetry: validity and limits of the constant phase element parameterization,” *Physical Chemistry Chemical Physics*, vol. 23, no. 37, pp. 21097–21105, Jan. 2021, DOI: https://doi.org/10.1039/d1cp03381f.

[98] Z. Chen, M.C. Wasson, R.J. Drout, L. Robison, K.B. Idrees, J.G. Knapp, F.A. Son, X. Zhang, W. Hierse, C. Kühn, S. Marx, B, Hernandez, O.K. Farha, “The state of the field: from inception to commercialization of metal–organic frameworks,” *Faraday Discussions*, vol. 225, no. 0, pp. 9–69, Feb. 2021, DOI: https://doi.org/10.1039/D0FD00103A.

[99] R. Kikuchi, “A Theory of Cooperative Phenomena,” *Physical Review*, vol. 81, no. 6, pp. 988–1003, Mar. 1951, DOI: https://doi.org/10.1103/physrev.81.988.

[100] K. J. Aoki, “Molecular interaction model for frequency-dependence of double layer capacitors,” *Electrochimica Acta*, vol. 188, pp. 545–550, Jan. 2016, DOI: https://doi.org/10.1016/j.electacta.2015.12.049.

[101] D. J. Griffiths, *Introduction to electrodynamics*, 2nd ed. Upper Saddle River, N.J.: Prentice-Hall, 1989, pp. 158–164.

[102] K. J. Aoki, Y. Liu, and J. Chen, “Irreversible oxidation of hydroxide ion in the light of negative capacitance by fast scan voltammetry,” *Journal*

of Electroanalytical Chemistry, vol. 926, p. 116919, Dec. 2022, DOI: https://doi.org/10.1016/j.jelechem.2022.116919.

[103] P. W. Atkins and J. D. Paula, *Atkins' Physical chemistry*. Oxford ; New York: Oxford University Press, 2014.

[104] R. G. Compton and C. E. Banks, *Understanding voltammetry*. Singapore ; London: World Scientific, 2011.

[105] M. J. Weaver, "Chapter 1 Redox Reactions at Metal–Solution Interfaces," *Deleted Journal*, pp. 1–60, Jan. 1988, DOI: https://doi.org/10.1016/s0069-8040(08)70015-3.

[106] R. A. Marcus and N. Sutin, "Electron transfers in chemistry and biology," *Biochimica et Biophysica Acta (BBA) - Reviews on Bioenergetics*, vol. 811, no. 3, pp. 265–322, Aug. 1985, DOI: https://doi.org/10.1016/0304-4173(85)90014-x.

[107] N. S. Hush, "Electron transfer in retrospect and prospect 1: Adiabatic electrode processes," *Journal of electroanalytical chemistry*, vol. 470, no. 2, pp. 170–195, Jul. 1999, DOI: https://doi.org/10.1016/s0022-0728(99)00168-0.

[108] W. R. Fawcett and M. Opallo, "The Kinetics of Heterogeneous Electron Transfer Reaction in Polar Solvents," *Angewandte Chemie*, vol. 33, no. 21, pp. 2131–2143, Nov. 1994, DOI: https://doi.org/10.1002/anie.199421311.

[109] Henstridge, M.C.; Laborda, E.; Wang, Y.; Suwatchara, D.; Rees, N.; Molina, A.; Martínez-Ortiz, F.; Compton, R.G, "Giving physical insight into the Butler–Volmer model of electrode kinetics: Application of asymmetric Marcus–Hush theory to the study of the electroreductions of 2-methyl-2-nitropropane, cyclooctatetraene and europium(III) on mercury microelectrodes," *Journal of electroanalytical chemistry*, vol. 672, pp. 45–52, May 2012, DOI: https://doi.org/10.1016/j.jelechem.2012.02.028.

[110] M. J. Weaver, "Dynamical solvent effects on activated electron-transfer reactions: principles, pitfalls, and progress," *Chemical reviews*, vol. 92, no. 3, pp. 463–480, May 1992, DOI: https://doi.org/10.1021/cr00011a006.

[111] A. D. Clegg, N. V. Rees, O. V. Klymenko, B. A. Coles, and R. G. Compton, "Marcus Theory of Outer-Sphere Heterogeneous Electron

Transfer Reactions: Dependence of the Standard Electrochemical Rate Constant on the Hydrodynamic Radius from High Precision Measurements of the Oxidation of Anthracene and Its Derivatives in Nonaqueous Solvents Using the High-Speed Channel Electrode," *Journal of the American Chemical Society*, vol. 126, no. 19, pp. 6185–6192, Apr. 2004, DOI: https://doi.org/10.1021/ja040014v.

[112] X. Zhang, H. Yang, and A. J. Bard, "Variation of the heterogeneous electron-transfer rate constant with solution viscosity: reduction of aqueous solutions of [(EDTA)chromium(III)]- at a mercury electrode," *Journal of the American Chemical Society*, vol. 109, no. 7, pp. 1916–1920, Apr. 1987, DOI: https://doi.org/10.1021/ja00241a005.

[113] K. Aoki, K. Honda, K. Tokuda, and H. Matsuda, "Voltammetry at microcylinder electrodes : Part II. Chronoamperometry.," *Journal of electroanalytical chemistry and interfacial electrochemistry*, vol. 186, no. 1–2, pp. 79–86, May 1985, DOI: https://doi.org/10.1016/0368-1874(85)85756-7.

List of Publications

[1]“Delay of reaching the Nernst equilibrium by ac-impedance,” Koichi Jeremiah Aoki, Yuanyuan Liu and Jingyuan Chen, *Journal of Solid State Electrochemistry*, Dec. **2023**. (No including in this thesis)

[2]“The Difference in the Effects of IR-Drop from the Negative Capacitance of Fast Cyclic Voltammograms,” Yuanyuan Liu, Koichi Jeremiah Aoki, and Jingyuan Chen, *Electrochem, Special Issue: Fundamentals and Modem Applications*, vol. 4, no. 4, pp. 460–472, Oct. **2023**. (No including in this thesis)

[3]“Similarity of Heterogeneous Kinetics to Delay of Double-Layer Capacitance Using Chronoamperometry,” Yuanyuan Liu, Koichi Jeremiah Aoki, and Jingyuan Chen, *Electrochem, Special Issue: Fundamentals and Modem Applications*, vol. 4, no. 2, pp. 301–312, Jun. **2023**. (Chapter 2, 6)

[4]“Irreversible oxidation of hydroxide ion in the light of negative capacitance by fast scan voltammetry,” Koichi Jeremiah Aoki, Yuanyuan Liu and Jingyuan Chen,, *Journal of Electroanalytical Chemistry*, vol. 926, no. 1572–6657, pp. 1572–6657, Dec. **2022**. (Chapter 5)

[5]“A loss of Charge at Reduction of Hydrogen Ion by Fast Scan Voltammetry,” Yuanyuan Liu, Koichi Jeremiah Aoki, and Jingyuan Chen, *Journal of The Electrochemical Society*, vol. 169, no. 3, p. 036510, Mar. **2022**.
(Chapter 4)

[6]“Peak potential shift of fast cyclic voltammograms owing to capacitance of redox reactions,” Koichi Jeremiah Aoki, Jingyuan Chen, Yuanyuan Liu, and Bei Jia, *Journal of Electroanalytical Chemistry*, vol. 856, no. 113609, p. 113609, Jan. **2020**.
(Chapter 2,3)